M.Sc. Thesis

Breach flow slides

Gijs Peelen
April 7, 2016

Delft University of Technology

Deltares
Enabling Delta Life

M.Sc. Thesis

Breach flow slides

Submitted in partial fulfilment of the requirements for the degree

Master of Science

In

Hydraulic Engineering

Track

Dredging Engineering

Faculty of 3ME

Delft University of Technology

by
M.Sc Gijs Peelen
G.p.peelen@student.tudelft.nl
1321277

April 7, 2016

Graduation committee:

prof.dr.ir. C. Van Rhee	(Delft University of Technology)
dr.ir. G.H. Keetels	(Delft University of Technology)
dr.ir. M Van Damme	(Delft University of Technology)
ir. D.R. Mastbergen	(Deltares)
dr. G.A. Van Den Ham	(Deltares)

Delft University of Technology

Delft University of Technology
P.O. Box 5048,
2600 GA, Delft
The Netherlands

Deltares
Enabling Delta Life

Deltares
P.O. Box 177
2600 MH, Delft
The Netherlands

PREFACE

This document is the result of my Master of Science degree in Hydraulic Engineering at Delft University of Technology. Within the specialisation of Dredging Engineering, it contains the research study of breach flow slides, made possible by Deltares under supervision and with the help of Dick Mastbergen, Geeralt van den Ham and Maarten de Groot.

ACKNOWLEDGEMENTS

First of all I am grateful for all the effort my graduation committee, Cees van Rhee, Geert Keetels and Myron van Damme put into this graduation project. During several meetings they asked critical questions which helped me during the entire process.

Second, I would like to thank the institute Deltares for giving me the opportunity, resources and patience to carry out this interesting research project.

Gijs Peelen
Delft, April 2016

SUMMARY

The stability of subaqueous slopes is often studied to determine the probability of failure of hydraulic structures. Slope failures have been widely studied to increase the understanding of this complex failure mechanism. However, after a failure it is often hard to figure out the type of failure mechanism: static liquefaction or breach flow. Densely packed soil show dilatant behavior when its subjected to shear, and therefore its stability is temporarily guaranteed. The slope gradual loses grains, which may initiate turbidity currents. This current can be accelerated over the entire slope, until far downstream the flow decelerates (decreased gravitational force and the bed friction) and settles eventually.

1D-equations are derived from conservation of mass and momentum along slopes, which results in an adaptation with respect to the equations of Mastbergen (2013) in the model HMBreach, namely the system is extended to non-stationary conditions. The 1D equations are the framework of the numerical model: BreachFlow. A first order upwind scheme is applied and the transition equations from Eke, Viparelli, & Parker (2011) form the boundary at the breach. This boundary provides initial conditions of thickness, velocity and density and are based on breach height, like in HMBreach and therefore change when the breach retrogrades in time. Due to the chosen numerical scheme hydraulic jumps cause errors when super critical flows decelerate and become sub-critical. Therefore, sedimentation cannot be modelled and the final slope is not found. However, several time steps at the toe of the breach can be modelled and provide information about the development of the breach height, which is important for the initial condition at the first grid point.

In conclusion, with BreachFlow is not yet possible to model the entire final slope, when the breach height reduces to zero. However, it is compared to HMBreach/HMTurb and Retrobreach a promising model, which is easy to adapt to different parameters (including profile) and more accurate regarding the calculation of three variables instead of one (transport of sand). Future work should be based on the implementation of a higher order explicit scheme or even an implicit scheme, in order to model the sedimentation. Then the model can be compared to several case studies including tidal flat of Walsoorden (Van den Ham et al, 2015) in order gain insight what type of mechanism occurred and what parameters correspond to the final slope and retrogressive length.

SAMENVATTING

The stabiliteit van zand hellingen onderwater is vaak onderwerp van onderzoek om de kans op falen van waterbouwkundige objecten beter te kunnen voorspellen. Opgetreden vloeiingen leveren veel informatie om de kennis te vergroten over dit complexe mechanisme. Het is echter vaak lastig na te gaan welk type faalmechanisme is opgetreden: statische verweking of bresvloeiing. Dicht gepakte zandlagen gedragen zich dilatant wanneer er een toename in schuifspanning ontstaat, dit zorgt voor een tijdelijke stabiliteit van het gehele zandpakket. Doordat water aan de rand van de helling het zandpakket binnenstroomt verliezen deze zandkorrels hun stabiliteit en vallen langs de helling naar beneden, wat kan resulteren in een dichtheidsstroom. Deze stroom van zand en water kan versnellen en pas ver benedenstrooms sedimenteren (onder invloed van afnemende hellingshoek) .

1D-vergelijkingen zijn afgeleid van de massa en momentum balans van hellingen, welke resulteren in een uitbreiding naar niet-stationaire condities ten opzichte van de afgeleide vergelijkingen van Mastbergen (20123) in het HMBreach model. Deze 1D vergelijkingen vormen de basis voor het numerieke model: BreachFlow. Een eerste orde schema is toegepast en de transitie vergelijkingen van Eke, Viparelli, & Parker (2011) vormen de overgang van het zand dat erodeert vanuit de bres naar het benedenstroomse onderwatertalud. Afhankelijk van de breshoogte zorgt deze randvoorwaarde voor de benodigde initiële waardes (dikte, snelheid en dichtheid) en dus voor een variabele input als gevolg van een veranderende breshoogte. Mengselsprongen (overgang van superkritische naar sub-kritische stromingen) zijn door de toepassing van dit numerieke schema niet te modelleren in BreachFlow. Hierdoor kan de sedimentatie van zand benedenstrooms niet worden gemodelleerd en is de uiteindelijk helling in dit gebied niet te vinden. Echter, in het superkritische gedeelte van de stroming is de ontwikkeling in tijd goed te modeleren en zorgt voor nauwkeurige informatie voor het verdere verloop van de bres.

Al met al is het met BreachFlow nog niet mogelijk de uiteindelijke helling te voorspellen wanneer de breshoogte is gereduceerd tot nul. Echter, in tegenstelling tot HMBreach/HMTurb en Retrobreach, is BreachFlow een veelbelovend model waarin aanpassingen van parameter (inclusief het profiel) makkelijk kunnen worden doorgevoerd en zorgen voor nauwkeurige resultaten van extra parameters in plaats van alleen het zandtransport. De ontwikkeling van BreachFlow zal gericht moeten zijn op de implementatie van een hoger orde expliciet numeriek schema, of zelfs een impliciet schema zodat mengselsprongen gemodelleerd kunnen worden. Dit zorgt voor een betere validatie wat betreft de case studies op de Plaat van Walsoorden (Van den Ham et al, 2015) en meer inzicht het achterhalen van het type faalmechanisme en belangrijke parameters die zorgen voor het uiteindelijke schadeprofiel.

CONTENTS

LIST OF FIGURES

LIST OF TABLES

LIST OF SYMBOLS

$A[-]$ = coefficient

$A_1[Pa]$ = total friction

$c[-]$ = volumetric sand concentration

$\bar{c}[-]$ =mean volumetric sand concentration

$c'[-]$ = the fluctuating part of the concentration

$c_b[-]$ = volumetric concentration of the bed

$c_0[-]$ = initial flow concentration

$c_v[-]$ = consolidation coefficient

$d[m]$ = thickness flow

$d_0[m]$ = initial flow thickness

$D_*[-]$ = Dimensionless grain size parameter (Bonnefile)

$D_{15}[m]$ = grain size of which 15% of the soil weight is finer

$D_{50}[m]$ = median grain size

$e_w[-]$ = coefficient for water entrainment,

$E[kg\ s^{-1}m^{-2}]$ = sediment pick up rate perpendicular to slope

$E_s[-]$ = coefficient sand bed entrainment factor

$E_w[-]$ = water entrainment rate

$F[kg\ \mathrm{s}^{-1}\ \mathrm{m}^{-1}]$ = product of $u\ d\ \rho_m$

$F_h[N/m]$ = horizontal intergranular force

FoS [-] = Factor of Safety

$Fr[-]$ = internal Froude number

$f_0[-]$ = Darcy-Weisbach friction coefficient of sand bed

$f_1[-]$ = friction coefficient of internal boundary layer

$g[m\ s^{-2}]$ = gravity acceleration

$H_0[m]$ = initial breach height

$k[m/s]$ = intrinsic permeability

$k_0[m/s]$ = permeability of undisturbed sand bed

$k_1[m/s]$ = permeability of loose sand bed

$K[J/kg]$ = mean turbulent kinetic energy

$m[-]$ = erosion power function

$M[kg\ \mathrm{m}^{-2}]$ = product of $d\ \rho_m$

$n[-]$ = erosion power function

$n_1[-]$ = porosity of loose sand bed

$n_0[-]$ = actual porosity of sand bed

$q[m^2/s]$ = specific discharge

$r_0[-]$ = ratio between the near bed concentration of suspended sediment and the layer averaged concentration

$Ri[-]$ = Richardson number

$R_p[-]$ = particle Reynolds number

$S[kg\ s^{-1}\ m^{-2}]$ = sedimentation rate of sand bed

$T[N/m]$ = friction force

$T_1\ [°]$ = temperature of water

$u[m/s]$ = flow velocity

$\bar{u}[m/s]$ = mean flow velocity

$u'[m/s]$ = the fluctuating part of the flow velocity

$u_0[m/s]$ = initial flow velocity

$u_*[\mathrm{m/s}]$ = bed shear velocity

$v[m^2\ \mathrm{s}^{-1}]$ = kinematic viscosity of water

$v_e[m/s]$ = sand bed erosion perpendicular to bed

$v_s[m/s]$ = shields velocity for sand grains

$v_{s,z}[m/s]$ = shields velocity for sand grains perpendicular to bed

$v_{sed}[m/s]$ = sedimentation velocity perpendicular to bed

$v_{wall}[m/s]$ = breach velocity

$v_{wall,90}[m/s]$ = vertical wall velocity

$V[m/s]$ = velocity of the dredger

$W[m/s]$ = vertical flow velocity

$w[m/s]$ = sedimentation velocity of flow

$\overline{w}[m/s]$ = mean sedimentation velocity of flow

$w'[m/s]$ = the fluctuating part of the fall velocity

$w_e[m/s]$ = entrainment water rate

$w_s[m/s]$ = fall velocity of single particle

$w_{s,z}[m/s]$ = fall velocity of single particle perpendicular to bed

$x[m]$ = distance along the slope

$u'[m/s]$ = the fluctuating part of the flow velocity

$z[m]$ = distance to the bed

$z_1[m]$ = boundary between the bottom of the slope and the current

$z_2[m]$ = boundary between the current and ambient water

$\alpha[°]$ = local slope angle

$\beta[°]$ = angle frame of reference

$\chi[m]$ = horizontal axis

$\delta[m]$ = thickness of the intermediate layer between density flow and ambient water

$\varepsilon[-]$ = relative density difference between suspension flow and ambient water

$\varepsilon_0[-]$ = layer averaged mean rate of dissipation of turbulent energy due to viscosity

$\varphi[^\circ]$ = internal friction angle sand

$\varsigma[m]$ = vertical axis

$\gamma_w[kN/m^3]$ = unit weight of submerged soil

$\eta[-]$ = constant that defines the rate of stress decay with distance

$\mu[-]$ = dynamic viscosity

$\theta[-]$ = shields; particle mobility parameter

$\theta_{cr}[-]$ = critical value particle mobility

$\theta^*_{cr}[-]$ = modified critical value particle mobility

$\rho_w[kg\ m^{-3}]$ = density water

$\rho_{m,z1}[kg\ m^{-3}]$ = density bed

$\rho_s[kg\ m^{-3}]$ = density of particles

$\rho_m[kg\ m^{-3}]$ = density of sand-water suspension

$\rho_{m,0}[kg\ m^{-3}]$ = initial flow density

$\rho_v[kg/m^3]$ = density at the toe of the breach front

$\sigma[kN/m^2]$ = total stress

$\sigma_h[N/m^2]$ = horizontal stress

$\tau_c[N/m^2]$ = bed-shear stress

$\tau_{c,cr}[N/m^2]$ = critical bed-shear stress

$\tau_o[Pa]$ = bed shear stress

$\tau_1[Pa]$ = shear stress internal boundary layer

$\Delta[-]$ = relative density water

$\Delta n[-]$ = porosity increase of the sand bed from undisturbed to loose condition

CHAPTER 1

BREACH FLOW SLIDES

1.1 INTRODUCTION

In the area of streaming alluvial valleys and deltaic plains, consisting of fine to medium grained sand, bank failures occur frequently. For example, incised channels are often seen due to the unstable streams (Simon & Rinaldi, 2000). The adjustments of the width of the channel can be several meters a year. The Brahmaputra River varies even 50-1100 meters/year (Coleman, 1969). Diverting gullies and channels in sand are often associated with bank failures, whereby the dominant factor is often not clear. Slumping, toppling, sliding or erosion of individual grains are controlled by different properties of the soil. Evidence of ancient bank failures can be seen in stratigraphic records. These records are used to roughly explain the type of process. By applying multi-beam bathymetry and seismic reflection profiles also submerged slopes can be evaluated. Well documented examples of large submarine flow slides that were mapped can be found in e.g. New Jersey continental slope (Pratson, Ryan, Mountain, Twichell, 1994) and retrogressive failures in the Ursa Basin, Gulf of Mexico (Sawyer, Flemings, Dugan & Germaine, 2009). In the Netherlands, most of the documentation of large channel bank failures is in the Scheldt estuaries. More than 1000 slopes failures were documented over the past 200 years (Wilderom, 1979). It makes this area suitable for in-situ experimental research.For the design of the Eastern Scheldt storm surge barrier many lab and flume scale tests have been performed in the past, but the complete process has never been observed yet. Recently a large field test has been performed near the tidal flat of Walsoorden (STOWA, 2015, Mastbergen, 2015). Also observations in Australia were reported (Beinssen, 2014), Figure 1.1.

Figure 1.1: Inskip point, Queensland, June 27th 2011

1.2 STABILITY OF SUBMERGED SLOPES IN SAND

The stability of subaqueous slopes in fine sand is often studied to determine the probability of failure of hydraulic structures. Slope failures have been widely studied to increase the understanding of this complex failure mechanism (Bolton, 1986). Shear slide is well known, flow slide in fine sands, however, resulting in very gentle deposition slopes, is a more complex failure mechanism (CUR, 2008). Instabilities of sandy slopes are reported in different environmental conditions like: large submarine landslides (Terzaghi, 1957), artificially placed sandy slopes in coastal areas, influenced by erosion and dredging and excavation (Meyer & van Os, 1976) which emphasises the value of new research. The liquefaction phenomenon is often addressed to be the most common cause of flow slides. Soils that consist of loosely packed, fine, and clean sand turn out to be more susceptible to static liquefaction. This type of soil behaves in a contracting manner. Above a critical shear stress, the soil becomes liquefiable. The flow of pore water controls the rate at which the pore volume increases, and the internal friction angle shear resistance of the soil decreases (Been & Jefferies, 1985; Been & Jefferies, 1991). The reduction in effective stress may result in large liquefaction, depending on the size of the bank, the size of the weak sand layer, the location of the incipient liquefaction and the density of the soil. Several triggers lead to increased shear stresses; extreme drops water levels in rivers where tides prevail, micro-seismic vibrations, cyclic stresses during earthquakes, local steep slopes due to an earlier liquefaction and rapid accumulation of sediments (Prisco, 2015).

When soil is more densely packed, an increase in shear stresses leads to dilative behavior resulting in suction in the pores. The temporarily increase in shear resistance disappears as the inflow of water reduces the suction. The grains located at the border of the bank loose their stability first and rain downwards. As the inflow of water mitigates the increase in pore pressure, grains gradually retreat. In the case of large sand deposits the breach continues over a large distance (figure 1.2). In order to prevent misleading interpretations and incorrect designations, in this report the failure mechanism will be called breach failure according to the following definition by Van den Berg, Van Gelder, & Mastbergen (2002):

''a gradual retreat of a subaqueous slope which is steeper than the angle-of-repose near the top of the slope, in non-cohesive, dilatant sands.''

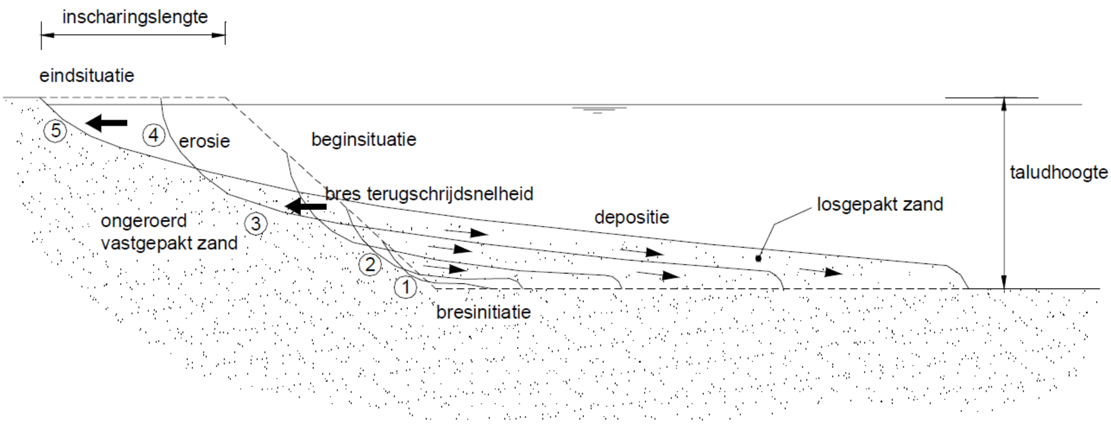

Figure 1.2: Breach Flow Slide (Mastbergen, 2009)

1.3 HMBREACH/HMTURB & RETROBREACH

Models have been developed in order to predict breach flow slides. Two types can be distinquished, models which predict the behaviour of a breach flow slide; HMBreach/HMTurb and models which also can predict the damage profile; Retrobreach .
HMBreach is the model designed by Deltares to simulate the turbidity current and successive erosion or sedimentation initiated by a breach on a certain randomly shaped subaqueous slope with specified sand properties. The 1D steady state two-layer model is able to calculate the equilibrium bottom slope iteratively. HMTurb is an extension of HMBreach which uses a fixed bottom slope. HMBreach is used for predictive analysis of unprotected submerged sandy slopes for dredging purposes and for stability analyses for levees.

Retrobreach (De Groot, 2014) is developed in the context of the WTI 2017 program (Wettelijk Toetsinstrumentarium) which contains new regulations regarding the maximal permissible risk of flooding. This model is a parameterized morphological model based on HMTurb calculations, which can predict the retrogressive length of breach flow slides. A local disruption is applied somewhere along a submerged slope, which is steeper than the internal friction angle and will be the trigger to initiate turbulent density currents. The area of interest is divided into four regimes based on the slope angle and the local transport of sand:
1. Wall regime
2. Erosion regime
3. Equilibrium regime
4. Sedimentation regime.

The first regime is that part of a slope which is disturbed and featured by a local steepening. The slope in this part is too steep to maintain its stability and particles will start to erode. The second regime is characterized by continuation of erosion at the bed. The boundary between the first and second regime equals the internal friction angle of sand. In both regimes gravity and the erosional effect of the overflowing water/sediment mixture destabilize sand particles at the bottom. When slopes angle decreases (further downwards) and therefore the velocity of the current becomes smaller, at some point there is equilibrium between the frictional component and the gravity component. There is an equal amount of sediment picked-up and settled in this regime; therefore the sand transport remains the same. Further downstream, when the slope angle even more decreases, the frictional component outbalances the gravity component and there is a net sedimentation. This fourth regime extends until all the sediment in the current has settled.

1.4 OBJECTIVES

The main objectives in this study is to set-up and improve 1D modeling to predict a complete breach flow slide to answer the question: what is the retrogression length of a breach flow slide in pre-specified conditions?

To reach this objective we have to answer the following questions:

1. Which mechanisms are involved when breach flow slides occur?
2. What set of equations can be used for 1D (unsteady state) modelling?
3. How to implement our findings in a numerical model?
4. How do the results match previous 1D models?

1.5 METHOD

In order to answer the sub-questions and consequently the research question several steps are required. The order of subjects treated in the upcoming chapters is given by:

Chapter2: All the mechanisms involving breach flows are discussed also the research conducted so far is presented shortly.

Chapter 3: Simplification of breach flow slides: a full derivation of the 1D set of continuity equations and momentum equation is given.

Chapter 4: By applying the schematized breach flow slide under constraint conditions the numerical model is presented.

Chapter 5: The numerical model is validated and compared with HMTurb/HMBreach and Retrobreach.

The first step is to map all the mechanisms involving breach flows slides. A constrained 1D model which uses several parameters (slope angle, internal friction, permeability and porosity) needs to be able to describe four regimes during the breaching. The morphological model only describes the sediment transport s_z , along a slope over a certain period. The four parts each consists of different equations based on calculations with the 1D steady state model HMTurb (Deltares, 2003). The parameterized expressions of Retrobreach form a useful prediction of the development of a breach flow in time.

The second step is to study the set of equations which are based on several assumptions which can be used. A full derivation of the 1D Navier-Stokes equations are required which form the framework of the model The equations are compared with the used equations of HMBreach, (Mastbergen & Van den Berg, 2003) based on the work of (Parker, Fukushima & Pantin, 1986 and Winterwerp, de Groot, Mastbergen, & Verwoert, 1990).These equations contain three variables all defined in x-direction: thickness $d[m]$, velocity $u[m/s]$ and concentration of the current $c[-]$. Likewise three equations are necessary to solve each variable. The continuity of sand, the continuity of the mixture (sediment/water) and the momentum equation are used to solve this set of variables.

The next step is to apply our findings in a large-scale model which is based on our improved simplified 1D equations. After discretising the improved equations in order to solve each variable along the slope in time, the model is tested for stability by using two different cases:

- A horizontal slope
- An equilibrium flow

The final step is to validate the model by comparing the results with those of HMBreach/HMTurb and Retrobreach.

CHAPTER 2

MECHANISMS INVOLVED

Albert Einstein (1879-1955) wrote: ''Nothing happens until something moves ''. A certain trigger is required to initiate the breaching process. In this chapter a single grain is followed from incipient motion until it comes to rest downstream. The entire process is divided into four regimes. In each regime dominant mechanisms are explained by the descriptive model Retrobreach (Deltares, 2012).

2.1 WALL REGIME

The retrogressive breach is defined as the wall regime in Retrobreach. This regime is typified by the wall velocity which is the consequence of dilatancy.

2.1.1 DILATANCY

In granular soils dilatancy is the volume increase that may occur during shear. This phenomenon is first reported by Reynolds (1885). The degree of which soil behaves dilative depends on the density of the considered soil. When a dense soil (figure 2.2) is subjected to shear stresses, it can only deform by rolling and gliding over each other, thereby increasing the space between particles. When considering submerged slopes steeper than the natural angle of repose, the shear stress component due to gravity, parallel to the slope, is larger than the shear strength leading to continuous failures. The only direction of volume increase is towards the ambient water. The additional volume of pores (decrease of pore pressure) induces an inflow of water. Because of the inflow, the soil does not lose its stability directly, only when the pore pressure drop is recovered, the effective stress (the mutual connectivity of grains) becomes zero close to the boundary and grains start to erode. In contrary, more loosely packed soil (figure 2.1) do not increase in volume, when subjected to shear stress grains can find a better spot and the pore volume is decreased eventually (water flows out of the soil). Because the total load must be carried, the effective stress is reduced and therefore the particles lose their connection.

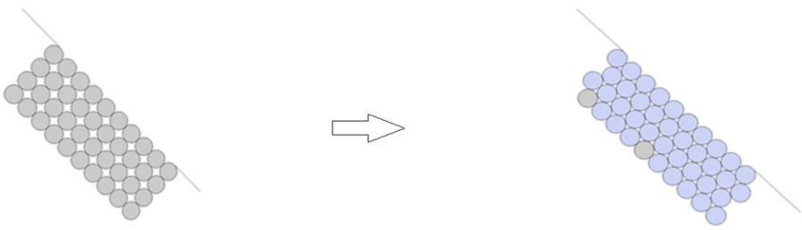

Figure 2.1: loosely packed grains under shear after consolidation

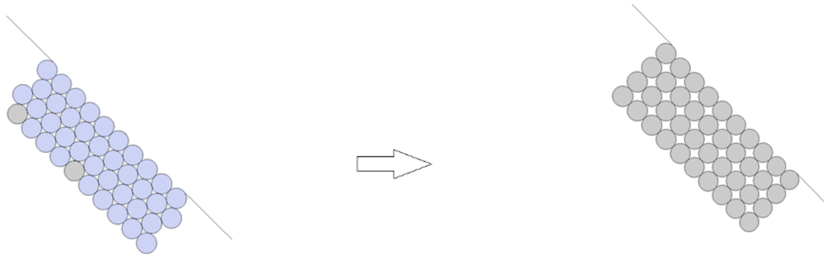

Figure 2.2: densely packed grains under shear after consolidation

The inward hydraulic gradient which pushes the outer grains closer to the each other, because the pore space cannot be filled immediately, decreases with the permeability of the sand. Figures 2.1 and 2.2 are a simplification of the soil, besides porosity, particle size and composition (mineralogy) influences the permeability (Lambe & Whitman, 1969).

The deformation of the porous material and flow pore fluid is the subject of the theory of consolidation. The theory was developed by Terzaghi (1925) for 1D purposes. By assuming a linear material, pseudo-static deformations only in perpendicular to the slope(disregarding inertial force), small strains, fully saturated soil, Darcy's law and if the compressibility of water is negligible compared to the compressibility of the soil.

For dredging purposes, Meijer & Van Os (1976) derived an expression for a moving boundary under steady state conditions and only lateral volume strains. From experiments the existence of a steady state is assumed to be realistic (Meijer & Van Os, 1967; Van Rhee & Bezuijen, 1998). Experimental data accompanied with numerical simulations show the large effect of dilatancy on pore pressure generation, whereby the numerical results fit quite well with the experimental results (Meijer & Van Os, 1967). Therefore, it can be concluded that it is necessary to incorporate dilatancy into the stress-strain relations. Additional experiments of Breusers (1974) showed that the slowly retrograding wall velocity (figure 2.3) mainly depends on grain size and permeability. If the velocity of a dredger equals the wall velocity the front slope is vertical. The relation is given by:

$$\frac{\cot\alpha}{\cot\varphi} = 1 - \frac{V}{v_{wall}} \tag{2.1}$$

In which, $\alpha[°]$ is the slope angle, $\varphi[\deg]$ is the internal friction angle, $V[m/s]$ is the velocity of the dredger and $v_{wall,90}[m/s]$ is the vertical wall velocity, which is defined as (Van Rhee & Bezuijen, 1998):

$$v_{wall,90} = \frac{k_1}{\Delta n}\Delta(1-n_0)\cot\varphi \tag{2.2}$$

Slopes between a vertical angle and the internal friction angle are determined by (van Kesteren et al,. 1992);

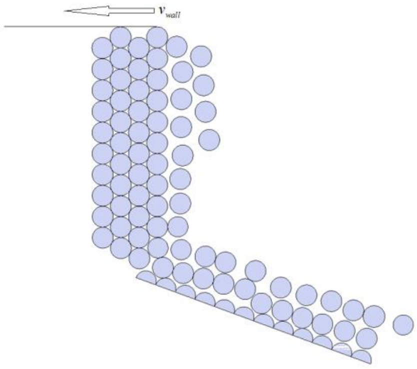

Figure 2.3 schematized breach flow

$$v_{wall} = \frac{k_1}{\Delta n}\Delta(1-n_0)\frac{\sin(\varphi-\alpha)}{\sin\varphi} \tag{2.3}$$

The intrinsic permeability of the loose sand bed $k_1[m/s]$, the relative porosity increase $\Delta n[-]$, the initial porosity $n_0[-]$ and the relative density $\Delta[-]$ determine the wall velocity.

The intrinsic permeability of the loose sand bed is slightly higher compared to the undisturbed sand k_0, because of the increase of porosity from n_0 to n_1 and is given by (Mastbergen & Van den Berg, 2003);

$$k_0 = \frac{gD_{15}^2}{160\nu}\frac{n_0^3}{(1-n_0)^2} \tag{2.4}$$

In which, $g[m/s^2]$ is the gravitational constant, $\nu = \dfrac{40}{20+T}10^{-6}\,[m^2/s]$ is the kinematic viscosity of water, $T_1\ [°]$ is the temperature of water and $D_{15}[m]$ is the grain size of which 15% of the soil weight is finer.

2.1.2 BREACHING/SLIDING

A similar 1D steady state model as in Meijer & Van Os (1967) is used by You, Flemings & Mohrig (2012). However, it simplifies the expression in order to yield an analytical solution. However, instead of the linear elastic model (Meijer & Van Os, 1967), You et al (2012) uses an exponentially drop in distance from the breaching front in pore pressure, which results in more dilation close to the front. An interesting result of the analysis of You et al (2012) is the independency of the erosion with respect to the dilation potential. According to his theory the increase in porosity due to shear is counterbalanced by the larger rate of water inflow due to larger under pressures. This theory is however only based on the assumption of linearity of the material parameters and no vertical water inflow (no vertical pore pressure dissipation). Above a certain value of the dilation potential (according to You, 2012 this value equals 4) the drop in pore pressure is high enough to keep the deposit stable, in which steady state breaching occurs.

However, for values beneath that critical parameter another mechanism occurs. (You, Flemings & Mohrig, 2014) describe this type of failure as sliding. The drop in pore pressure is not enough to provide a temporary stability resulting in sudden erosion of larger volumes of sand (figure 2.4). As a consequence, this sliding positively affects the drop in pore pressure further inside the deposit. Therefore the increase in dilation potential is large enough to switch to a temporary breaching mode. Both mechanisms may alternate in assumption of uniform material properties.

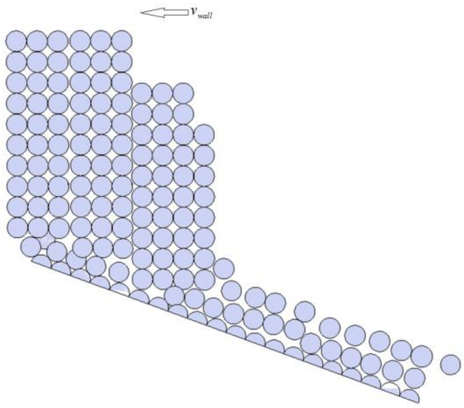

Figure 2.4: schematized sliding mechanism

The assumption of no vertical inflow of water does however influence the maximum drop in pore pressure. Numerical results give much better fits with the experimental data (You, 2012). It can be explained by a reduced maximum drop in pore pressure which temporarily decreases the stability of the soil and hence moves the maximum pressure drop towards the breaching front. This implies that the erosion rate is faster at the top of the deposit, which is observed during experimental studies (Eke, Viparelli & Parker, 2011).

2.1.3 BREACH HEIGHT

Differences in height are suggested to influence the type of failure. Smaller initial heights with the same type of deposit show only the breaching type. By increasing breach heights the dual failure mode arises (alternation of sliding and breaching, see 2.1.2). It has been shown that larger drops in pore pressure positively affect the stability by means of a larger FoS (Factor of Safety), which describes the ratio between stabilising forces and de-stabilising forces (You, 2012): friction force (T), gravitational force (W), horizontal inter-granular force (Fh) and force from pore pressure acting on the slope (P) (figure 2.5).

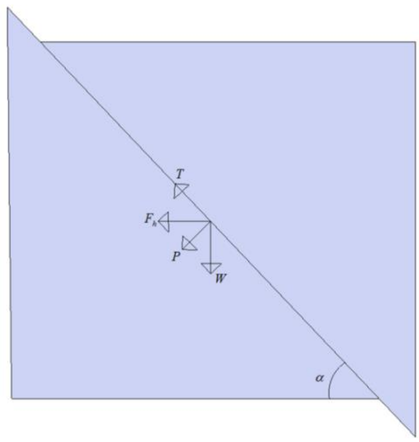

Figure 2.5: Stability analysis of a wedge

When FoS<1 for a certain slope α the deposit is not stable and sliding occurs (resistance factor is smaller than the downward force due to gravity). During the inflow of water the pressure dissipates, resulting in a smaller FoS. By increasing the height the FoS tends to result in values smaller than 1 (You, 2012). The maximum breach height in the experiments of You was limited to 1m. The sudden release of a wedge over larger heights than the experimental set-up are expected to be of a combination of breaching and sliding (dual failure mode: You et al., 2014). In addition, larger initial breach heights may provide an increase in breach height in time because of the erosional effect of a sand/water mixture with high velocity (see chapter 2.3). The importance of breach heights is suggested by Van Rhee & Bezuijen (1998) supported by field experiments and numerical studies.

2.14 CONCLUDING REMARKS

The presence of dilatancy is a necessary condition for breach flow slides to occur. In the wall regime, this feature prevents submerged slopes to shear immediately with large volumes of soil. For modeling purposes, it is chosen to use a constant wall velocity based on the vertical wall velocity of Van Kesteren, Steeghs & Mastbergen (1992) (2.2). As a consequence, permeability, grain size and the increase in porosity are considered to be constant. The role of fines on the permeability is therefore neglected. This constant velocity is also reported in Mastbergen & Van den Berg (2003), this simplification seems to be acceptable for 1D modeling. It also implies the velocity is the product of sliding and steady state breaching (You, 2012). When the breach retrogrades into the zone of the slope that is above water, the sand will behave cohesive due to stresses in the unsaturated zone, causing the sliding of lumps of sand (see figure 1.1). There is no difference between the distinctive velocities that both mechanisms show. Even if the breach height increases, and according to the stability analysis (You, 2012) it is most likely that sliding is also involved, the wall velocity remains constant in this model. Therefore, it is hypothesized the model underestimates the wall velocity in real circumstances.

2.2 EROSION REGIME

The erosion regime is the transformation of a retrograding breach into a density current or turbidity current. This current is fed by the breach but will erode sand from the bed also thus enhancing flow velocity and potential erosion capacity. This so-called self-acceleration that can result in a flow slide can occur only under specific conditions. These conditions can be determined with HMTurb. If the turbidity current is not able to erode and transport the sand, the sand will settle and the flow slide will stop.

2.2.1 TURBIDITY CURRENTS

Turbidity currents are sediment-laden underflows which occur in presence of subaqueous slopes of certain height and slope angle, for example in the ocean and lakes (Parker et al., 1986). The transport of littoral sediment with velocities of 8-14 m/s (Kamphuis, Davies, Nairn & Sayao, 1986) to deeper parts is still not yet fully understood. Turbidity currents are suspended sediment flows exchanging bed-sediment.

Sediment is forced downstream because of gravity, at the same time the shear stresses between the sediment flow and sea bed and water induce a turbulent water flow, enabling the entrainment or vertical diffusion of sediment, resulting in a suspended sand concentration distribution (Rouse vertical). The suspension of sediment is influenced by turbulence and fall velocity. Net erosion of particles from the bed leads to a turbidity current with a higher density and thus an increased gravity as a driving force (self-acceleration). The expanding turbidity current causes a wider sedimentation zone at the toe of the bank.

Parker et al. (1986) used a 1 dimensional layer averaged model to describe the mechanism. The volume balance equation for water and sand and the momentum equation for the sand-water mixture are being used to model turbidity currents: The mass/ volume balance equation for water is given by a rotated coordinate system in which the x-axis is defined along the slope and the z-axis perpendicular to the slope (positive upwards).

$$\frac{\partial d}{\partial t}+\frac{\partial ud}{\partial x}=e_w u, \tag{2.5}$$

In this equation the volumetric effect of sand (1-c) is neglected, so this holds for relatively low concentrations. In Winterwerp et al, 1992 and Mastbergen & Van den Berg, 2003 (HMBreach) this effect is included, resulting in separate continuity equations for water and sand.

The volume balance equation for sediment is:

$$\frac{\partial cd}{\partial t}+\frac{\partial ucd}{\partial x}=w_s(E_s-r_0), \tag{2.6}$$

The momentum balance equation for the mixture is

$$\frac{\partial ud}{\partial t}+\frac{\partial u^2 d}{\partial x}+\frac{1}{2}\Delta g\frac{\partial cd^2}{\partial x}+\Delta\,\mathrm{gcd}\,\alpha-u_*^2=0 \tag{2.7}$$

With, $r_0=\frac{c_b}{c}$, $\Delta=\frac{\rho_m-\rho_w}{\rho_w}$ and $e_w=\frac{w_e}{u}$

In which, $d[m]$ is the layer thickness, $u[m/s]$ is the mean flow velocity, $c[kg/\mathrm{m}^3]$ is the layer averaged concentration of suspended sediment, $w_e[m/s]$ is the velocity of entrainment of ambient water, $c_b[kg/m^3]$ is the near-bed volumetric sediment concentration, $E_s[-]$ is the dimensionless coefficient of bed sediment entrainment, $u_*[\mathrm{m/s}]$ is the bed shear velocity, $\Delta[-]$ is the submerged specific gravity of the sediment, $\alpha[°]$ local slope angle, $e_w[-]$ is the coefficient for water entrainment, $\rho_m[kg/m^3]$ is the density of the sediment, $w_s[m/s]$ is the non-cohesive sediment fall velocity, $r_0[-]$ is the ratio between the near bed concentration of suspended sediment and the layer averaged concentration and $\Delta[-]$ is the relative density of particles.

In order to arrive at these equations several approximations and constraints have been imposed. First of all the hydrostatic pressure-approximation is assumed to be valid; the thickness of the density flow is much less than any scale height, and the motion-induced fluctuations in density and pressure do not exceed the total static variation of these quantities (Spiegel & Veronis, 1960). Second, the kinematic viscosity is assumed to equal the value for clear water (but this is not relevant for turbulent flows). Third, the boundary layer approximations are assumed, which hold; the turbidity current is fully turbulent, the velocity of the flow is significant larger than the fall velocity due to gravity along the slope because of the rotated coordinate system, $w_{s,x} << u_x$ and the Reynolds stress in x-direction is ignored $u'c=0$. Fourth, the similarity assumptions are applied: the parameters u and c are assumed to maintain similar profiles in the z-direction as they change in time.

For steady state conditions of a flow in downstream direction with a fixed slope S the equations can be solved analytically (Eke et al., 2011);

$$\frac{\partial d}{\partial s}=\frac{-Ri\alpha+\left(2-\frac{1}{2}Ri\right)e_w+\frac{u_*^2}{u^2}+\frac{1}{2}Ri\frac{r_o w_s}{u}\left(\frac{E_s/r_0}{u}-1\right)}{(1-Ri)} \quad (2.8)$$

$$\frac{\partial d}{\partial s}=\frac{u}{d}\frac{Ri\alpha-\left(1+\frac{1}{2}Ri\right)e_w-\frac{u_*^2}{u^2}-\frac{1}{2}Ri\frac{r_o w_s}{u}\left(\frac{E_s/r_0}{u}-1\right)}{(1-Ri)} \quad (2.9)$$

And

$$\frac{\partial ucd}{\partial s}=cv_s r_o\left(\frac{E_s/r_0}{u}-1\right) \quad (2.10)$$

With $Ri=\frac{R\,\mathrm{gcd}}{u^2}$

In which, $Ri[-]$ is gradient Richardson number.

In order to be able to compute the steady state equations, some assumptions have to be made concerning the water entrainment (e_w), dimensionless sediment entrainment (E_s), shear velocity (u_*), and concentration ratio (r_0). The relation for water entrainment $e_w=\frac{w_e}{u}$ is taken to be $e_w=\frac{0.00153}{0.0204+Ri}$ (Egashira, Ashida, Yajima & Takahama, 1989). A value of r_0 =1.6 is based on laboratory tests and is a reasonable approximation (Parker et al., 1986).

In 1986 flume tests were performed on high density flows and also the model ZSTORT was developed (Winterwerp et al, 1990). From this model later the model HMBreach was derived for high-density flows under water (Mastbergen & Van den Berg, 2003, Delft Cluster, 2006). The models of Parker (1986) and Mastbergen & Van den Berg (2003) are more or less comparable and describe a 1-al 2 layer model of turbidity currents with erosion of sand (which is conserved in lateral direction) and entrainment of ambient water. However, the model of Mastbergen & Van den Berg, 2003, includes the difference in momentum by development of density differences in addition to the gravity effect. The Boussinesq approximation is not implemented and the model is valid for high concentrations also. HMTurb is the basic version of HMBreach with a fixed geometry. In HMbreach an iterative computation of the bed slope is an option. The model is now part of D-Flow slide (Deltares) to assess slope stability for dike-safety. HMBreach can be used to model resulting equilibrium slopes under assumption of a steady dredging process (Mastbergen, 2009) by using the same coordinate system as Parker (1986).

The continuity equation of sand;

$$\frac{\partial cd}{\partial t} + \frac{\partial ucd}{\partial x} = (1-n_0)v_e \tag{2.11}$$

The continuity equation of water:

$$\frac{\partial(1-c)d}{\partial t} + \frac{\partial(1-c)ud}{\partial x} = w_e\Big|_{z2} + n_0 v_e\Big|_{z1} \tag{2.12}$$

And the momentum equation:

$$\frac{\partial\rho_m ud}{\partial t} + \frac{\partial\rho_m u^2 d}{\partial x} + \frac{1}{2}\cos\alpha g d^2 \frac{\partial(\rho_m-\rho_w)}{\partial x} + (\rho_m-\rho_w)gd\cos\alpha\frac{\partial d}{\partial x} - (\rho_m-\rho_w)\mathrm{g}\sin\alpha d + \frac{f_0+f_1}{8}\rho_m u_s^2 = 0 \tag{2.13}$$

With, the density of the current: $\rho_m = \rho_w(1+\Delta c)$.

In which, $c[-]$ is the depth averaged concentration, $w_e[m/s]$ is the net velocity of water entrainment, $v_e[m/s]$ is the net sand bed erosion perpendicular to the bed, $n_0[-]$ is the undisturbed volume porosity of the sand bed, $\Delta[-]$ is the relative density of particles. The sand erosion velocity v_e (or sand entrainment flux E_s) is a very important, but still not accurately known parameter. In Mastbergen & Van den Berg (2003) an expression is implemented that accounts for dilatancy and under pressures in the sand at high flow velocities, actually the breaching effect derived by Meijer & van Os (1967) and Breusers (1974). It is validated with flume tests (Winterwerp et al 2002) but only scarse data are available in the high-velocity regime. It is a modification of the Van Rijn pick-up model. From these equations the steady state expressions can be solved analytically. Both forms of the momentum equation (2.7) and (2.13) are not much different. In Parker et al. (1986) all the terms are divided by the Richardson number, in contrast to Froude number which is used in the HMBreach equation. The Richardson number is related to the internal Froude number (Mastbergen & Van den Berg, 2003):

$$Ri = (Fr)^{-2}\frac{\delta}{d} = \left(\frac{u}{\sqrt{\varepsilon g d}}\right)^{-2}\frac{\delta}{d} \tag{2.14}$$

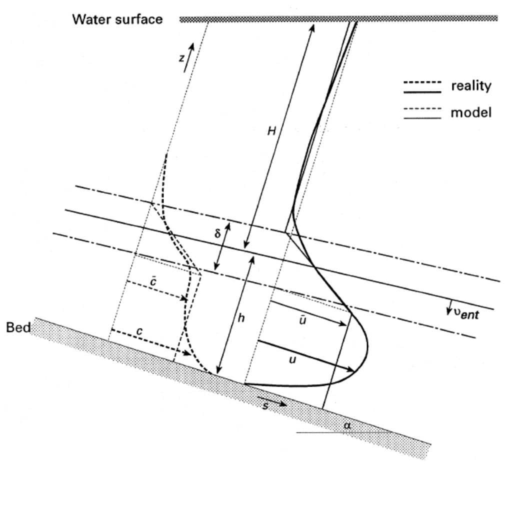

Figure 2.6: Two-layer model schematization of flow velocity and sand concentration distribution (Mastbergen & Van Den Berg, 2003)

In which, Fr[-] is the internal Froude number, $\delta[m]$ is the thickness of the intermediate layer (figure 2.6) between density flow and ambient water, $d[m]$ is the thickness of the flow, $\varepsilon[-]$ is the relative density difference between the suspension flow sub-layer and the ambient water upper layer.

2.2.2 EROSION RATE

Both models are reduced to steady state assumptions, which enable the expressions to be solved analytically. Parker et al. (1986) included a fourth equation (2.15) to take the energy balance into account. Because of the entrainment of new sediment and maintaining the existing load, the turbulent energy increases. The entrainment of sediment into the flow cannot be too large, it would settle out. So, the increase of energy is constrained by (Parker et al., 1986);

$$\frac{\partial Kd}{\partial t}+\frac{\partial uKd}{\partial x}=u_*^2u+\frac{1}{2}u^3e_w-\varepsilon_0 d-Rgw_s cd-\frac{1}{2}R\,\mathrm{gcd}\,ue_w-\frac{1}{2}Rgdw_s(E_s-r_0c) \qquad (2.15)$$

$K[J/kg]$ is the mean turbulent kinetic energy, $\varepsilon_0[-]$ is the layer averaged mean rate of dissipation of turbulent energy due to viscosity.

The reason why the model of Mastbergen & Van den Berg (2003) does not apply this energy constraint is because of the ambient water entrainment factor e_w which is a simple function of velocity, instead of computed based on the turbulent kinetic energy as Parker does. The sediment entrainment or erosion velocity in Parker, 1986 is quantified by Akiyama & Fukushima (1985), from data for open channel suspensions in flumes and rivers. The entrainment factor in this model, determined for grain diameters in the range of 0.06-1.00 mm.

The modelling of the erosion velocity or E_s in the model of Mastbergen & Van den Berg (2003) is based on the experiments by Van Rijn (1984), who provided an accurate expression for a wide range of particles (but no bed effects such as under-pressures at high flow velocities). By measuring the entrainment flux of several particles sizes, the following empirical relation was suggested:

$$E_s=0.00033D_*^{0.3}\left(\frac{\theta-\theta_{cr}}{\theta_{cr}}\right)^{1.5} \qquad (2.16)$$

With, $D_*=\left(\frac{\Delta g}{v^2}\right)^{1/3}D_{50}$

In which, $\theta[-]$ is the dimensionless bed-shear stress according to Shields, $\Delta[-]$ is the relative density of particles. $\theta_{cr}[-]$ is the critical dimensionless bed-shear stress, $D_*[-]$ is the dimensionless grain size parameter (Bonnefile).

However, pick-up relation by the experiments of Van Rijn (1984) was found by low values of the Shields parameter. Which is the relation between a dimensionless shear stress and the particle Reynolds-number holds (Shields, 1936):

$$\theta=\frac{\tau_c}{(\rho_s-\rho_w)\,\mathrm{gD}_{50}} \qquad (2.17)$$

In which, $\tau_c[N/m^2]$ is the bed-shear stress, $\rho_s[kg/m^3]$ is the density of sediment, $\rho_w[kg/m^3]$ is the density of water $g[m/s^2]$ is the acceleration of gravity and D[m] is the particle diameter of granular sediment.

The critical Shields parameter is given in dimensionless form (van Rijn, 1984):

$$\theta_{cr} = \frac{\tau_{c,cr}}{(\rho_s - \rho_w)\,\mathrm{g}\mathrm{D}_{50}} \tag{2.18}$$

In which, $\tau_{c,cr}[N/m^2]$ is the critical bed-shear stress and D_{50}[m] is the median particle diameter of granular sediment.

Erosion can only occur if $\theta > \theta_{cr}$. The empirical relation of Brownlie (1981) is used to quantify the critical shields parameter:

$$\theta_{\mathrm{cr}} = 0.22(\sqrt{\Delta}*\mathrm{Re})^{-0.6} + 0.06*(10)^{-7.7*(\sqrt{\Delta}*\mathrm{Re})^{-0.6}} \tag{2.19}$$

In which, $\Delta[-]$ is the relative density difference, $\mathrm{Re}[-]$ is the Reynolds number for the particles, $D[m]$ is the diameter of a single particle and $v[m^2/s]$ is the kinematic viscosity of the surrounding water.

Van Rhee and Talmon (2000) did experiments with a higher Shields parameter (up to 25) in combination with high sediment concentrations, which resulted in reduced pick-up of values because of the hindered erosion. At relatively low flow velocities grains are picked up grain by grain. Layers of grains are picked up when flow velocity and erosion increases (Bisschop, Visser, van Rhee & Verhagen, 2011). Due to this higher velocity dilatancy, permeability and the (un)drained shear strength of the soil become important and reduce the erosion rate (hindered erosion), comparable with the method described previously by Mastbergen & Van den Berg, 2003. In densely packed soil the top layer is exposed to flow velocities. In order to induce horizontal movement of single grains, shearing grains increase the porosity. As a consequence, inflow of water pushes the top layer on the bed and hinders erosion (figure 2.7).

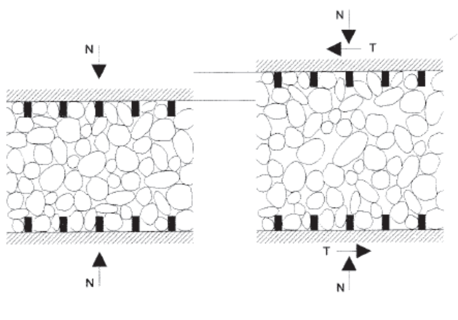

Figure 2.7: increasing vertical pressure on the bed (Bisschop et al., 2011)

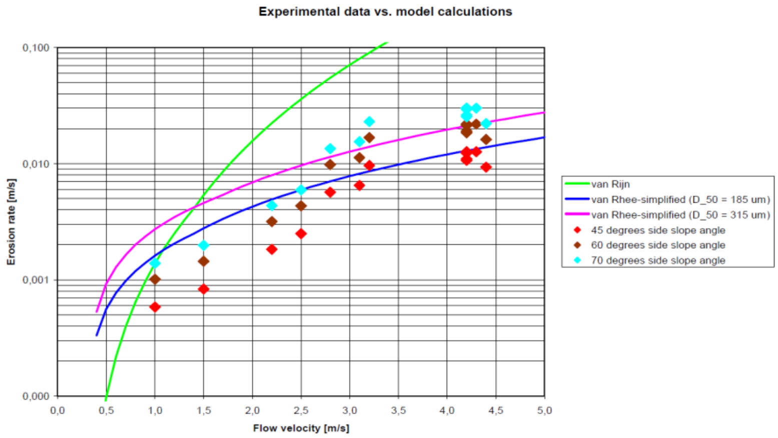

Figure 2.8: Erosion rate in high flow velocities (Bisschop et al., 2011)

The original expression of Van Rijn (1984) is therefore adopted by Van Rhee (2010), which more accurately predicts the pick-up at high velocities by taking dilatancy into account. The expression yields:

$$v_e = \frac{E_s v_s}{1 - n_0 - c_b} \tag{2.20}$$

In which $v_e[m/s]$ is the sand bed erosion perpendicular to bed, $v_s[m/s]$ is shields velocity for sand grains, $n_0[-]$ is the initial porosity (prior to erosion), $c_b[-]$ is the volumetric concentration of the bed and $E_s[-]$ is the coefficient sand bed entrainment factor (also known as the dimensionless pick-up parameter) which is modified to (Van Rhee, 2010):

$$E_s = 0.00033 D_*^{0.3} \left(\frac{\theta - \theta_{cr}^*}{\theta_{cr}^*}\right)^{1.5} \tag{2.21}$$

And, $\theta_{cr}^* = \theta_{cr}\left(\dfrac{\sin(\varphi - \alpha)}{\sin\varphi} + \dfrac{1}{\Delta(1-n_0)}\dfrac{v_e}{k}\dfrac{n_i - n_0}{1 - n_i}\right)$

In which, $\theta_{cr}^*[-]$ is the modified critical Shields parameter, $\alpha[°]$ is the local slope angle, $\varphi[°]$ is the angle of internal friction and $n_i[-]$ is the bed porosity (estimated as maximal porosity).

Due to the presence of the v_e term, this expression needs to be solved numerically. Therefore, Mastbergen & Van den Berg (2003) proposed an expression which also is valid for higher flow velocities but can solved analytically without the sedimentation velocity of particles due to gravity, in the case the erosion flux is significant higher than the sedimentation velocity (figure 2.8). Compared to the formulation of Van Rhee, 2010, in this expression (2.22) slope angle dependency of the critical Shields parameter is not taken into account.

$$v_e = \sqrt{\frac{A(\theta - \theta_{cr})^m \, \mathrm{D}_*^n \, k_1 \sqrt{\Delta^3 g D_{50}}}{\Delta n}} \tag{2.22}$$

2.2.3 WATER ENTRAINMENT

Besides the sediment entrainment at the lower boundary, there is also entrainment of ambient water at the upper boundary, which increases the thickness of the turbidity current downstream. The range of internal Froude numbers which are valid for modelling turbidity currents is quite small. The thickness of the intermediate layer δ (figure 2.6), $Fr_i < 1$ is suggested to be at most half of the currents thickness, which equals an internal Froude number of about 2.8. Also subcritical flows $Fr_i < 1$ require a downstream boundary condition. Turbidity currents which are strongly supercritical are expected to be unstable and dilute rapidly (Mastbergen & Van den Berg, 2003).

The rate at which the entrainment occurs is defined as (Mastbergen & Van den Berg, 2003):

$$w_e = \frac{1}{666} u Fr_i^2 \qquad (2.23)$$

2.2.4 CONCLUDING REMARKS

The unsteady state expressions of Mastbergen & Van den Berg (2003) are used for modelling, because the inclusion of density differences. The model of Parker (1986) uses a constraint energy assumption, by adding a fourth equation, in order to reduce the erosion rate. Mastbergen & Van den Berg (2003) use a different definition of the sediment entrainment factor based on the experiments of Van Rijn and modified for the effect of dilatancy at high flow velocities (hindered erosion). The entrainment of ambient water is described with a simple expression and therefore do not require a fourth equation. Additional research by Van Rhee (2010) provided another expression for the reduction of the erosion rate, explained the hindered erosion in high flow velocities. However, the v_e term in expression (2.21) need to be solved numerically. Therefore, the simplified erosion flux expression of Mastbergen & Van den Berg (2003) is used for modeling. The same holds for the simplified expression of the water entrainment at the upper boundary of the current.

2.3 EQUILIBRIUM + SEDIMENTATION REGIME

If the erosion of water and sediment equals the sedimentation rate, there is no net erosion. The process is considered to be in equilibrium if, moreover, entrainment of ambient water can be neglected. More downstream, where slopes become gentler the sedimentation rate increases since the erosion rate will decrease. This net sedimentation continues until all sediment is released from the current.

2.3.1 EQUILIBRIUM FLOW

The thickness, velocity and density of the flow do not vary over distance $\frac{\partial u d \rho_m}{\partial x} = 0$ and are constant in time $\frac{\partial u d \rho_m}{\partial t} = 0$. The momentum equation (2.13) is reduced to:

$$(\rho_m - \rho_w) g \sin\beta d = \frac{f_0}{8} \rho_m u^2 \qquad (2.24)$$

It requires that there is an 1D equilibrium between gravity along the bed slope and bed shear stress (neglecting water entrainment), which results in an expression of the velocity of the flow with:

$$u = \sqrt{8(\varepsilon g d)/f_0} \tag{2.25}$$

In which, $\varepsilon[-]$ is the relative density difference between the suspension flow sub-layer and the ambient water.

2.3.2 HINDERED SETLLING

Turbidity currents result from suspension of meanwhile falling grains along the bed slope. If the grains start falling, the constant terminal velocity is given by the empirical relationship (Van Rijn & Kroon, 1992);

$$\begin{aligned} w_s &= \frac{1}{18}\frac{\Delta g D_{50}^2}{\nu} \text{ when; } \mathrm{D} \le 100\mu\mathrm{m} \\ w_s &= \frac{10\nu}{D_{50}}\left[\sqrt{1+\frac{\Delta g D_{50}^3}{100\nu^2}}-1\right] \text{when; } 100 < D < 1000\mu m \end{aligned} \tag{2.26}$$

If no more erosion takes place, when the flow velocity is below the critical value, the suspended sand will slowly settle and the turbidity current will lose momentum and eventually vanish. If the velocity reduces due to decreasing slopes at some point (2.22) is not valid any more. The sediment starts to settle but is affected by the concentration (the effect is not negligible for high concentrations above 1–5%). This process is called hindered settling and is the counterpart of hindered erosion. According to the hindered settling effect modeled by Richardson & Zaki (1954), the expression is:

$$v_{sed} = \frac{w_s c(1-c)^n}{1-n_0} \tag{2.27}$$

In which, $v_{sed}[m/s]$ is the settling velocity, upwards defined in positive z- direction, $c[kg/m^3]$ is the near bed volumetric concentration. The concentration is assumed to be constant over the layer. The power n is equal to (Rowe, 1987):

$$n = \frac{4.7+0.41\mathrm{R}_p^{0.75}}{1+0.175\mathrm{R}_p^{0.75}} \tag{2.28}$$

In modeling turbidity currents, the use of this expression is necessary, In the case of low concentrations the effect of hindered settling is reduced to $v_{sed} = \frac{w_s c}{1-n_0}$.

2.3.3 BED FORMS

Turbidity currents are classified in the group of sediment waves. By studying different bed forms with bathymetrical maps and by simulation of bed form evolution with flume experiment, more information is gathered to understand different types of cross-sectional geometries. Besides symmetrical profiles with the top of the crest in the middle and asymmetrical profiles including downslope asymmetry or upslope asymmetry, another type is seen in nature: cyclic steps. These profiles were already recognised during dredging works by De Koning (1970) and are seen in nature. Parker (1996) defined cyclic steps as: ''a series of slowly upstream-migrating bed forms (steps), where each downward step (the lee side of the bed form) is manifested by a steeply dropping flow passing through a hydraulic jump before reaccelerating on flat stoss side''. Detailed experiments were performed by Mastbergen & Bezuijen, 1988 (subaqueous) and Winterwerp et al., 1986 (subaerial), which triggered the development of numerical modelling of cyclic steps. Recently the cyclic steps hypothesis is tested for a wide range of turbidity currents (Cartigny, Postma, Van den Berg & Mastbergen, 2011). Mastbergen (1989) and Winterwerp (1992) simplified the process into three parts. First the hydraulic jump is described, where the flow decelerates into a subcritical flow (Perng & Capart, 2008). The second part is characterized by an acceleration (up to a critical flow) of the flow towards the crest; the stoss side. In the last part, the flow accelerates further towards the trough until the slope is strongly reduced.

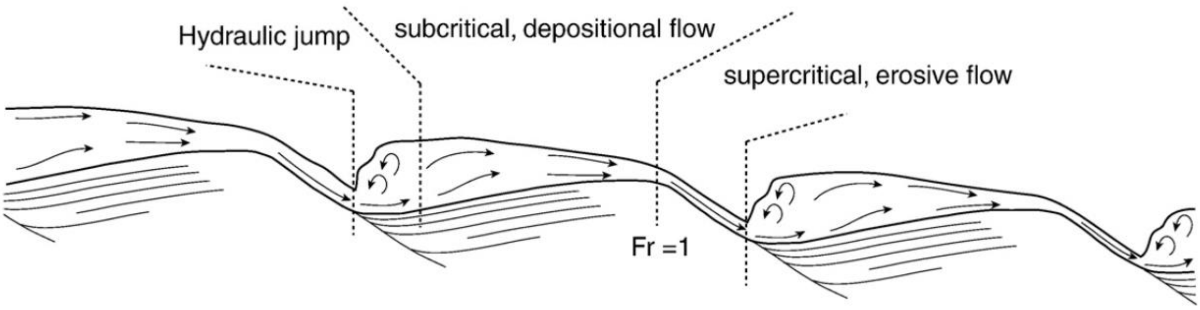

Figure 2.9: cyclic step schematization (Cartigny et al., 2011)

Numerical results in Cartigny et al. (2011) show that indeed many sediment waves can be interpreted as upslope migrating cyclic steps (figure 2.9), located at the upper flow regime, but there are bounded by the densimetric Froude number (depending on flow velocity, thickness and density). First, the incoming flow needs to be supercritical (Fr>1) to form a hydraulic jump. Second, after the hydraulic jump the slope needs to be steep enough to return the flow into its initial Froude number. In the numerical analysis with a lee side of $\alpha = 0.33$, a Froude number of 5 formed the upper limit of cyclic steps. Together with the specific discharge, the combination of Froude numbers as a consequence of the imposed or initial geometry is crucial in the development of cyclic steps. Cyclic steps or anti-dunes were also observed during the dumping of dredged sediments during the IJkdijk test (Vellinga, 2015), whereas dunes were observed moving with the tidal current (STOWA 2015).

2.3.4 CONCLUDING REMARKS

If due to decreased slopes, equilibrium flows keep decelerating, turbidity currents start to release sediment. Due to the hindered settling effect the sedimentation is less than the fall velocity of a single grain. Large differences in bed forms may provide an alternation between net erosion and sedimentation. Therefore the initial profile largely determines development of the slope in time.

2.4 CONCLUSION CHAPTER 2

The goal of this chapter was to identify the mechanisms involved during breach flow slides. The entire process from the retrogressive breach until sedimentation is described in a simplified 1D environment. Several assumptions were made to reduce its modeling complexity:

-Constant breaching process without sliding with vertical breach

-The simplified erosional flux and water entrainment of Mastbergen & Van den Berg (2003)

-The hindered settling effect of Mastbergen (2009)

The next chapter provides a full derivation of the 1D Navier-stokes equations combined with the assumptions made in chapter 2 including a comparison with the equations provided by Mastbergen & Van den Berg (2003).

CHAPTER 3

EQUATIONS

In this chapter the required 1D-equations are elaborated in order to model turbidity currents. The 1D-equations are derived from conservation of mass and momentum along slopes. After the definitions, the sediment continuity equation is derived, followed by the mass balance equation of the sediment/water mixture. Finally the momentum equation is derived and the expressions are compared with Mastbergen (2009). The derived expressions are fully coupled, which means that the effects of sediment density and bed deformation are incorporated into the flow mass and momentum conservation, as in HMBreach and in contrast to decoupled (Di Cristo, Iervoline & Vacca, 2006) and partially coupled models (Lesser, Roelvink, Van Kester & Stelling, 2004).

3.1. DEFINITIONS

Figure 3.1 shows the definitions used in this report. Instead of the use of a horizontal x-axis and vertical z-axis the frame of reference is rotated clockwise with angle β, which matches the mean slope angle. By choosing this mean slope angle, large local variations in direction have negative effects on the accuracy of the results, but it simplifies the numerical computation. The water level is considered to be horizontal.

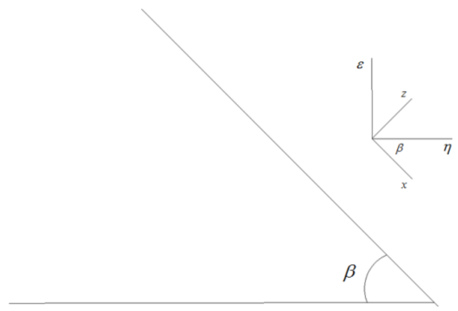

Figure 3.1: definition coordinates

By definition, transport of sediment is considered to be positive from left to right direction with velocity $u[m/s]$. In contrast to the retrogressive wall velocity $v_{wall}[m/s]$, which is defined upstream (in x-direction; figure 3.2). The height of the breach is defined as $H[m]$. The current which is a mixture of water and sand has a density of $\rho_m[kg/m^3]$, the thickness is defined as $d[m] = z_2 - z_1$. z_1 is the boundary layer between the undisturbed sand bed with density $\rho_s[kg/m^3]$ at the bed and the sediment flow. Likewise, z_2 determines the upper boundary layer between the flow and the ambient water with density $\rho_w[kg/m^3]$.

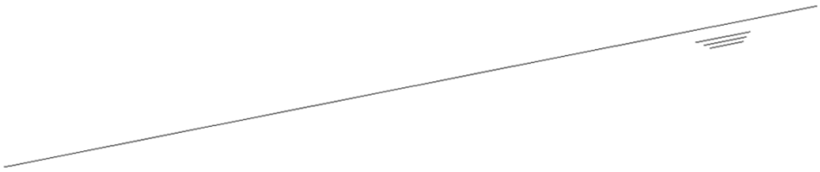

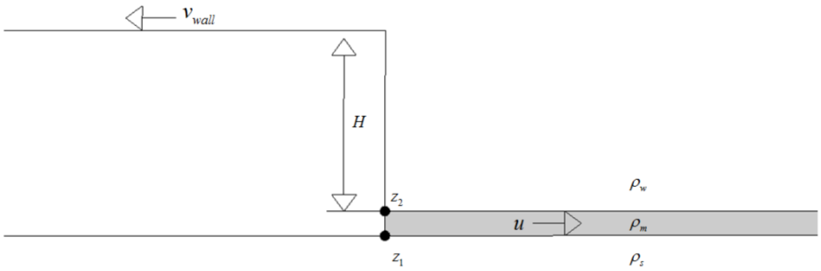

Figure 3.2: definition variables

3.2 ASSUMPTIONS

The degree of simplification is based on the scale of interest. In this problem, concerning flow and sediment transport at the scale of dunes and ripples, simplification is based on Reynolds-averaged Navier-Stokes equations. Often density flows can be assumed constant in density. However, in turbidity currents, the suspended sediment concentration is not constant due to interaction with the bed (erosion and sedimentation). The first assumption of a constant density is therefore not valid. However, complete mixing of sand grains and water is assumed, except for the fall velocity (one phase flow), so the mixture is considered as a homogeneous fluid with varying density. The changing density of the mixture also affects the Boussinesq approximation (Boussinesq, 1877). It states that density differences between two fluids are only incorporated in the gravity term. The density difference in the inertia term is neglected.

The second assumption is the Reynolds-averaging, whereby the velocity and pressure are averaged over turbulence by using a mean and fluctuating part:

$$c=\bar{c}+c';u=\bar{u}+u';w=\bar{w}+w'$$

Third, the slender flow approximations assume that lateral changes in flow are significantly smaller than changes in upward direction (assumption of hydrostatic pressure). Therefore in the continuity equation the Reynolds stresses associated to turbulence in horizontal directions (parallel to the slope) are neglected.

$$\frac{\partial(u'c)}{\partial x} << \frac{\partial(w'c')}{\partial z}$$

In which, $u'[m/s]$ is the Reynolds stress parallel to the slop and $w'[m/s]$ is the Reynolds stress perpendicular to the slope, which is not be cancelled.

The velocity and concentration of the flow are considered one dimensional (depth averaged). Normally the velocity and concentration vary with depth in non-uniform flows. Due to this assumption the flow velocity $u[m/s]$ can be defined by integration of the flow thickness perpendicular to the bed $d[m]$.

3.3 SEDIMENT CONTINUITY EQUATION

In deriving the continuity equation for 1D unsteady flow, an infinitesimal control volume of sides Δx , Δy and Δz is considered with velocity components u , v and w , and the concentration c (figure 3.3). For flow in along the slope in x-direction the mass influx across square ABCD in time interval Δt is given as:

$$G_{in} = [uc - \frac{\partial uc}{\partial x}\frac{\Delta x}{2}]\Delta z \Delta y \Delta t \tag{3.1}$$

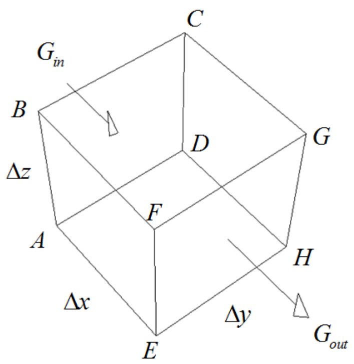

Figure 3.3: flow into volume

The efflux is over square EFGH in time interval Δt is given as:

$$G_{out} = [uc + \frac{\partial uc}{\partial x}\frac{\Delta x}{2}]\Delta z \Delta y \Delta t \tag{3.2}$$

Similar expressions can be obtained for the y and z directions. The net mass influx into the control surface in time can be expressed, after summation as:

The net mass flux is: $G_{net} = G_{in} - G_{out}$, which results in:

$$G_{net} = \left(\frac{\partial uc}{\partial x} + \frac{\partial vc}{\partial y} + \frac{\partial wc}{\partial z}\right)\Delta x \Delta y \Delta z \Delta t \tag{3.3}$$

For the corresponding increase of mass defined as $c\Delta x \Delta y \Delta z$ in time between $t + 1/2\Delta t$ and $t - 1/2\Delta t$, the net increase is described as:

$$G_{\Delta t} = \frac{\partial}{\partial t}(c\Delta x \Delta y \Delta z)\Delta t \tag{3.4}$$

Equating the net mass influx with the net mass increase the 3D continuity equation yields:

$$\frac{\partial c}{\partial t}+\frac{\partial uc}{\partial x}+\frac{\partial vc}{\partial y}+\frac{\partial wc}{\partial z}=0 \tag{3.5}$$

Here the x-axis is defined parallel to the slope, and the z-axis is perpendicular to the slope. This equation applies for all types of flow including unsteady, turbulent compressible flow (Falconer, 1993). By integration this equation over the breadth, which is considered constant and introducing the terminal fall velocity w_s [m/s] in quiescent water in both x and z direction because of the rotated coordinate system. The expression yields a 2D continuity equation.

$$\frac{\partial c}{\partial t}+\frac{\partial (u-w_{s,x})c}{\partial x}+\frac{\partial (w-w_{s,z})c}{\partial z}=0 \tag{3.6}$$

In which, $c[-]$ is the concentration of the current, $u[m/s]$ is the velocity of the current along the slope, $w_{s,z}=w_s\cos\beta$ [m/s] is the vertical velocity of the current and $w_{s,x}=w_s\sin\beta$ (fall velocity along the slope).

The parameters: c , u and w are split into mean (with overbar) and fluctuating parts (Reynolds averaging):

$$c=\bar{c}+c';u=\bar{u}+u';w=\bar{w}+w'$$

This results in:

$$\frac{\partial \bar{c}}{\partial t}+\frac{\partial (\bar{u}-w_{s,x})\bar{c}}{\partial x}+\frac{\partial (\bar{w}-w_{s,z})\bar{c}}{\partial z}=-\frac{\partial (u'c)}{\partial x}-\frac{\partial (w'c')}{\partial z} \tag{3.7}$$

It is assumed that $u'c'$ can be neglected compared to the fluctuation of $w'c'$ of the flow (slender flow approximation):

$$\frac{\partial \bar{c}}{\partial t}+\frac{\partial (\bar{u}-w_{s,x})\bar{c}}{\partial x}+\frac{\partial (\bar{w}-w_{s,z})\bar{c}}{\partial z}=-\frac{\partial (w'c')}{\partial z} \tag{3.8}$$

For many coastal and estuarine-flow problems the fall velocity in x-direction, present due to the rotated coordinate system, is relatively small in comparison with the flow along the slope and can be neglected (depth averaging). As a consequence, the continuity equation can be integrated over the depth and solved numerically to give the depth averaged velocity fields (dropping the overbar for convenience).

$$\frac{\partial}{\partial t}\int_{z1}^{z2}(c)dz+\frac{\partial}{\partial x}\int_{z1}^{z2}(uc)dz+\frac{\partial}{\partial z}\int_{z1}^{z2}(w-w_s)c=-\frac{\partial}{\partial z}\int_{z1}^{z2}(w'c') \tag{3.9}$$

By using the Leibnitz rule (Sokolnikoff & Redheffer, 1966) the expression yields:

$$\begin{gathered}\frac{\partial}{\partial t}\int_{z1}^{z2}\partial(c)dz-c\Big|_{z2}\frac{\partial z_2}{\partial t}+c\Big|_{z1}\frac{\partial z_1}{\partial t}+\frac{\partial}{\partial x}\int_{z1}^{z2}\partial(uc)dz-uc\Big|_{z2}\frac{\partial z_2}{\partial x}+uc\Big|_{z1}\frac{\partial z_1}{\partial x}+\\ c(w-w_s)\Big|_{z2}-c(w-w_s)\Big|_{z1}=-(c'w')\Big|_{z2}+(c'w')\Big|_{z1}\end{gathered} \tag{3.10}$$

The partial derivative of the mean fall velocity holds:

$$w\big|_{z1} = \frac{Dz}{Dt} = \frac{\partial z}{\partial t} + \frac{\partial z}{\partial x}\frac{\partial x}{\partial t}\bigg|_{z1} = \frac{\partial z}{\partial t} + u_s \frac{\partial z}{\partial x}\bigg|_{z1} \quad (3.11)$$

$$w\big|_{z2} = \frac{Dz}{Dt} = \frac{\partial z}{\partial t} + \frac{\partial z}{\partial x}\frac{\partial x}{\partial t}\bigg|_{z2} = \frac{\partial z}{\partial t} + u_s \frac{\partial z}{\partial x}\bigg|_{z2}$$

By substitution, the expression (3.7) yields:

$$\frac{\partial}{\partial t}\int_{z1}^{z2}\partial(c)dz + \frac{\partial}{\partial x}\int_{z1}^{z2}\partial(uc)dz - (cw_s)\Big|_{z2} + (cw_s)\Big|_{z1} = -(c'w')\Big|_{z2} + (c'w')\Big|_{z1} \quad (3.12)$$

This expression can be further elaborated into:

$$\frac{\partial c\left(z_2 - z_1\right)}{\partial t} + \frac{\partial uc\left(z_2 - z_1\right)}{\partial x} - w_s c\Big|_{z2} = -(c'w')\Big|_{z2} - w_s c_b\Big|_{z1} + (c'w')\Big|_{z1} \quad (3.13)$$

The entrainment from the ambient sand into the current is described as

$$-w_s c\Big|_{z2} + (c'w')\Big|_{z2} = 0 \quad (3.14)$$

Because in this upper boundary only water is present, the fall velocity of sediment and the concentration are zero. Therefore both terms are cancelled. The net rate of sediment accumulation on the bed is determined by the sediment flux crossing the bed. The boundary at the bed, z_1 is influenced by the sediment due to gravity in the current and the re-suspension of sediment:

$$F_{sz}\Big|_{z1} = (-w_s c_b + c'w')\Big|_{z1} \quad (3.15)$$

In which the first term $-w_s c$ denotes the rate of depositional flux on the bed due to gravity. $c_b[-]$ is the volumetric concentration of the bed at the bottom z_1. The $w_s[m/s]$ is the fall velocity of single particles which is defined as (Van Rijn, 1992);

$$w_{s,z} = \frac{10\nu}{D_{50}}\cos\beta\left[\sqrt{1 + \frac{\Delta g D_{50}^3}{100\nu^2}} - 1\right] \text{ when; } 100 < D < 1000\mu m \quad (3.16)$$

The second term in (3.15): $c'w'$, denotes re-suspension of sediment at the bed (turbulent Reynolds flux). According to Parker (1986) this term is quantified by the fall velocity $v_s = -w_s$ (actually a negative fall velocity) times and a dimensionless sediment entrainment factor E_s.

$$-w'c'\Big|_{z1} = v_{s,z}E \quad (3.17)$$

$$F_{s,z}\Big|_{z1} = (v_{s,z}E - w_{s,z}c_b)\Big|_{z1} = v_{s,z}E_s - w_{s,z}c_b \quad (3.18)$$

Due to the dilatancy effect at high velocities the expression of Mastbergen & Van den Berg (2003) is used which also is valid for higher flow velocities and can be solved analytically. In that case the sedimentation velocity is small compared to the erosion velocity and can be neglected. (see chapter 2.2.2).

$$v_e = \sqrt{\frac{A(\theta - \theta_{cr})^m \, D_*^n \, k_1 \sqrt{\Delta^3 g D_{50}}}{\Delta n}} \tag{3.19}$$

In which, $\theta[-]$ is the dimensionless bed-shear stress according to Shields and $\theta_{cr}[-]$ is the critical dimensionless bed-shear stress. If $\theta - \theta_{cr} < 0$ sediment will settle according to the hindered settling expression (chapter 2.3.2)

Substituting the volumetric concentration of the flow, given by: $c = \frac{\rho_m - \rho_w}{\rho_s - \rho_w}$, and the concentration at the boundary z_1 : $c_b = \frac{\rho_{m,z1} - \rho_w}{\rho_s - \rho_w}$ into the final expression:

$$\frac{\partial(\rho_m - \rho_w)(z_2 - z_1)}{\partial t} + \frac{\partial u(\rho_m - \rho_w)(z_2 - z_1)}{\partial x} = c_b(\rho_s - \rho_w)v_e\Big|_{z1} \tag{3.20}$$

In which, $c_b = 1 - n_0$.

This expression can be simplified into:

$$\frac{\partial(\rho_m - \rho_w)(z_2 - z_1)}{\partial t} + \frac{\partial u(\rho_m - \rho_w)(z_2 - z_1)}{\partial x} = (\rho_{m,z1} - \rho_w)v_e\Big|_{z1} \tag{3.21}$$

3.4 CONTINUITY OF WATER

The second equation is the continuity of water. Conservation of mass is expressed like the continuity equation of only sediment. The concentration is however replaced by (1-c):

$$\frac{\partial 1 - c}{\partial t} + \frac{\partial \bar{u}(1-c)}{\partial x} + \frac{\partial \bar{w}(1-c)}{\partial z} = 0 \tag{3.22}$$

In which, $(1-c)[-]$ is the concentration of water, $u[m/s]$ is the velocity of the current along the x-axis, $w[m/s]$ is the fall velocity of the mixture perpendicular to the slope. By splitting the parameters likewise as in the derivation of the continuity equation of the sediment and under assumption of no Reynolds flux in direction of the flow (slender flow approximation), it results in:

$$\frac{\partial(1-c)}{\partial t} + \frac{\partial u(1-c)}{\partial x} + \frac{\partial w(1-c)}{\partial z} = -\frac{\partial w'(1-c)}{\partial z} \tag{3.23}$$

Integration over the height $(z_2 - z_1)$ of the current (depth averaging), it yields:

$$\frac{\partial}{\partial t}\int_{z1}^{z2}((1-c))dz + \frac{\partial}{\partial x}\int_{z1}^{z2}(u(1-c))dz + \frac{\partial}{\partial z}(w(1-c)) = -\frac{\partial}{\partial z}\int_{z1}^{z2}(w'(1-c)) \tag{3.24}$$

and by applying the Leibnitz rule (Sokolnikoff & Redheffer, 1966) the expression yields:

$$\frac{\partial}{\partial t}\int_{z1}^{z2}\partial(1-c)dz-(1-c)\Big|_{z2}\frac{\partial z_2}{\partial t}+(1-c)\Big|_{z1}\frac{\partial z_1}{\partial t}+\frac{\partial}{\partial x}\int_{z1}^{z2}\partial(u(1-c))dz-u(1-c)\Big|_{z2}\frac{\partial z_2}{\partial x}+u(1-c)\Big|_{z1}\frac{\partial z_1}{\partial x}+$$
$$(1-c)w\Big|_{z2}-(1-c)w\Big|_{z1}=-((1-c)w')\Big|_{z2}+((1-c)w')\Big|_{z1} \tag{3.25}$$

The partial derivative of the mean fall velocity holds:

$$w\Big|_{z1}=\frac{Dz}{Dt}=\frac{\partial z}{\partial t}+\frac{\partial z}{\partial x}\frac{\partial x}{\partial t}\Big|_{z1}=\frac{\partial z}{\partial t}+u\frac{\partial z}{\partial x}\Big|_{z1} \tag{3.26}$$

$$w\Big|_{z2}=\frac{Dz}{Dt}=\frac{\partial z}{\partial t}+\frac{\partial z}{\partial x}\frac{\partial x}{\partial t}\Big|_{z2}=\frac{\partial z}{\partial t}+u\frac{\partial z}{\partial x}\Big|_{z2}$$

By substitution, expression (3.24) yields:

$$\frac{\partial(1-c)(z_2-z_1)}{\partial t}+\frac{\partial u(1-c)(z_2-z_1)}{\partial x}=-w'(1-c)\Big|_{z2}+w'(1-c)\Big|_{z1} \tag{3.27}$$

Because the continuity water is considered, the concentration of the current with respect to water is substituted by: $c=\frac{\rho_m-\rho_w}{\rho_s-\rho_w}$, at boundary z_1 : $c\Big|_{z1}=\frac{\rho_{m,z1}-\rho_w}{\rho_s-\rho_w}$ and at boundary z_2 : $c\Big|_{z2}=\frac{\rho_{m,z2}-\rho_w}{\rho_s-\rho_w}$ it yields:

$$\frac{\partial d}{\partial t}-\frac{\partial d(\rho_m-\rho_w)}{\partial t}+\frac{\partial ud}{\partial x}-\frac{\partial ud(\rho_m-\rho_w)}{\partial x}=-w'\Big|_{z2}+w'(\rho_m-\rho_w)\Big|_{z2}+w'\Big|_{z1}-w'(\rho_m-\rho_w)\Big|_{z1} \tag{3.28}$$

At z_2, there is no sediment entrained by the flow. Also it is assumed that no sediment is entrained by the ambient water due to lateral flows, this is solely the water entrainment into the current at z_2 (concentration equals zero). The entrainment of water is defined in negative z direction. It however leads to an increase of the layer thickness (in positive direction). At z_1, the current entrains water and particles which is the same expression of v_e, but for the water fraction (1-c). An alternative equation is found by adding the continuity sediment and the continuity of water. The expression yields:

$$\frac{\partial(z_2-z_1)}{\partial t}+\frac{\partial u(z_2-z_1)}{\partial x}=w_e\Big|_{z2}+v_e\Big|_{z1} \tag{3.29}$$

3.5 MOMENTUM EQUATION

In deriving the x-direction momentum equation for turbulent flow, Newton's second law of motion states that the sum of the external forces acting on a volume must equal the rate of change of linear momentum. In x-direction, the continuity equation (3.5) is multiplied by $u[m/s]$. The local acceleration and advective acceleration are (no incompressibility):

$$F_{total} = \Delta x \Delta y (\frac{\partial \rho_m u(z_2 - z_1)}{\partial t} + \frac{\partial \rho_m u^2 (z_2 - z_1)}{\partial x}) \tag{3.30}$$

The equation can be expanded by including pressure, gravitational and shear stress components:

$$\frac{\partial \rho_m u(z_2 - z_1)}{\partial t} + \frac{\partial \rho_m u^2 (z_2 - z_1)}{\partial x} + \sum \sigma_x + \sigma_{shear} = 0 \tag{3.31}$$

In order to maintain the x-axis and z-axis, the coordinate system needs to be rotated due to the bed slope. The χ, ς coordinates represent respectively the horizontal and vertical axis. The rotation of the axes yields:

$$\frac{\partial p}{\partial \chi} = 0 \Rightarrow \frac{\partial p}{\partial \chi} = \frac{\partial p}{\partial z}\frac{\partial z}{\partial \chi} + \frac{\partial p}{\partial x}\frac{\partial x}{\partial \chi} \Rightarrow \frac{\partial p}{\partial \chi} = (\frac{\partial p}{\partial x}\cos\beta + \frac{\partial p}{\partial z}\sin\beta) = 0 \tag{3.32}$$

$$\frac{\partial p}{\partial \varsigma} = -\rho_m g \Rightarrow \frac{\partial p}{\partial \varsigma} = -(\frac{\partial p}{\partial z}\frac{\partial z}{\partial \varsigma} + \frac{\partial p}{\partial x}\frac{\partial x}{\partial \varsigma}) \Rightarrow \frac{\partial p}{\partial \varsigma} = (-\frac{\partial p}{\partial x}\sin\beta + \frac{\partial p}{\partial z}\cos\beta) = -\rho_m g \tag{3.33}$$

$$\begin{pmatrix} \cos\beta & \sin\beta \\ -\sin\beta & \cos\beta \end{pmatrix} \begin{pmatrix} 0 \\ -\rho_m g \end{pmatrix} = \begin{pmatrix} \frac{\partial p}{\partial x} \\ \frac{\partial p}{\partial z} \end{pmatrix}$$

It yields;

$$\frac{\partial p}{\partial z} = -\rho_m g \cos\beta \text{ and } \frac{\partial p}{\partial x} = -\rho_m g \sin\beta \tag{3.34}$$

First, by integrating $\frac{\partial p}{\partial x}$ over the height of the current in z direction, it yields;

$$\int_{z1}^{z2} \frac{\partial p}{\partial x} dz = \frac{\partial}{\partial x}\int_{z1}^{z2} p dz - p_{z2}\frac{\partial z_2}{\partial x}|z_2 + p_{z1}\frac{\partial z_1}{\partial x}|z_1 \tag{3.35}$$

With a linear distribution between in positive direction $p_{z1} = \rho_m g(z_2 - z_1)\cos\beta + P_0$ and $p_{z2} = P_0$, and $p = \rho_m g(z_2 - z)\cos\beta + P_0$, which can be written in the form;

$$= \frac{\partial}{\partial x}\int_{z1}^{z2} (\rho_m g \cos\beta (z_2 - z) + P_0) dz - P_0 \frac{\partial z_2}{\partial x}|z_2 + (\rho_m g(z_2 - z_1)\cos\beta + P_0)\frac{\partial z_1}{\partial x}|z_1 \tag{3.36}$$

The first term is integrated over the layer thickness.

$$\begin{aligned} &= \frac{\partial}{\partial x}\left(\frac{1}{2}\rho_m g\, z_2^2 \cos\beta + (\rho_m g\, z_2 z_1 \cos\beta) + \frac{1}{2}\rho_m g\, z_1^2 \cos\beta + P_0(z_2 - z_1)\right) - \\ &P_0 \frac{\partial z_2}{\partial x}|z_2 + (\rho_m g(z_2 - z_1)\cos\beta + P_0)\frac{\partial z_1}{\partial x}|z_1 \end{aligned} \tag{3.37}$$

This can be rewritten into:

$$= \frac{\partial}{\partial x}[\frac{1}{2}\rho_m g\cos\beta(z_2 - z_1)^2 + P_0(z_2 - z_1)] - P_0\frac{\partial z_2}{\partial x}|z_2 + \\ (\rho_m g(z_2 - z_1)\cos\beta + P_0)\frac{\partial z_1}{\partial x}|z_1 \tag{3.38}$$

The first term in (3.38) can be simplified by separation of the variables ρ_m and $z_2 - z_1$:

$$= \rho_m g\cos\beta(z_2 - z_1)\frac{\partial}{\partial x}(z_2 - z_1) + \frac{1}{2}g\cos\beta(z_2 - z_1)^2\frac{\partial}{\partial x}\rho_m + \frac{\partial}{\partial x}P_0(z_2 - z_1)] - \\ P_0\frac{\partial z_2}{\partial x}|z_2 + (\rho_m g(z_2 - z_1)\cos\beta + P_0)\frac{\partial z_1}{\partial x}|z_1 \tag{3.39}$$

This expression can be simplified because the sum of the first term and the fifth term equals:

$$\rho_m g\cos\beta(z_2 - z_1)\frac{\partial}{\partial x}(z_2 - z_1) + (\rho_m g(z_2 - z_1)\cos\beta\frac{\partial z_1}{\partial x}|z_1 = \\ \rho_m g\cos\beta\left(z_2 - z_1\right)\frac{\partial\left(z_2\right)}{\partial x} \tag{3.40}$$

The residual terms of P_0 can be rewritten as:

$$\frac{\partial}{\partial x}P_0(z_2 - z_1)] - P_0\frac{\partial z_2}{\partial x}|z_2 + P_0\frac{\partial z_1}{\partial x}|z_1 = \frac{\partial}{\partial x}P_0(z_2 - z_1)] - P_0\frac{\partial(z_2 - z_1)}{\partial x} = \left(z_2 - z_1\right)\frac{\partial P_0}{\partial x} \tag{3.41}$$

The expression $\frac{\partial p}{\partial z}$ equals:

$$\int_{z1}^{z2}\frac{\partial p}{\partial x} = \rho_m g\cos\beta\left(z_2 - z_1\right)\frac{\partial\left(z_2\right)}{\partial x} + \left(z_2 - z_1\right)\frac{\partial P_0}{\partial x} + \frac{1}{2}g\cos\beta(z_2 - z_1)^2\frac{\partial}{\partial x}\rho_m \tag{3.42}$$

This equation is also valid if there is a no horizontal water level. The increase of water pressure along the top of the current is expressed in the change of P_0. In which the first term determines the change in the thickness of the current. Second, integrating in x-direction yields:

$$\int_{z1}^{z2}(-\rho_m g\sin\beta))dz = (-\rho_m g\sin\beta(z_2 - z_1)) \tag{3.43}$$

By substituting this expression into the pressure part, it yields:

$$= \rho_m g\cos\beta\left(z_2 - z_1\right)\frac{\partial\left(z_2\right)}{\partial x} + \left(z_2 - z_1\right)\frac{\partial P_0}{\partial x} + \frac{1}{2}g\cos\beta(z_2 - z_1)^2\frac{\partial}{\partial x}\rho_m - \\ \rho_m g\sin\beta(z_2 - z_1)) \tag{3.44}$$

The change of water pressure right above the current along the slope (figure 3.4), $\Delta P_0[kN/m^2]$ can be defined as $P_{right} - P_{left}$, in which $P_{right} = \rho_w g h_w \cos\beta + \rho_w g \Delta x \tan\beta \cos\beta - \frac{\partial z_2}{\partial x} \Delta x \rho_w g \cos\beta$ and in addition: $P_{left} = \rho_w g h_w \cos\beta$. (3.45)

In which, $h_w[m]$ is the height of the water column above the sand/water mixture.

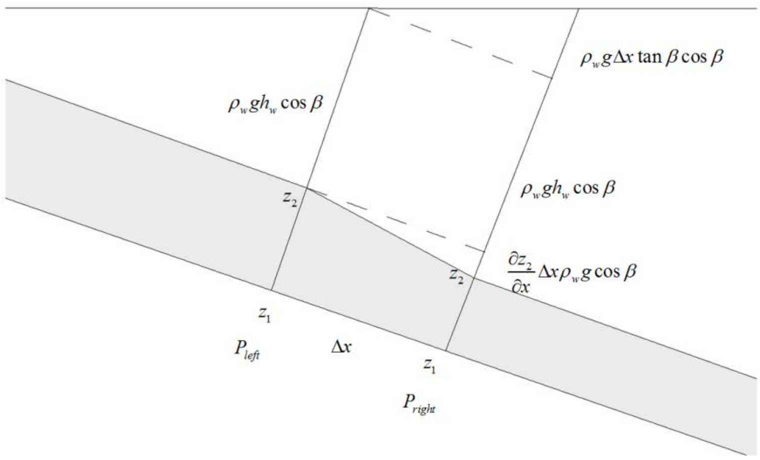

Figure 3.4: pressure difference

By taking the limit $\Delta x \to 0$, the expression yields;

$$\frac{\partial P_0}{\partial x} = \rho_w \,\mathrm{g} \sin\beta - \frac{\partial z_2}{\partial x} p_w g \cos\beta \tag{3.46}$$

(3.46) can now be substituted into (3.44):

$$\begin{aligned}\sum \sigma_x &= \rho_m g \cos\beta \left(z_2 - z_1\right) \frac{\partial\left(z_2\right)}{\partial x} + \frac{1}{2} g \cos\beta (z_2 - z_1)^2 \frac{\partial}{\partial x} \rho_m + \\ &\left(z_2 - z_1\right)(\rho_w \,\mathrm{g} \sin\beta - \frac{\partial z_2}{\partial x} p_w g \cos\beta) - (\rho_m g \sin\beta (z_2 - z_1))\end{aligned} \tag{3.47}$$

In which, it yields the combination of pressure term and the gravitational term.

Finally, we elaborate the additional term due to the shear stress. The shear force on top of the current (expressed in negative x direction) and at the bed is;

1) $-F_{bed} = \tau_{bed} \Delta y \Delta x$ (3.48)

2) $-F_{top} = \tau_{top} \Delta y \Delta x$ (3.49)

Dividing by $\Delta x \Delta y$ yields,

$$-\sigma_{shear} = (\tau_{top} + \tau_{bed}) \tag{3.50}$$

In which, $\tau_{top} = \frac{f_1}{8}\rho_m u_s^2$ and $\tau_{bed} = \frac{f_0}{8}\rho_m u_s^2$

By substitution, the momentum equation yields:

$$\frac{\partial \rho_m u(z_2 - z_1)}{\partial t} + \frac{\partial \rho_m u^2 (z_2 - z_1)}{\partial x} + \rho_m g\cos\beta\left(z_2 - z_1\right)\frac{\partial\left(z_2\right)}{\partial x} + \frac{1}{2}g\cos\beta(z_2 - z_1)^2\frac{\partial}{\partial x}\rho_m - \left(z_2 - z_1\right)(-\rho_w g\sin\beta + \rho_w g\cos\beta\frac{\partial z_2}{\partial x}) - (\rho_m g\sin\beta(z_2 - z_1)) + (\tau_{bed} + \tau_{top}) = 0 \tag{3.51}$$

Finally, it results in three expressions, in which (3.52) is continuity of sediment (3.53) is the continuity of sediment/water mixture and (3.54) is the momentum equation.

$$\frac{\partial(\rho_m - \rho_w)\left(z_2 - z_1\right)}{\partial t} + \frac{\partial u(\rho_m - \rho_w)\left(z_2 - z_1\right)}{\partial x} = (\rho_{m,z1} - \rho_w)v_e\Big|_{z1} \tag{3.52}$$

$$\frac{\partial\left(z_2 - z_1\right)}{\partial t} + \frac{\partial u\left(z_2 - z_1\right)}{\partial x} = w_e\Big|_{z2} + v_e\Big|_{z1} \tag{3.53}$$

$$\frac{\partial \rho_m u(z_2 - z_1)d}{\partial t} + \frac{\partial \rho_m u^2 (z_2 - z_1)}{\partial x} + \rho_m g\cos\beta\left(z_2 - z_1\right)\frac{\partial\left(z_2\right)}{\partial x} + \frac{1}{2}g\cos\beta(z_2 - z_1)^2\frac{\partial}{\partial x}\rho_m - \left(z_2 - z_1\right)(-\rho_w g\sin\beta + \rho_w g\cos\beta\frac{\partial z_2}{\partial x}) - (\rho_m g\sin\beta(z_2 - z_1)) + (\tau_{bed} + \tau_{top}) = 0 \tag{3.54}$$

We simplify the expression by substituting an expression for $d[m]$, which is $d = z_2 - z_1$.

$$\frac{\partial(\rho_m - \rho_w)d}{\partial t} + \frac{\partial u(\rho_m - \rho_w)d}{\partial x} = (\rho_{m,z1} - \rho_w)v_e\Big|_{z1} \tag{3.55}$$

$$\frac{\partial d}{\partial t} + \frac{\partial ud}{\partial x} = w_e\Big|_{z2} + v_e\Big|_{z1} \tag{3.56}$$

$$\frac{\partial \rho_m ud}{\partial t} + \frac{\partial \rho_m u^2 d}{\partial x} + \rho_m g\cos\beta d\frac{\partial\left(z_2\right)}{\partial x} + \frac{1}{2}g\cos\beta d^2\frac{\partial}{\partial x}\rho_m - d(-\rho_w g\sin\beta + \rho_w g\cos\beta\frac{\partial z_2}{\partial x}) - (\rho_m g\sin\beta d) + (\tau_{bed} + \tau_{top}) = 0 \tag{3.57}$$

If the density of the mixture and the density of the water are combined, it leaves us a more clear momentum equation.

$$\frac{\partial \rho_m ud}{\partial t} + \frac{\partial \rho_m u^2 d}{\partial x} + (\rho_m - \rho_w)g\cos\beta d\frac{\partial\left(d + z_1\right)}{\partial x} - (\rho_m - \rho_w)g\sin\beta d + (\frac{f_0 + f_1}{8}\rho_m u_s^2) + \frac{1}{2}g\cos\beta d^2\frac{\partial}{\partial x}\rho_m = 0 \tag{3.58}$$

Delft 3D-flow, designed by Deltares and originally used for fluid mud calculations is adapted for the applicability of breach for modelling. In (Mastbergen, 2013) the set of equations of HMBreach are extended with time dependency for unsteady state modelling. The set of equations are shown by (see also chapter 2 equations 2.11, 2.12 and 2.13):

$$\frac{\partial cd}{\partial t}+\frac{\partial ucd}{\partial x}=(1-n_0)v_e \tag{3.59}$$

$$\frac{\partial(1-c)d}{\partial t}+\frac{\partial(1-c)ud}{\partial x}=w_e\Big|_{z2}+n_0v_e\Big|_{z1} \tag{3.60}$$

$$\frac{\partial\rho_m ud}{\partial t}+\frac{\partial\rho_m u^2 d}{\partial x}+\frac{1}{2}\cos\alpha g d^2\frac{\partial(\rho_m-\rho_w)}{\partial x}+(\rho_m-\rho_w)gd\cos\alpha\frac{\partial d}{\partial x}-(\rho_m-\rho_w)\mathrm{g}\sin\alpha d+\frac{f_0+f_1}{8}\rho_m u_s^2=0 \tag{3.61}$$

In which (3.59) is the continuity of the sediment, (3.60) is the continuity of the water and (3.61) is the 1D- momentum equation.

In the momentum equation (3.61) a difference is noticed. The pressure term (fourth term of 3.61) depends only on the change in thickness of the current, because $\alpha[°]$ is defined as the local slope. However, according to the derivation of the momentum equation, if the pressure gradient is integrated over the depth by using a linear distribution (hydrostatic pressure) the change in pressure due to the change in bed level is also included in the equation.

$$\int_{z1}^{z2}\frac{\partial P}{\partial x}dz=\frac{\partial}{\partial x}\int_{z1}^{z2}Pdz-P_{z2}\frac{\partial z_2}{\partial x}\Big|_{z2}+P_{z1}\frac{\partial z_1}{\partial x}\Big|_{z1} \tag{3.62}$$

In which, $p_{z1}=\rho_m g(\mathrm{z}_2-\mathrm{z}_1)\cos\beta+P_0$, $p=\rho_m g(\mathrm{z}_2-\mathrm{z})\cos\beta+P_0$ and $p_{z2}=P_0$.

This difference is the result the rotated frame of reference, in which β is constant. However, the assumption of hydrostatic water pressure still holds. Therefore, if the thickness of the current remains the same over a certain distance Δx but at the bottom z_1 erosion occurs, a correction of the pressure term is required, which is the term: $(\rho_m-\rho_w)gd\cos\beta\frac{\partial z_1}{\partial x}$. In the model of Mastbergen (2013) this change in bed level is taken into account in the local bed slope α , in which erosion at the bed leads to an increase in pressure.

CHAPTER 4

MODEL: BREACHFLOW

In this chapter the numerical implementation of the new model BreachFlow is described, which serves as a tool for qualifying and quantifying important parameters like (initial breach height, grain size, initial slope height and the location of the initial breach. Decisions for choosing an appropriate computational method have to meet the required accuracy and efficiency. Also, numerical challenges like the wetting/drying problem and moving grids has to be overcome, therefore numerical modelling of turbidity currents is considered as highly complicated (Kostic & Parker, 2003). The main source of inaccuracy however is the expression of the erosion velocity, since the models are various but the validation data scarce.
The numerical solution of BreachFlow is simple however, since a stable forward method can be applied (as in HMBreach), at least for supercritical flow. If subcritical flow or hydraulic jumps are encountered, however, the solution is much more complicated.

4.1 NUMERICAL IMPLEMENTATION

The solution of BreachFlow is found by means of integration in time and space. An appropriate numerical discretisation is required by considering the physical behaviour, the accuracy and the efficiency of the model. The first consideration is the use of either an explicit or implicit solver. Implicit methods are unconditionally stable, whereas the stability of explicit methods depends on the Courant Number, which for stability needs to be less or equal than unity:

$$\sigma \geq \frac{u\Delta t}{\Delta x} \leq 1 \tag{4.1}$$

Implicit models are however unconditionally stable and couple all the cells together through an iterative solution. This iterative process requires a lot computational effort and is preferred by steady state solutions. Because the maximum flow velocity physically will not exceed 10 m/s, the time step requires being 10 times as small as the grid size. Therefore an explicit method is preferred over an implicit method.

4.1.1 FIRST ORDER UPWIND SCHEME

A simple first order upwind scheme is applied which implies that the information is obtained from backward direction. The mass and momentum expressions are all convection equations which can be rewritten in conservative form if the time variation of the solution inside a volume is only due to the boundary fluxes. The velocity $u[m/s]$, thickness $d[m]$ and density $\rho_m[kg/m^3]$ in the sediment continuity, sediment/water continuity and momentum equation are rewritten by F and M:

$$\frac{\partial M}{\partial t} - \rho_w \frac{\partial d}{\partial t} + \frac{\partial F}{\partial x} - \rho_w \frac{\partial ud}{\partial x} = (\rho_{m,z1} - \rho_w) v_e \Big|_{z1} \tag{4.2}$$

$$\frac{\partial d}{\partial t}+\frac{\partial ud}{\partial x}=w_e\Big|_{z2}+v_e\Big|_{z1} \tag{4.3}$$

$$\frac{\partial F}{\partial t}+\frac{\partial Fu}{\partial x}+(\rho_m-\rho_w)g\cos\beta d\frac{\partial d}{\partial x}-(\rho_m-\rho_w)g\sin\beta d+\frac{f_0+f_1}{8}\rho_m u_s^2+\frac{1}{2}g\cos\beta d^2\frac{\partial}{\partial x}\rho_m=0 \tag{4.4}$$

In which, M is the product of the density and the thickness $\rho_m d$ and F is the product of $\rho_m ud$

If (4.3) is substituted into (4.2), it yields:

$$\frac{\partial M}{\partial t}+\frac{\partial F}{\partial x}=\rho_{m,z1}v_e\Big|_{z1}+\rho_w w_e\Big|_{z2} \tag{4.5}$$

The upwind flux F is discretized backward in space (FTBS scheme):

$$\frac{\partial M}{\partial t}+\frac{F_i-F_{i-1}}{\Delta x}=\rho_w w_e\Big|_{z2}+\rho_{m,z1}v_e\Big|_{z1} \tag{4.6}$$

The same procedure is applied by discretizing the continuity of sediment and momentum equation:

$$\frac{\partial d}{\partial t}+\frac{F_i/\rho_{m,i}-F_{i-1}/\rho_{m,i-1}}{\Delta x}+w_e\Big|_{z2}+v_e\Big|_{z1} \tag{4.7}$$

$$\begin{aligned}&\frac{\partial F}{\partial t}+\frac{(\rho_{m,i}u_i^2d_i-\rho_{m,i-1}u_{i-1}^2d_{i-1})}{\Delta x}+(\rho_m-\rho_w)g\cos\beta d\frac{(d_i+z_{1,i}-d_{i-1}+z_{1,i-1})}{\Delta x}-\\&(\rho_m-\rho_w)g\sin\beta d_i+\left(\frac{f_0+f_1}{8}\rho_m u_s^2\right)+\frac{1}{2}g\cos\beta d^2\frac{(\rho_{m,i}-\rho_{m,i-1})}{\Delta x}=0\end{aligned} \tag{4.8}$$

4.1.2 MODELLING PROPAGATION OF CURRENT

In the ongoing process of turbidity current, the model needs to handle shocks and discontinuities properly, which implies conservation of mass and momentum across the shock. An example of a shock is sharp hydraulic jumps (from super-critical to sub-critical flows) but also the sharp front of the turbidity current which propagates with a characteristic speed. This complex process is called the 'wetting and drying' problem. Initially the current is not present over the entire slope, implying **dry** conditions downstream of the front of the **wet** flow. Pre-specified conditions are required in order to generate results.

One solution is the treatment of dry/partially dry and wet cells as proposed by (Li, Vriend, Wang & Maren, 2013), where specified tolerance depths allocate the different states. In this model there is been chosen to make a distinction between dry and wet cells, and therefore only use one tolerance depth to separate the two states. At the start of the simulation all grid points, except the grid point at the incoming boundary, are in a dry state, which implies zero speed, thickness and a density equals to ambient water. Numerical models are not able to handle these zero values. So in order to compute the dry points are removed by small values (0.0001; significant smaller compared to the initial condition). The error which arises can therefore be neglected (figure 4.1).

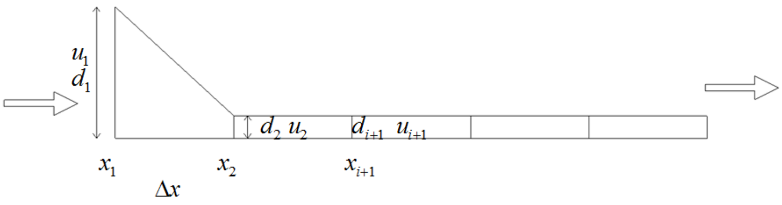

Figure 4.1: wet/dry cells

4.1.3 MOVING GRID

Finally the boundaries are not fixed but move in time along the flow field. The inflow, which is fed by the retrogressive breach, moves according to the specified wall velocity upstream (order mm/s). On contrary, the outflow boundary condition moves much faster (m/s) with the head of the turbidity current downstream. The problem is solved by Kostic & Parker (2003) by using a transformation of the spatial domain with $x \in [0,1]$ by which 0 marks the inflow and 1 the outflow at the front of the current. It is also possible to use fixed boundaries at both ends of the domain, which is used more often (Choi & Garcia, 1995; Bradford, 1996). A disadvantage is the requirement of a large grid size, because the sediment needs to be all settled at the boundary downstream. However in this model the downstream boundary is fixed and the boundary at the breaching front moves with a constant wall velocity upstream. A small grid size of 0.1 m and a time step of 0.01 s are used in BreachFlow. As the breach retrogrades with wall velocity; v_{wall}, grid points are shifted leftwards when the distance of Δx has been reached. An additional grid point at the right boundary is introduced (figure 4.2).

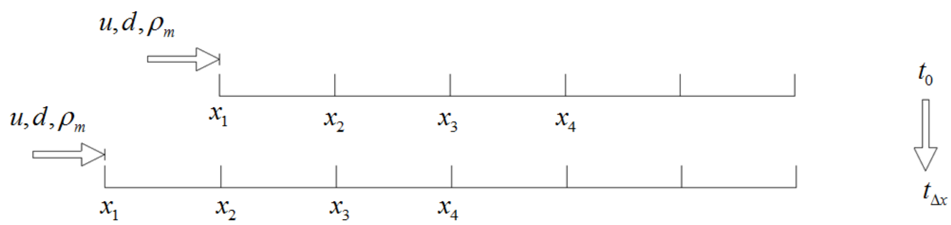

Figure 4.2: moving grid

4.2 HYDRODYNAMIC BOUNDARY CONDITIONS

For a hyperbolic system of equations the number and location of a physical boundary condition are specified by the in- and outflowing number of characteristics. For supercritical flows there need to be an upstream boundary as the information propagates downstream (closed boundary). Downstream, there is no need to define a boundary condition, however to limit the extent of computation it is necessary to introduce an artificial boundary. This boundary can however not be zero, because of the wetting/drying problem, so at the boundary the values are equal with the fore last grid values. Subcritical flows also require downstream boundary conditions. Because there is been chosen for only an upstream moving grid, the conditions of the downstream boundary are not influenced by sedimentation of the turbidity current.

4.2.1 MODELLING BREACH

The boundary condition at the breach is known in the form of an incoming amount of sediment with a specified assumed thickness, velocity and density. This upstream boundary is based on continuity by the retrogressive breach velocity $v_{wall}[m/s]$, the initial breach height $H_0[m]$ and the density of soil $(1-n_0)\rho_s[kg/m^3]$ that equals to the incoming amount of sediment (figure 4.3). However, the way these parameters are transformed into a flow velocity, a thickness and a concentration follows from continuity of sediment. For the amount of water (so the concentration and the flow velocity or Froude number: in HMBreach 12% resp. 2 for instance) an assumption is required.

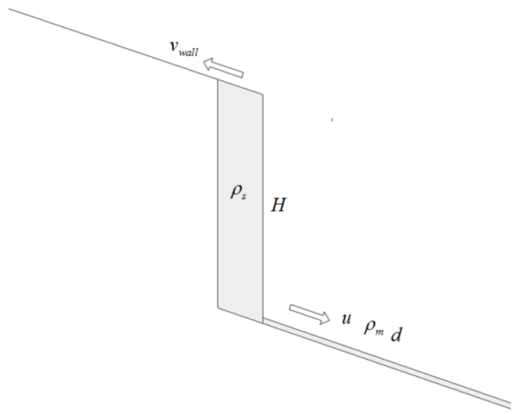

Figure 4.3: boundary condition at breach

If an initial breach height of 1m is imposed, including a wall velocity of 1 mm/s (assuming $(1-n_0)\rho_s = 1600\ kg/m^3$) the incoming flux $F = 2.00 kg/m/s$. As the sediment falls down, it also entrains water and sediment before it reaches the incoming boundary. Because the initial condition might be critical for the development of possible turbidity currents (and thus the progressive erosive character), the transition of the breach into the current requires attention. If initial velocities and sediment transport rate are sufficiently large, the turbid underflow strongly self-accelerates (Parker et al., 1986). Without an additional formulation two parameters needs to be estimated in order to provide three boundary conditions.
Eke et al. (2011) provided three additional expressions for the transition from breach to turbidity current including the entrainment of water and sediment (figure 4.4):

$$H_0 = \frac{3}{4} e_w z \tag{4.9}$$

$$W = v_{wall}(1-n_0)(\frac{5}{4}e_w + f_0)^{-1/3}(\frac{\Delta gz}{(v_{wall}(1-n_0))^2})^{1/3} \quad (4.10)$$

$$\rho_v = \frac{4(\rho_s - \rho_w)}{3e_w}(\frac{5}{4}e_w + f_0)^{1/3}(\frac{\Delta gz}{(v_{wall}(1-n_0))^2})^{-1/3} + \rho_w \quad (4.11)$$

In which, $H_0[m]$ is the initial breach height, $W[m/s]$ is the vertical flow velocity, $\rho_v[kg/m^3]$ is the density at the toe of the breach front, $e_w[-]$ is the entrainment of water coefficient, $z[m]$ is the (near) vertical downward coordinate, $n_0[-]$ is the porosity of undisturbed soil, $f_0[-]$ is the wall friction coefficient and $\Delta[-]$ is the submerged specified gravity of sediment grains.

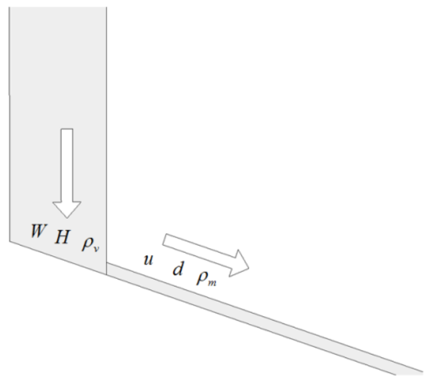

Figure 4.4: transitions u, d and ρ_m

For simplification the entrainment of water is considered to be constant (in contrast to the water entrainment in the turbidity current).

According to the example of the initial breach of 1m with a wall velocity of 1 mm/s, the initial conditions become:

$H = 0.05625\ m$; $W = 0.4287\ m/s$; $\rho_v = 1047\ kg/m^3$

4.2.2 DOWNSTREAM BOUNDARY

Supercritical flows require only boundary condition information upstream. However, when flows decelerate because of decreasing slopes, flows become subcritical, which require also a downstream boundary condition. This boundary can be chosen far away from any disturbance of the flow, which means that all sediment is settled and therefore the initial height of the last grid point remains the same during modelling. However, this is not possible since the assumption of a 2-layer flow is not valid anymore and the amount of water in the flow cannot be defined anymore. According to the model equations the flow depth would go to infinity when the flow velocity and concentration go to 0. Another drawback is the amount of grid points that is required, which may be too inefficient. Therefore an open fixed boundary condition is applied in BreachFlow with an additional constraint that prevents the thickness and velocity to become zero.

4.3 TEST RESULTS

In order to test BreachFlow on its stability two cases are applied. The first case shows a horizontal bed. The second shows a submerged slope under a constant angle in equilibrium state. To be consistent, the flow direction is always to the right. The grid is fixed, which means that the changing initial conditions discussed in 4.2.1 are not used, but a fixed amount of sediment is used instead.

4.3.1 TEST: HORIZONTAL FLOW

To test the transition of super- to subcritical flows a horizontal slope is considered. The initial condition is specified in which with the inflow direction to the right (no moving grid is used, so no retrogressive breach). The initial conditions entering the domain are set on: $d = 0.065\ [m]$, $u = 0.6\ [m/s]$ and $\rho_m = 1090\ [kg/m^3]$. The domain equals $8\ m$ divided into steps of $0.1\,m$. Because of the horizontal slope $\beta = 0$ which reduces the momentum equation by:

$$\frac{\partial \rho_m u d}{\partial t} + \frac{\partial \rho_m u^2 d}{\partial x} + (\rho_m - \rho_w) g d \frac{\partial (d + z_1)}{\partial x} + \frac{f_0 + f_1}{8} \rho_m u_s^2 + \frac{1}{2} g d^2 \frac{\partial \rho_m}{\partial x} = 0 \qquad (4.12)$$

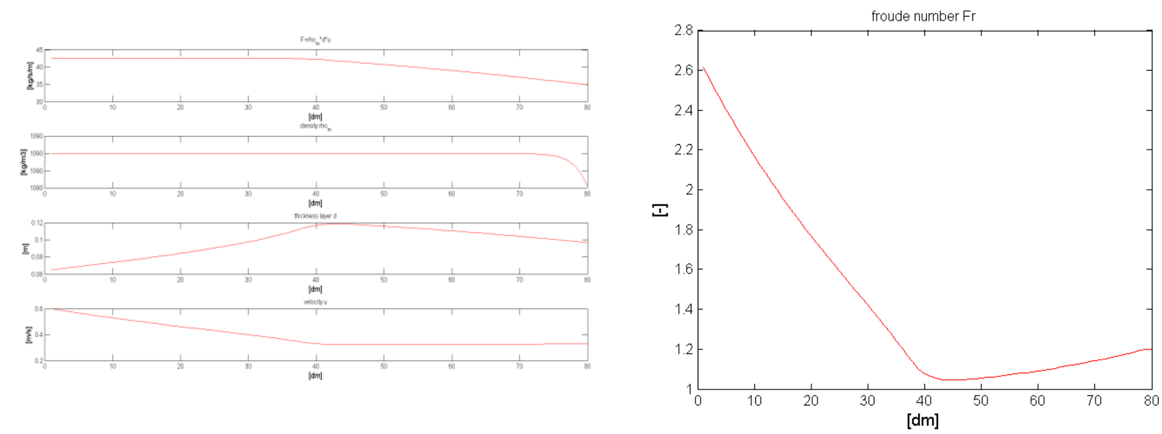

Figure 4.5: horizontal flow (30 sec)

Figure 4.5 shows a decrease in velocity for the first 4m, this is balanced by an increase in thickness. Figure 4.6 shows the hydraulic jump after 45 sec (Fr<1). The change in velocity of the flow becomes large and is balanced by a large increase of the thickness. Continuation of the simulation provides large peaks in thickness, velocity and its product F (including the constant density).

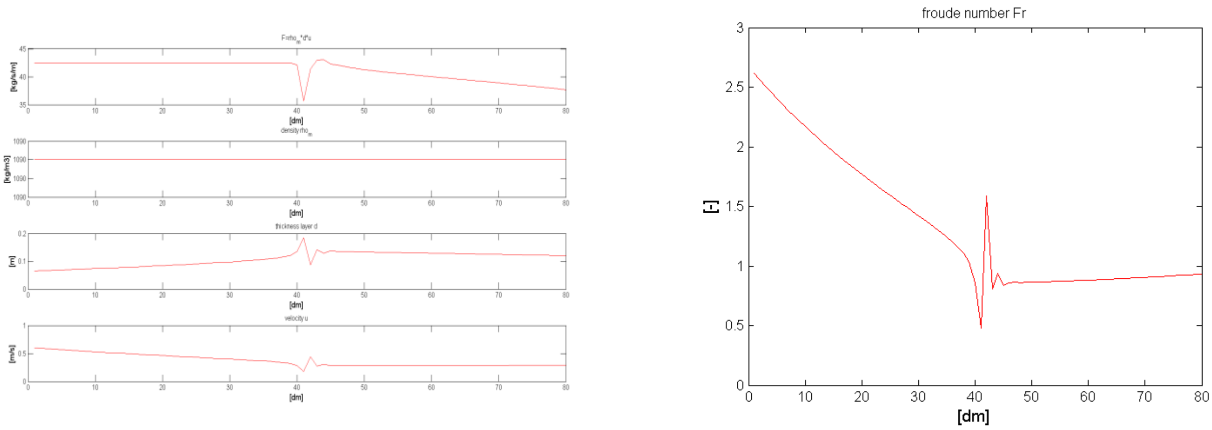

Figure 4.6: horizontal flow (45 sec)

4.3.2 TEST: EQUILIBIRUM FLOW

In the situation of submerged slopes with the assumption of a steady state condition and constant velocity, thickness and density, so with no net erosion and no entrainment, the momentum equation is reduced to:

$$-(\rho_m - \rho_w) g \sin \beta d + \frac{f_0 + f_1}{8} \rho_m u_s^2 = 0 \tag{4.13}$$

The force due to gravity equals the frictional force. The equation is rewritten by:

$$u_s = \sqrt{\frac{8}{f_0 + f_1} \frac{(\rho_m - \rho_w)}{\rho_m} g \sin \beta d} \tag{4.14}$$

The erosion and sedimentation module is set to zero, likewise the entrainment of water. The same initial conditions are used as in the test case of horizontal flow (see 4.3.1). The results are shown in figure 4.7 with an extended grid size of 2.8 m after 1000 sec. The flow remains supercritical over the entire slope.

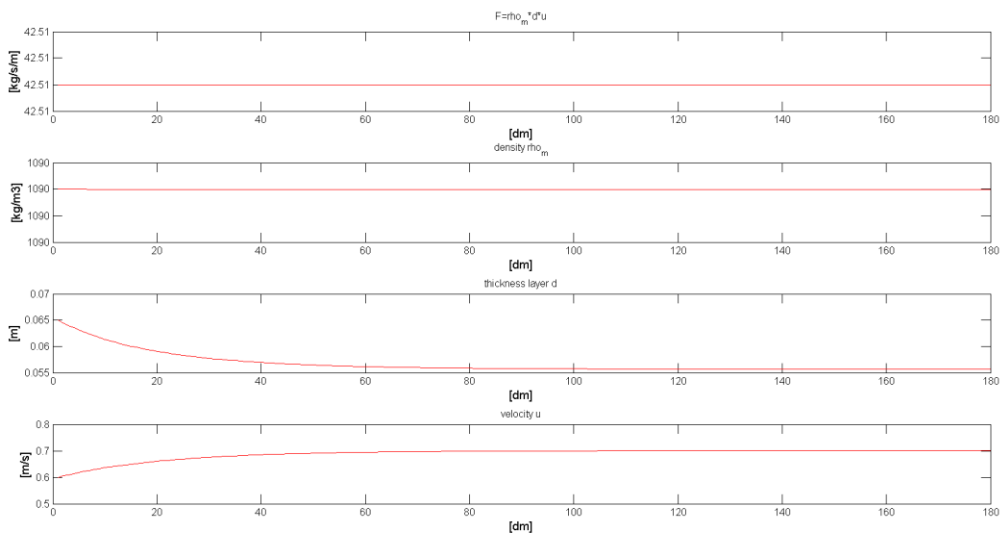

Figure 4.7: equilibrium flow 5° [1000sec]

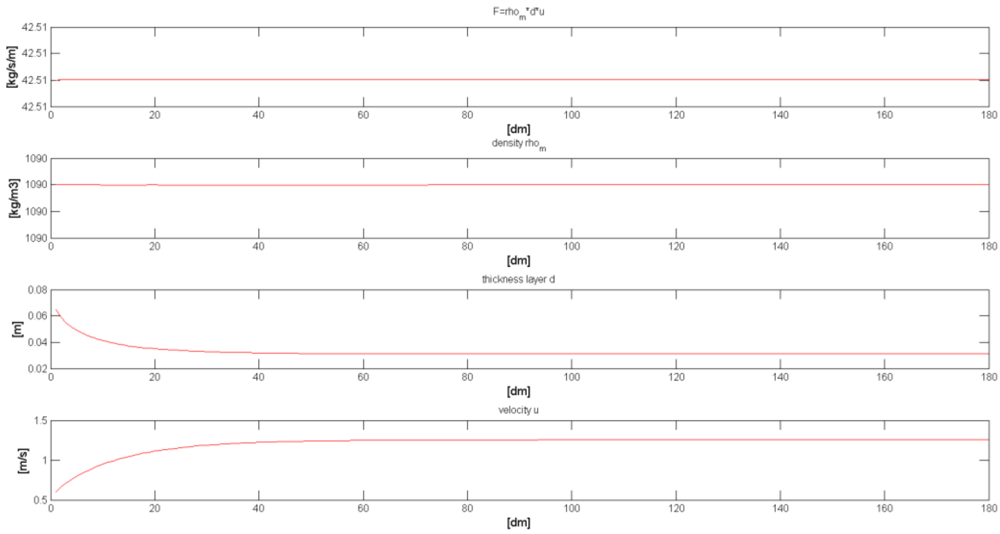

Figure 4.8: equilibrium flow 30° (10000 sec)

4.4 RESULTS RETROGRADING BREACH (VARIABLE PARAMETERS)

In order to model the retrograding breach along the slope in BreachFlow, an erosion and sedimentation module is applied including a moving grid, according to the expression formulated in chapter 2 and substituted in chapter 3. Several parameters are subject to the amount of erosion and sedimentation, which possibly affects the final slope and therefore are tested under pre-specified circumstances.

4.4.1 RESULTS HORIZONTAL SLOPE

The parameters which can be considered as constants are shown in table 4.1. The variable input parameters in table 4.2 are compared in the case of a horizontal slope (figure 4.9). The breach angle is considered to be perpendicular to the horizontal slope.

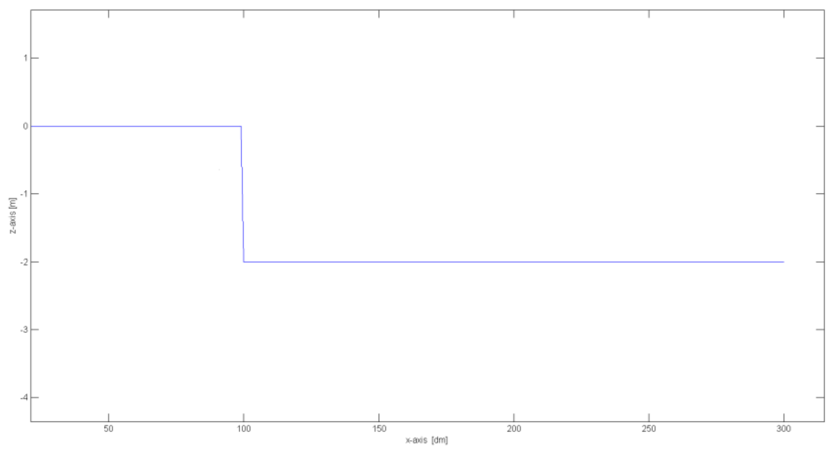

Figure 4.9: initial profile; breach height 2m

Physical constants	Value
D_{50}	0.0002 [m]
f_0	0.032 [-]
g	9.81 [m/s^2]
k_1	0.0003 [m/s]
n_0	0.3[-]
Δx	0.1 [m]
Δt	0.01 [sec]
ρ_s	2650 [kg/m^3]
ρ_w	1000 [kg/m^3]
φ	32 [°]

Table 4.1: constants

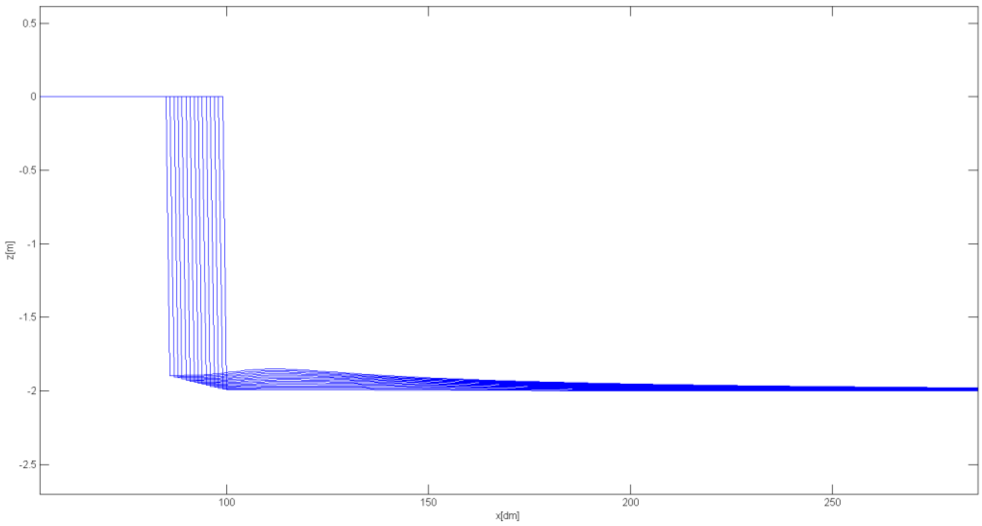

Figure 4.10: breach height 2m, profile 5 min

Variable Parameters	Value
Input	
c_0	0.064 [-]
d_0	0.11[m]
Fr	2.9[-]
H_0	2 [m]
u_0	0.96 [m/s]
v_{wall}	0.005 [m/s]
β	0[°]
$\rho_{m,0}$	1106 [kg/m^3]

Table 4.2: variable parameters, breach height 2m

Figure 4.10 shows the retrogressive breach at 0.005 m/s with associated parameters (table 4.2). Each line represents an update of the profile after 20 sec. The initial breach height of 2m has decreased after 5 min by 0.1 m, which also decreases the initial parameters u , d and ρ_m . Because of the horizontal slope the sediment settles close to the breach. If the initial breach height decreases to 1 m, the breach height decreases even more in time and the initial parameters decrease likewise. This result is in line with Eke et al. (2011). We call this 'nabressen'. The critical breach height is about 2.49m, which means that the breach height remains the same when it retrogrades. Sedimentation directly at the toe of the breach occurs with smaller values. When the breach is high enough, or the slope steep enough, or the sand fine enough, erosion will take place (figure 4.11 and table 4.3).

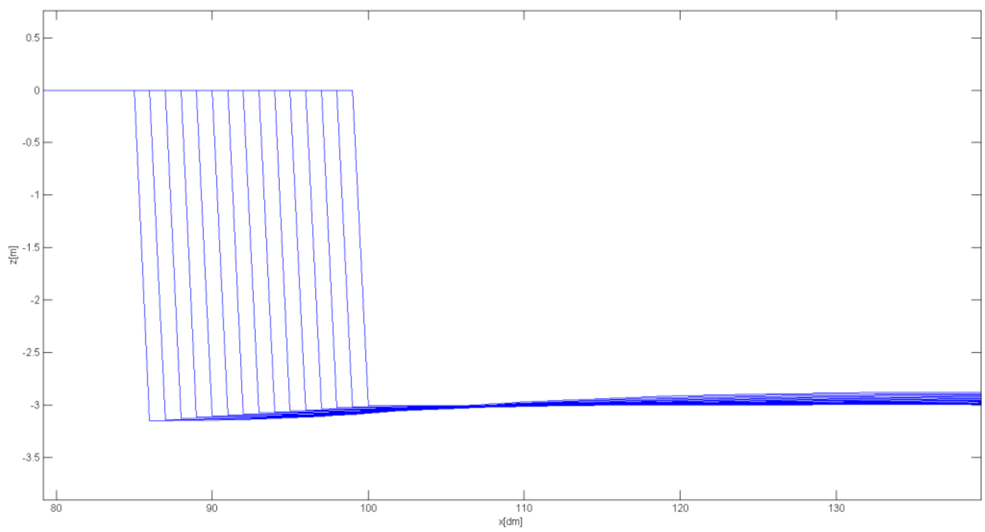

Figure 4.11: breach height 3m; profile 5 min

Variable Parameters	**Value**
Input	
c_0	0.055 [-]
d_0	0.168 [m]
Fr	3.0[-]
H_0	3 [m]
u_0	1.106 [m/s]
v_{wall}	0.005 [m/s]
β	0[°]
$\rho_{m,0}$	1092 [kg/m^3]

Table 4.3: variable parameters, breach height 3m

4.4.2 RESULTS OBLIQUE SLOPES

The slope downstream of the breach is important for sediment to accelerate and induce turbidity current. Thereby is it important to see at what critical slope angle erosion feed the turbidity current and lead to steeper slopes downstream of the initial breach. In appendix A, the initial breach height is varied from 1 to 3.5m and slope angles from $0° - 30°$ are shown. The initial parameters are shown in table 4.4. The first important aspect is the breach height. If the breach height is below the 3.5m, even if the downstream slope is horizontal, the breach decreases in time (appendix A: figure A.1, A.4 and A.7) and slowly retrogrades upstream with constant velocity ($v_{wall} = 0.0027\ m/s$). Each plotted line represents the development of the breach in 37 seconds. If the slope increases to 18° still no erosion takes place at the toe of the breach (figure A.2.2). This early sedimentation (which is based on the hindered settling equation of chapter 2.3.2) is not present if there is a slope angle of 30°. The bed level decreases about 0.05m, which is small but can be explained by a small breach height. By increasing the breach height a smaller slope angle is required for erosion. A lower bed level of 0.1m already occurs by using a breach height of 2m with a 10° slope angle. By further increasing the slope angle the bed level decreases from 0m to -0.7m and within 80m from the breach there is still no sedimentation (figure A.6)

When the breach height is modelled to 3.5m, including a slope angle of 10°, the erosion directly near the breach may cause problems (figure 4.12). The hole is about 2m deep and despite of the decreasing breach height it is expected that the breach retrogrades over a large distance. The sediment remains in suspension and does not settle within 20 meters. Increasing the downstream slope leads to severe erosion.

parameters	**Value**
D_{50}	0.00025 [m]
H_0	1-3.5 [m]
k_1	0.000193 [m/s]
n_0	0.38[-]
v_{wall}	0.0027 [m/s]
β	0-30[°]

Table 4.4: parameters oblique slopes

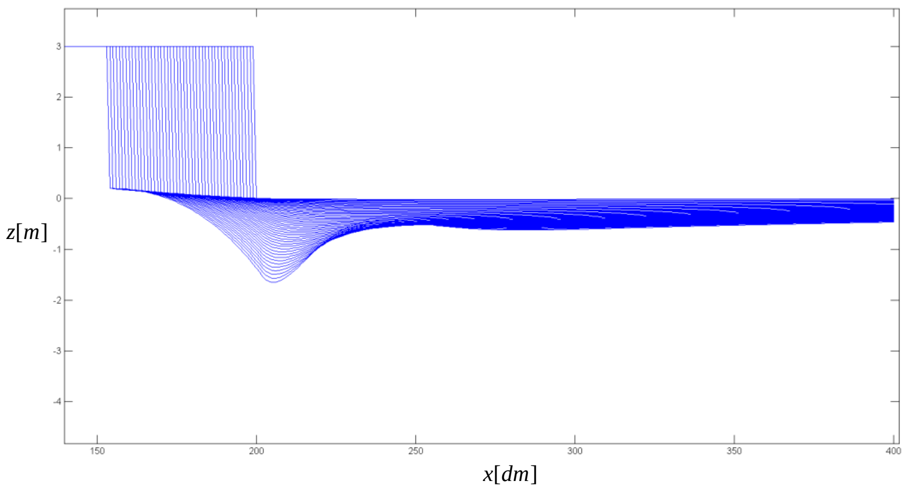

Figure 4.12: breach height 3.5m, beta 10°

4.4.3 RESULTS WALL VELOCITY

The left boundary is coupled to the wall velocity. When the wall velocity is reduced by 0.002 m/s, the initial velocity of the flow and the initial density, decreases. However, when the breach has reached the same location as in figure 4.10, the sediment has settled closer to the breach compared to a wall velocity of 0.005 m/s (figure 4.13), in which each line represents the development of the breach in 20 seconds.

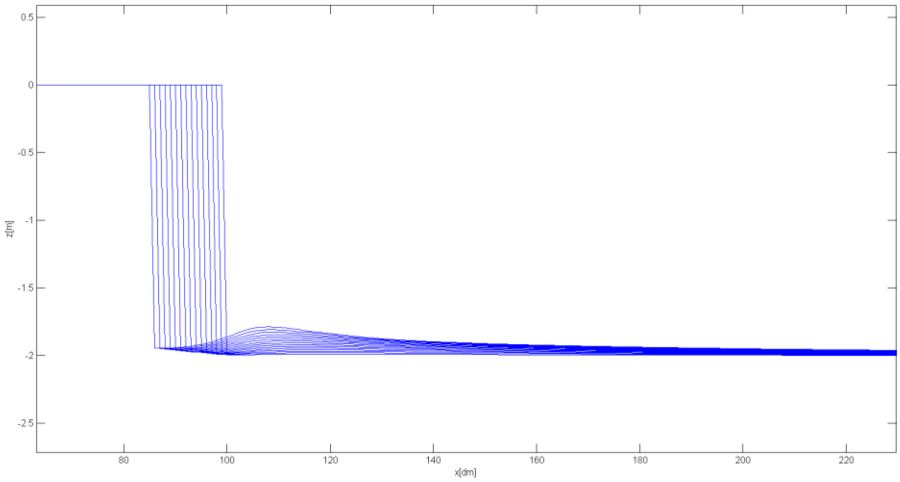

Figure 4.13: breach height 2m, wall velocity 0.002m/s

4.4.4 RESULTS BED FRICTION COEFFICIENT

A comparison of the numerical results shows that as the bed friction coefficient increases from 0.001 to 0.05 the turbidity current changes from acceleration with decrease in thickness (from 0.11 to 0.05) (figure 4.14) to acceleration with almost equal thickness along the slope.(figure 4.15). But friction (bed shear stress) has also an effect on the erosion.

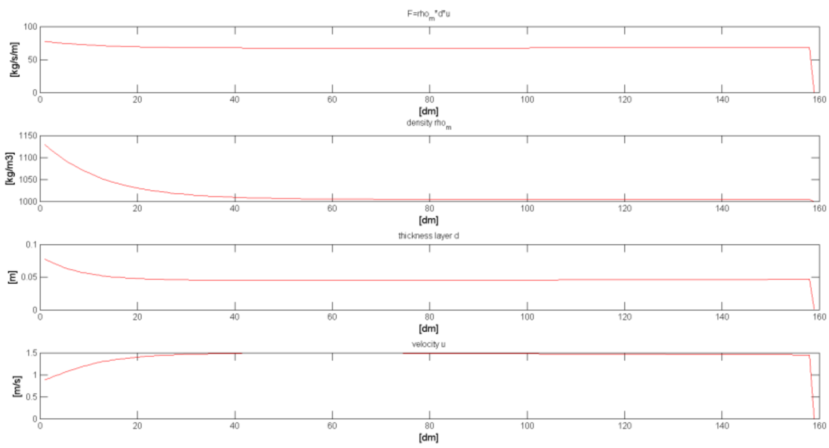

Figure 4.14: breach height 2m, bed friction 0.001

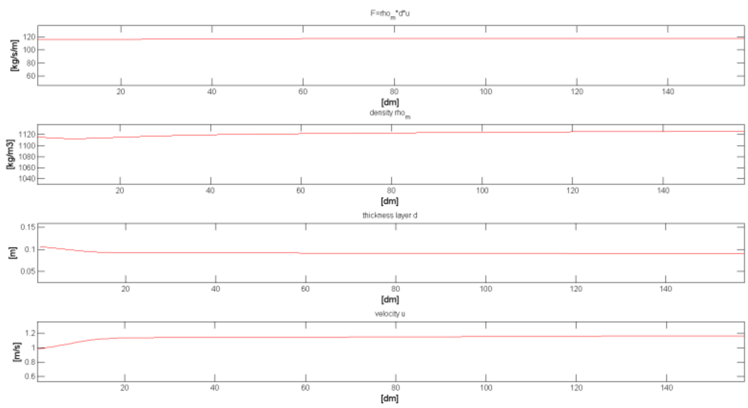

Figure 4.15: breach height 2m, bed friction 0.05

Downstream the current with the higher bed friction remains the same, whereby the lower bed friction loses its grains much faster. This result is comparable to Eke et al. (2011), whereby the breach height was 5m instead the used 2m in this model.

4.4.5 INITIAL CONDITIONS

For simplification the water entrainment of vertical breach is considered to be constant. The water entrainment downstream is however dependant on velocity and the internal Froude number. The maximum of 0.075[-] therefore, might be an overestimation of the entrainment, because it decreases with breach height. Smaller values will impede the continuation of the retrogressive breach, because its decreases the thickness and therefore increases the density.

4.5 RETROGRADING BREACH (FIXED PARAMETERS)

The derived relations of Eke et al. (2011) are used so far to model the retrogression of the breach. However, also independent relations can be used for modelling. In this paragraph the influence of the parameters are derived separately. First the breach height is varied by applying the parameters of table 4.5. The three variables u , d and ρ_m are changed (by which the product remains constant) in order to find critical values (values at which the breach height just decreases in time (figure 4.16) in contrast with an increasing breach height, figure 4.17).

Physical constants	**Value**
D_{50}	0.00014 [m]
f_0	0.032 [-]
g	9.81 [m/s^2]
k_1	0.000256 [m/s]
n_0	0.4[-]
Δx	0.1 [m]
Δt	0.01 [sec]
ρ_s	2650 [kg/m^3]
ρ_w	1000 [kg/m^3]
φ	32 [°]

Table 4.5: constants fixed parameters

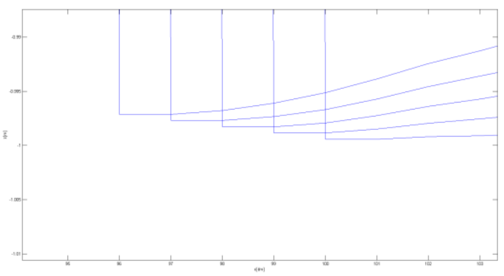

Figure 4.16: decrease in breach height

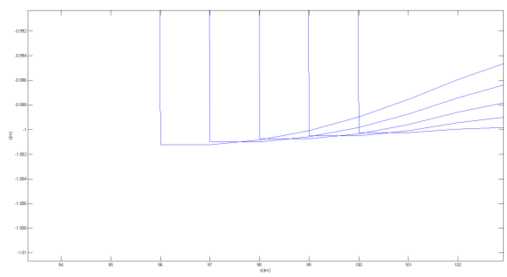

Figure 4.17: increase in breach height

If the density is imposed between $1050-1500\ kg/m^3$, variations of thickness and velocity are plotted in figure 4.18.

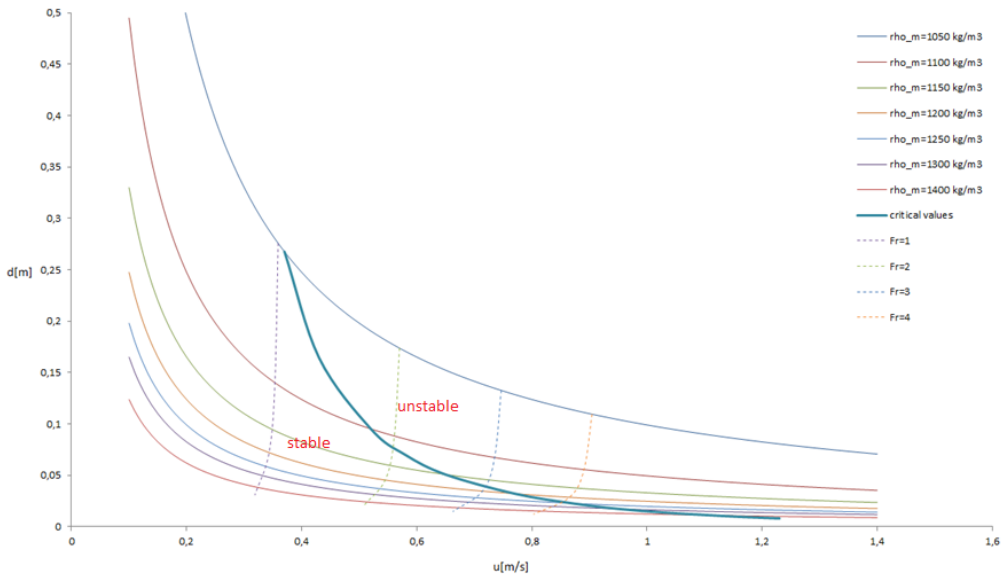

Figure 4.18: breach height 1m, wall velocity 0.005m/s, n0=0.4

Critical values at which the breach just decreases in time are also given in figure 4.18 (thick blue line). Combinations of thickness, velocity and density above the critical line cause an increase in breach height and thus provides unstable results. Below the blue line the breach height decrease and goes to zero (stable). Froude numbers 1-4 are shown by the dotted lines in figure 4.18.

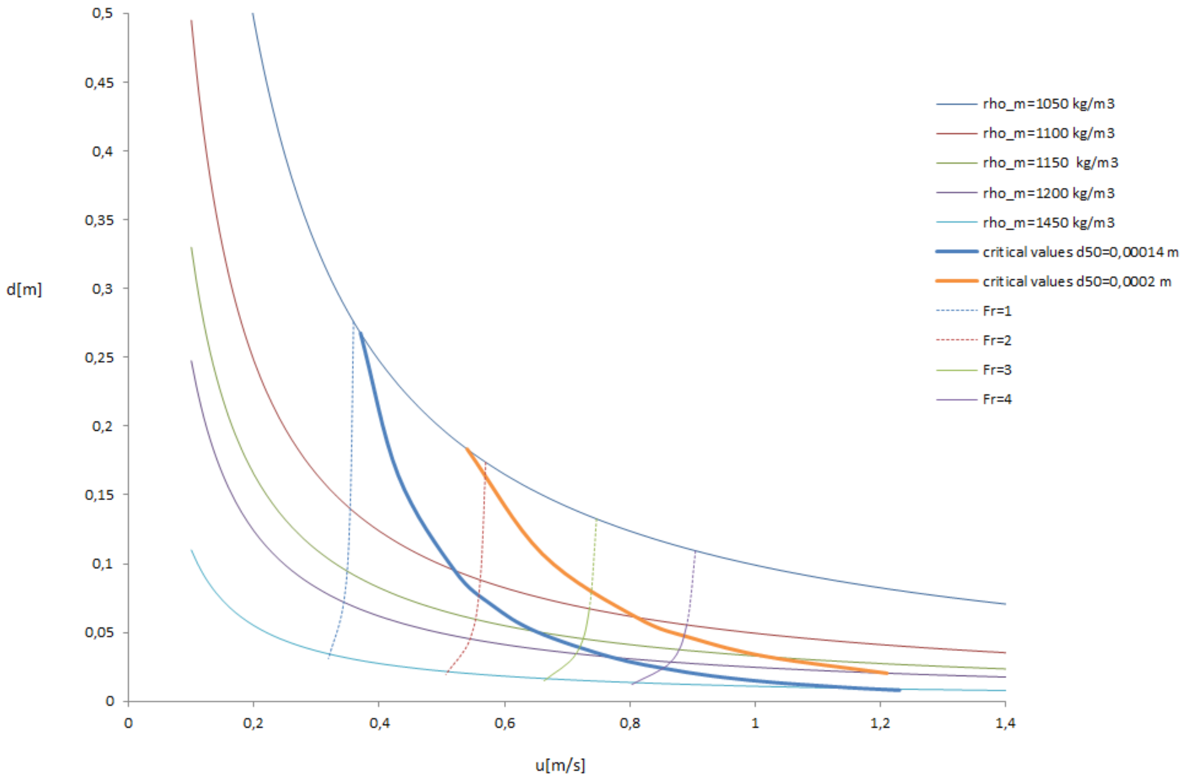

Figure 4.19: influence of d50

The influence of grain size is shown in figure 4.19. More combinations of thickness, velocity and density yield a decreasing breach height when a d50 of 200 μm is applied compared to the former used 140 μm . These results are compared to a lower value of initial porosity. More densely packed soil ($n_0 = 0.3$) leads to a wall velocity which is slower compared to loosely packed soil ($n_0 = 0.4$). In order to maintain the same amount of sediment as in figure 4.18 (product of wall velocity, concentration and breach height), the breach height is required to increase by 1.336m, which results in an initial breach height of 2.336m.

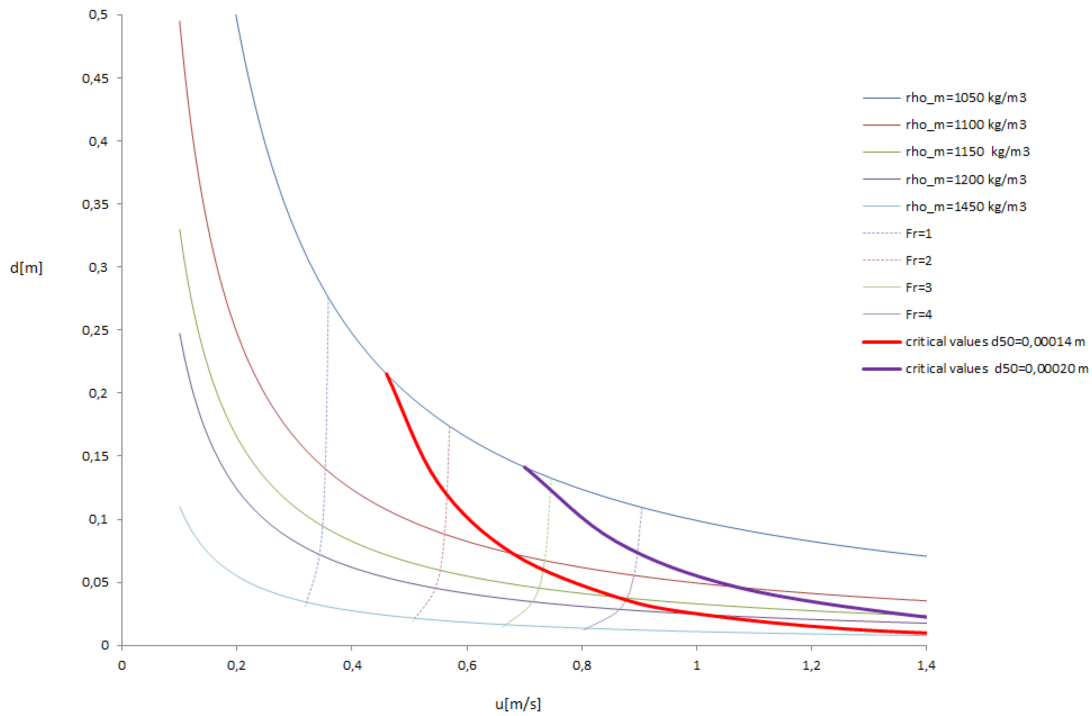

Figure 4.20: breach height 2.336m, wall velocity 0.0018m/s, n0=0.3

The critical values shift towards the right (see comparison 4.19 and 4.20), which means that more combinations of the product of thickness, velocity and density provide a decreasing breach height of the current, despite the initial breach height is more than doubled. Values with a Froude number below 2 show only decreasing breach heights when a d50 of 200 μm is applied.

When the production is doubled (from 0,003 to 0,006) , which is done by increasing the initial breach height to 2m, as expected more combinations of the initial conditions tend to show an increase in breach height (figure 4.21).

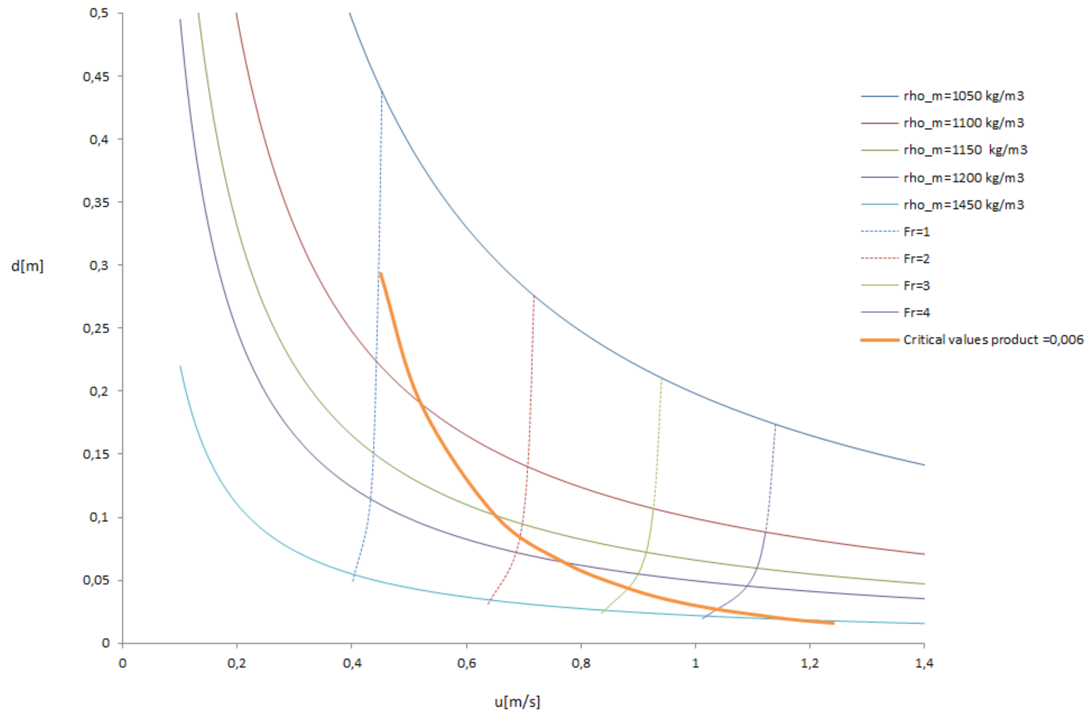

Figure 4.21: breach height 2m, wall velocity 0.005m/s, n0=0.4

The majority of possible combinations (surface between Fr=1-4 of figure 4.21) is above the critical line, which implies an increase in breach height when the breach retrogresses. With the use of these graphs it is possible see what combinations of sediment transport results in a decrease or increase in breach height for a given initial breach height, median grain size, wall velocity, porosity and permeability.

4.6 COMPARISON FIXED-VARIABLE CONDITIONS

The results of figures 4.18, 4.19 and 4.20 are combined with the initial parameters of Eke et al. (2011) as shown in 4.2.1. The transition equations are influenced by wall velocity $v_{wall}[m/s]$, porosity $n_0[-]$and breach height $H_0[m]$including the constants of water entrainment $e_w[-]$and wall friction $f_0[-]$. The red square in figure 4.22 represents the initial breach height of 1m, which provides with the initial conditions of: d =0.056 m, u =0.72 m/s and ρ_m = 1120 kg/m3. According to these transitional parameters the median grain size of 200 μm provides an decrease in breach height, in contrast to the median grain size of 140.

.

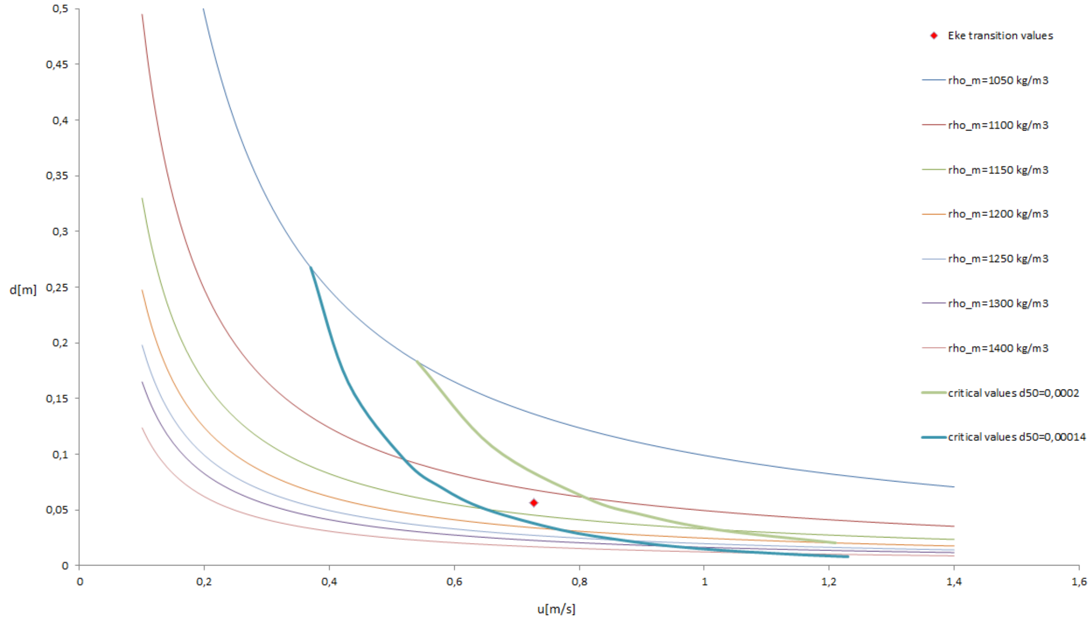

Figure 4.22: comparison transition values Eke et al., 2011, $n_0 = 0.4$

In densely packed soil with an porosity of 30%, both grain sizes provide an increase in breach height (figure 4.23).

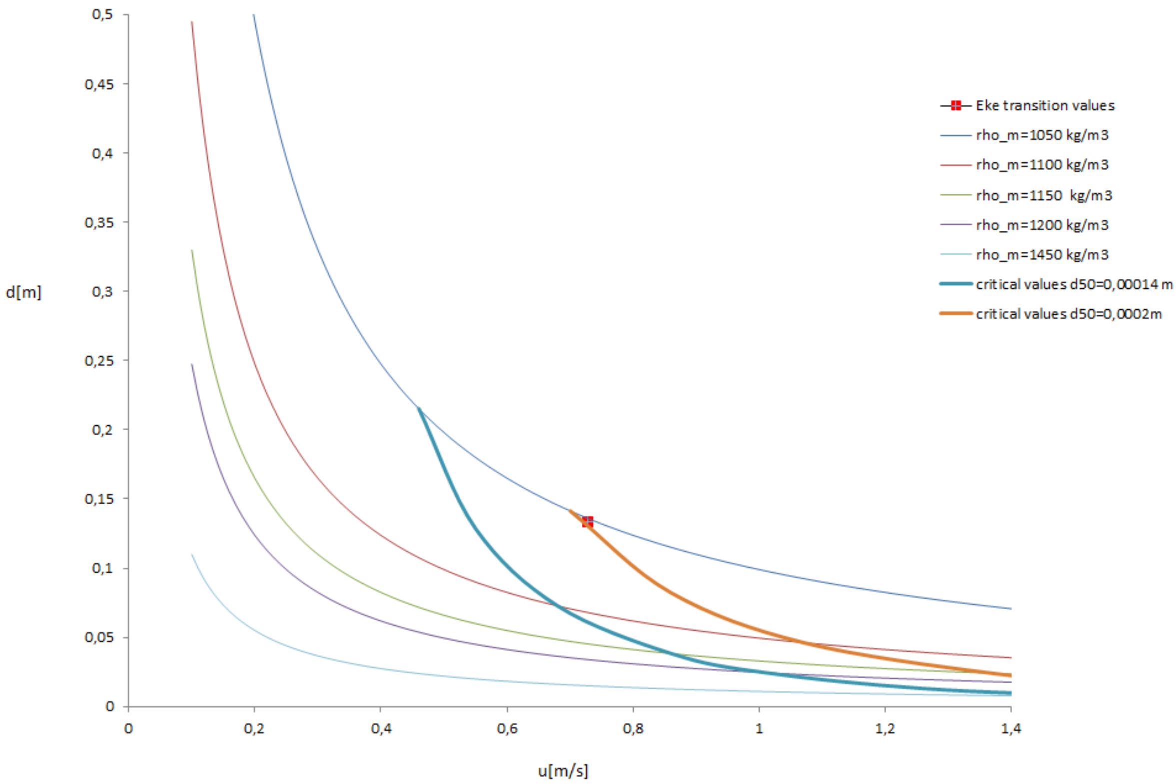

Figure 4.23: comparison transition values Eke et al., 2011; $n_0 = 0.3$

The results of several simulations provide knowledge of the sensitivity of the used parameters. The initial breach height, velocity and density of the flow are important for an increase in breach height and continuation of the breach with respect to fixed parameters and parameters depending on the development of breach height (transition equations of Eke et al., 2011).

A slower retrograding breach results in smaller values of the turbidity currents, which decreases the probability to provide an unstable breach. Sediment settles early compared to higher values of the wall velocity and therefore angle of repose is larger. However, when the amount of sediment per second is the same compared to the higher wall velocity (and thus the initial breach height needs to increase) it leads to more combinations in which the initial breach possibly decreases. In addition also the Eke's parameter (red square in figure 4.23) also differs (decrease in density and increase in thickness) and therefore the both grain sizes now lead to an increase in breach height.

4.7 CONCLUSION

The first order upwind scheme without any dissipation to avoid provide a useful model in order to simulate the first minutes of a 90 degrees slope with a certain initial breach height. By applying very small values for the velocity and thickness the initial wetting and drying problem at the start of the simulation is solved. With respect to hydraulic jumps the first order upwind simulation is not able to handle Fr<1. This is a major drawback of the model, because the sedimentation regime cannot be modelled to the point that all sediment has settled (figure 4.26). The upper limit of the internal Froude number of the initial thickness, velocity and density during simulation is high compared to the analysis of Mastbergen & Van Den Berg (2003). They proposed a criterion in which the internal Froude number cannot exceed a value of about 2.8, since they derived that in the case of strongly supercritical flows the intermediate mixing zone will dilute and the stratification would disintegrate, defined by the Richardson number. This implies that the presence of turbidity currents are quite narrow (1<Fr<2.8).

Further research should focus on the validation of the boundaries of these initial conditions in order to be able to compare the results with the transitional values of Eke et al., 2011. The variable parameters of Eke et al., 2011 are used in the next chapter in order to simulate breach flow slides.

In addition, the breach during the analysis of horizontal flows is not exactly 90°. This is a restriction of the numerical grid which is divided into $\Delta x = 0.1m$. However, because of the boundary condition immediately downstream of the breach, it does not affect the accuracy of the calculation.

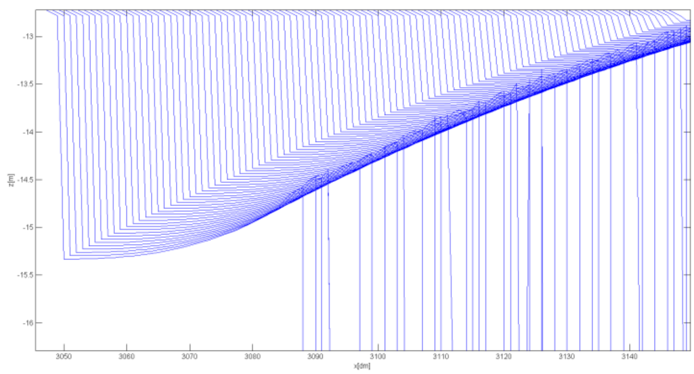

Figure 4.24: sedimentation error

CHAPTER 5

VALIDATION

In this chapter the results are compared and validated with two cases modelled with HMTurb/HMBreach and Retrobreach. HMBreach is a model designed by Deltares to simulate a turbidity current in time initiated by a certain breach. The 1D steady state two-layer model is able to calculate the equilibrium bottom slope iteratively. An extension of HMBreach is HMTurb which uses a fixed bottom slope per layer. HMBreach is used for predictive analysis of unprotected submerged sandy slopes for dredging purposes and for stability analyses for levees. Retrobreach is a parameterized model, based on HMTurb calculations, with four distinct phases and provides a descriptive prediction of the breach retrograding.

5.1 CASE STUDY: ROOMPOT

5.1.1 INTRODUCTION

The Roompot is part of the Oosterschelde, an estuary in Zeeland, the Netherlands. This estuary has been closed by a storm surge barrier and dam called the Oosterscheldekering. Because of this (partial) closure the water that enters the Oosterschelde during ebb and leaves during flood will flow faster than it formerly did and as a consequence more erosion will occur in the estuary.

Figure 5.1: location slope failure (Tabak 2011)

In 2004 such a flow slide occurred very close to the Oosterscheldekering on the edge of the bed protection (see Figure 5.1), during this collapse 850 000 m3 of sand was moved. This collapse was discovered from annual measurements by Rijkswaterstaat that monitors the water depth in the Oosterschelde. The profiles are shown in figure 5.2. The porosity is about $0.4[-]$. With respect to the mean grain size there are three distinct areas. Above NAP-28m the $D_{50} = 175 - 260[\mu m]$. Between NAP-28m and -33m the mean diameter is $240 - 380[\mu m]$ and below NAP-35m $170 - 220[\mu m]$ (De Groot, 2008). In between there is a clay layer, which hinders the breach to continue, but may cause a sudden increase in breach height after losing stability.

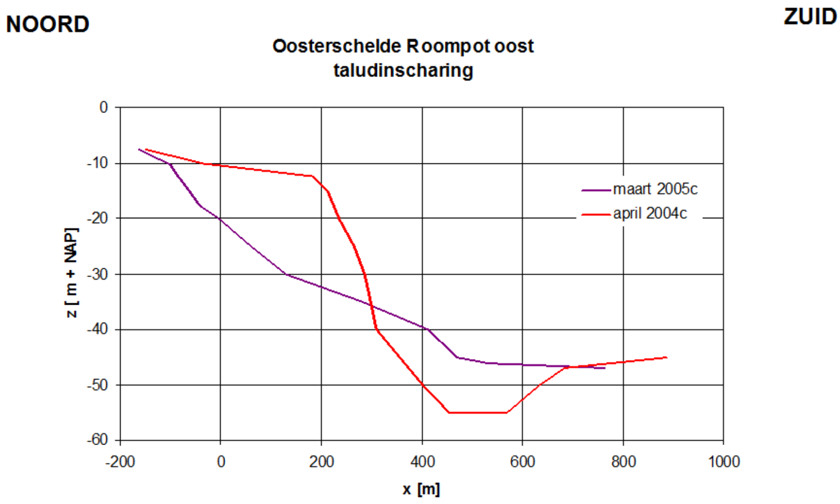

Figure 5.2: measured slope profile development Roompot (Tabak 2011)

5.1.2 VALIDATION ROOMPOT

The Roompot case is modelled with BreachFlow. The parameters are shown in Table 5.1 and the profile of the submerged slope is shown in figure 5.3.

Input	**value**
H_0	0.5 [m]
d_0	0.034 [m]
u_0	0.47 [m/s]
$\rho_{m,0}$	1198 [kg/m^3]
c_0	0.12 [-]
v_{wall}	0.005 [m/s]
n_0	0.4 [-]
β	10[°]
Fr	2[-]

Table 5.1: parameters Roompot fixed condition

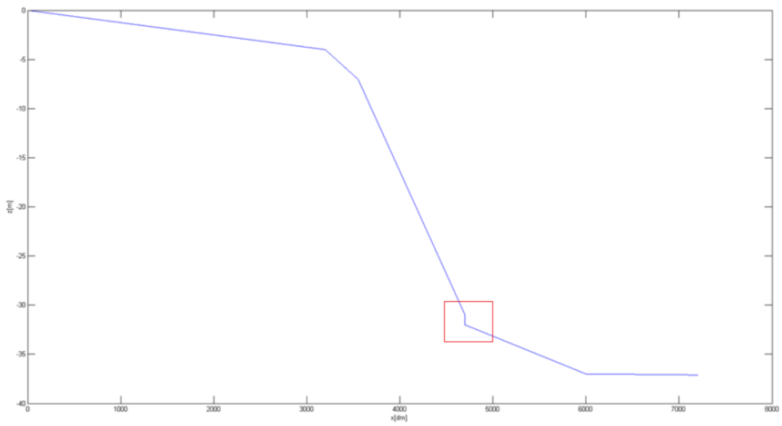

Figure 5.3: slope profile BreachFlow

The initial disturbance of 0.5m is applied at -40 m NAP (red square figure 5.3). By using the initial conditions without using the equations with respect to the left boundary the initial breach of 0.5 m decreases until after 2.3 min (0.7 m) there is no breach height left (figure 5.4). On the other hand, if the left boundary is applied by the use of the transformation formulas of the transition between sediment along the vertical breach and the transport downstream of the breach (table 5.2) the breach decreases also over time, but somewhat slower (3.3 min; 0.9m) (figure 5.5), where each line is plotted after 20 sec.

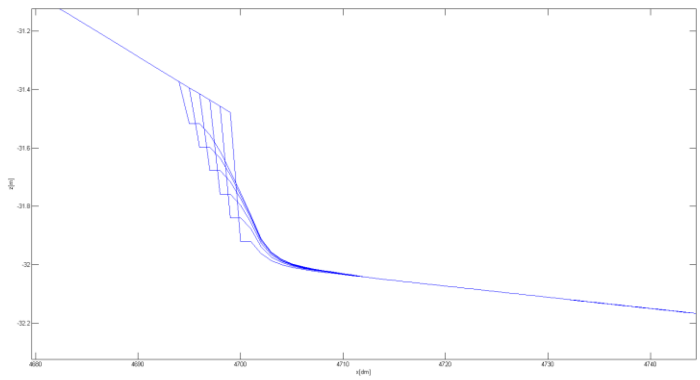

Figure 5.4: fixed initial breach conditions

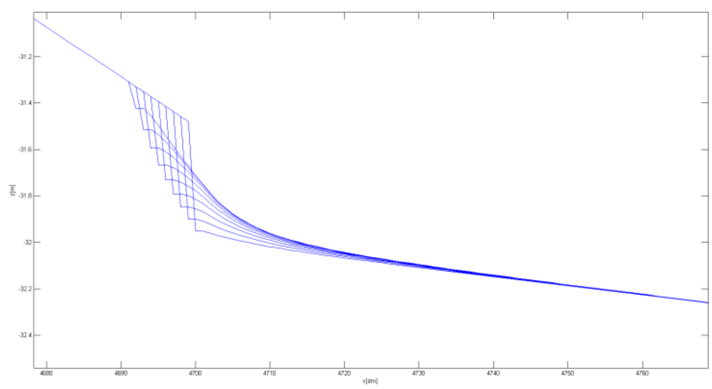

Figure 5.5: variable initial breach conditions

The velocity and density between both initial conditions cause differences in result. The higher velocity of the flow causes somewhat more sediment transport compared to the initial conditions of BreachFlow.

Variable Parameters	Value
Input	
c_0	0.108 [-]
d_0	0.030 [m]
Fr	3.0[-]
H_0	0.5 [m]
n_0	0.4[-]
u_0	0.63 [m/s]
v_{wall}	0.005 [m/s]
β	10[°]
$\rho_{m,0}$	1178 [kg/m^3]

Table 5.2: parameters Roompot, variable condition

When initial breach height is increased to 1m, it is seen form figure 5.6 that the breach continues to retrograde.

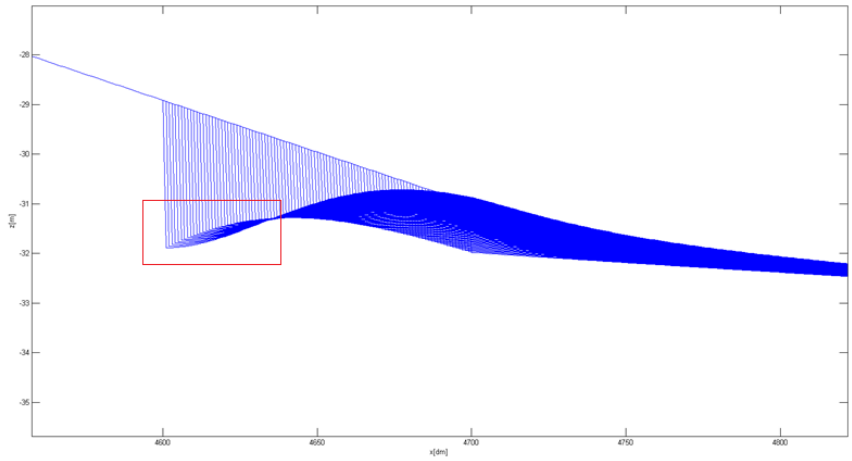

Figure 5.6: initial breach height 1m

In conclusion, according to BreachFlow the breach diminishes close to location of the initial breach. In order to show a longer retrogressive breach failure the initial breach height needs to be at least 1.0m. However, an erosive density current is not present at this breach height. In figure 5.6 it is clear to see that at the toe of the initial breach height the sediment settles directly. When the breach height has increased and likewise the initial parameters there is some erosion downstream of the breach (see red box figure 5.6), implying an increasing retrogressive breach height.

5.2.1 INTRODUCTION

In the Western Scheldt estuary, in the south-western part of the Netherlands, several flow slides of $10^5 - 10^6 [m^3]$ have occurred. Therefore, this area was chosen to be the test location of a large experiment. However, before the test was performed a large flow slide (almost $10^5 m^3$) occurred on 22nd of July 2014 (see figure 5.5). A week after the event, further activity was observed on the shoreline (Mastbergen et al., 2015). Given the occurrence of this recent failure, the test site was relocated 400 m to the east of figure 5.7. At this location, almost identical pre-failure conditions were found.

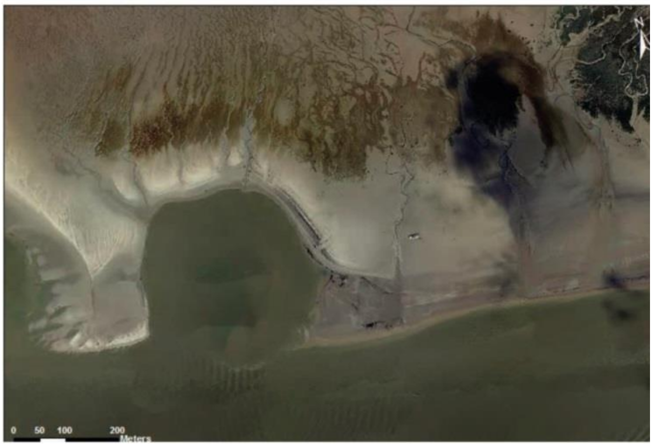

Figure 5.7: overview flow slide in the tidal flat of Walsoorden, 2014 (Van den Ham et al., 2015)

Soil investigation showed a generally uniform fine sand ($D_{50} = 140\mu m$, D_{60} / D_{10} = 1.5) with low clay content. In figure 5.8 the development of the slope is given. From experience it was predicted flow slides may occur spontaneously in fine sand with slope of at least 1:3 over a height of at least 5m and a total of 15m (Mastbergen et al. 2015). There are two distinct layers. A certain amount of sand is dredged at -8m N.A.P over a depth of 5m.

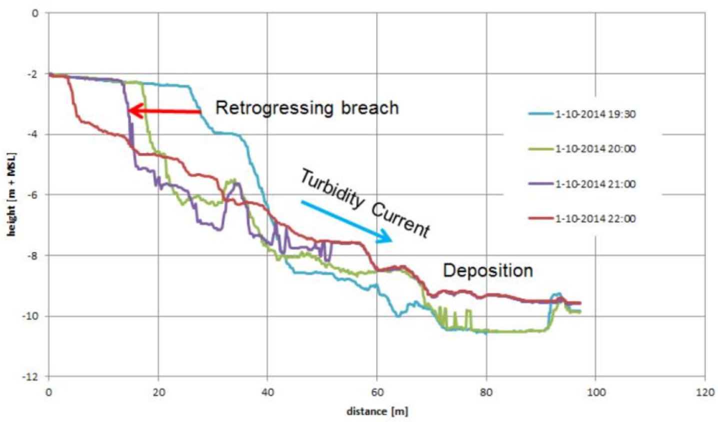

Figure 5.8 Breach flow development at Walsoorden, 2014 (Mastbergen et al., 2015)

Despite of the uncertainty of the occurrence of a pure breach slide, which causes fluctuations in retrogression velocity (figure 5.8), a constant wall velocity is applied. By applying D_{50} = 140 μm under assumption of $n_0 = 0.4[-]$ and $k_1 = 0.000193[m/s]$, a wall velocity of $0.0038[m/s]$ is found. When the initial boundary conditions are fixed, by using $d = 0.05[\mathrm{m}]$ $u = 0.45[m/s]$ and $\rho_m = 1100[kg/m^3]$ the breach slowly retrogrades by a decreasing breach height (figure 5.9)

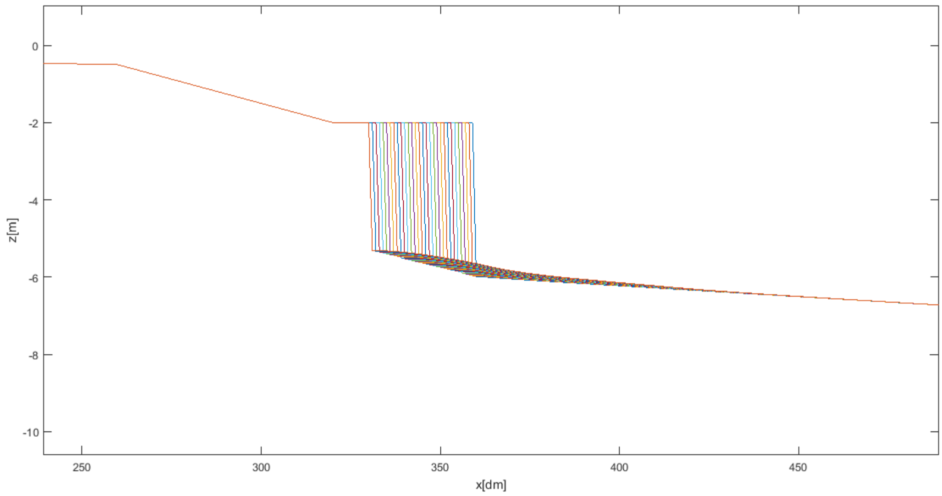

Figure 5.9: development breach with fixed parameters

By using the transition equation of Eke et al. (2011) the breach now grows in time (figure 5.10), because the modelled initial velocity and thickness are larger $d = 0.22[\mathrm{m}]$ and $u = 1.05[m/s]$. The density decreases to $\rho_m = 1063[kg/m^3]$.

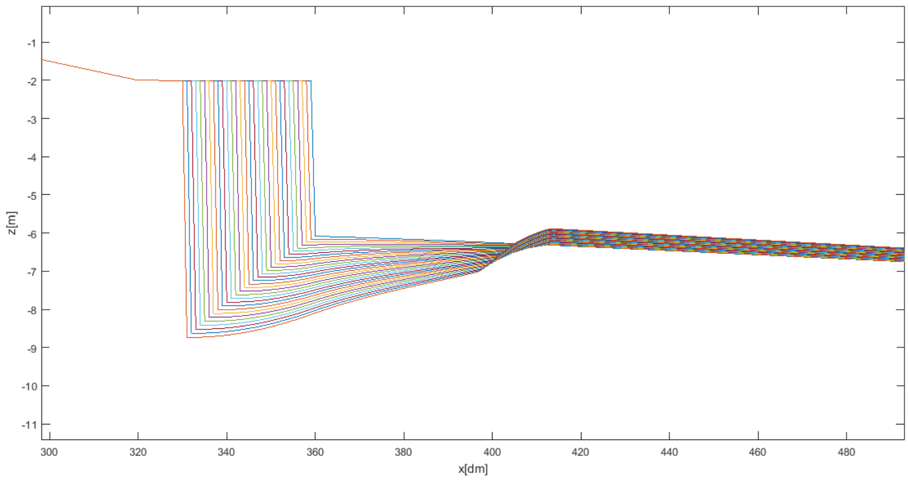

Figure 5.10: development breach with variable parameters

The measured profile shows a decreasing breach height in time, which is in agreement with the run with fixed parameters.

Because the actual initial breach has a milder slope than 90 ° , there are two options to compensate for this error. The first option is to reduce the initial breach height. By reducing it from 4 m to 2.5m the development is shown in figure 5.11.

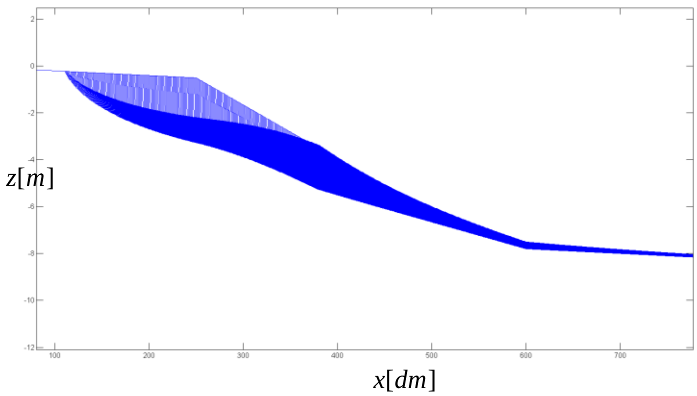

Figure 5.11: result BreachFlow, reduced breach height

The second option is to modify the transition equations (see chapter 4.2.1). The initial velocity needs to be smaller in order to show a decrease in breach height. Because of the slope of the breach, compared to the prediction of Eke et al. (2011) the velocity is probably overestimated. In order to show a decrease in breach height the velocity is reduced by a factor 3. The result of the reduced parameter by BreachFlow is shown in figure 5.12.

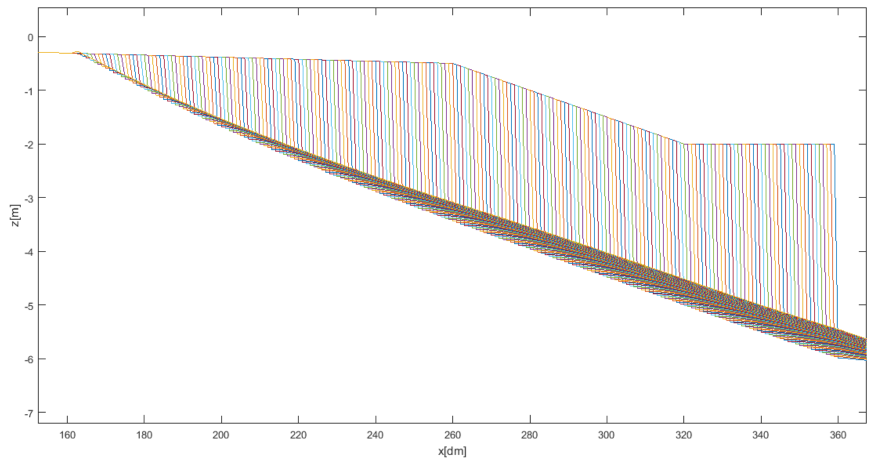

Figure 5.12: result BreachFlow, reduced velocity

This flow slide is also modelled with Retrobreach (predicted) and provides a prediction of the retrogressive length when pure breaching is applied (figure 5.13). This prediction is however less accurate because the actual initial profile is not known in detail.

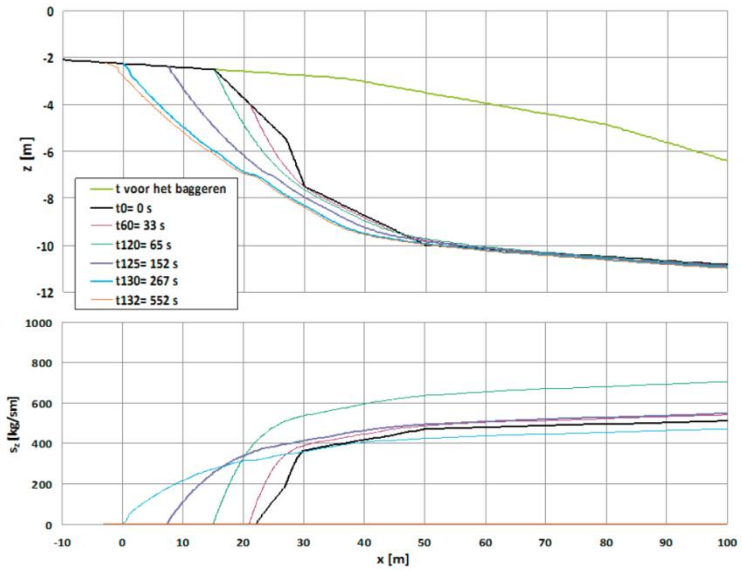

Figure 5.13: result Retrobreach

With respect to the actual measured length of the breach flow, the post diction of BreachFlow is quite accurate, however the location of the sedimentation did not agree, implying the sand transport was predicted too high. The location of sedimentation is however more accurately modelled in BreachFlow compared to the pre-diction of Retrobreach.

5.3 CONCLUSION

When there is no net erosion present and grains start to settle, it is seen in BreachFlow that the increase in slope angle just downstream of this sedimentation can initiate new erosion (figure 5.4). This feature is also recorded during experiments and explains the presence of alternating bed forms.

Both cases show the thin boundary between erosion at the toe of the breach, which lead to higher breach heights, and direct sedimentation. In BreachFlow it is assumed that the breach is vertical (rotated x-axis) and its wall velocity is located at the breach top. Therefore, no retrogressive breach was found in modelling the Roompot case when 0.5 m was applied. A breach height of 1m was necessary to initiate an increase in breach height, although no initial erosion was present downstream the breach.

Just like the Roompot Case, the in-situ experiment at the tidal flat of Walsoorden shows also only steep slopes (1:3). Therefore the accompanied breach height needs to be corrected in order to use the transition equations by Eke et al. (2011). The result of figure 5.11 and 5.12 shows the post-diction of the entire breaching process. Both runs show an underestimation of the retrogressive length. With respect to the sedimentation the reduced breach height simulation shows more sedimentation close to the breach compared to the reduced velocity. The measured profile is between both simulations.

BreachFlow is able to give a prediction when there is a certain (vertical) breach height. However, more research is required to provide accurate relations between the thickness, velocity and density falling down from the breaching front and the incoming boundary condition, which are the initial parameters of the model. The formulations of Eke et al. (2011) provide an overestimation of the amount of erosion near the beach front. More research should focus on whether a reduction of this relationship is a good way to compensate for this overestimation.

CHAPTER 6

CONCLUSION

The main objectives in this study was to set-up and improve a schematized 1D model that give predictions for the retrogression length of a breach flow slide.

To reach this objective we have attempted to answer the following questions:

1. Which mechanisms are involved when breach flow slides occur?
2. What set of equations can be used for 1D (unsteady state) modelling?
3. How to implement our findings in a numerical model?
4. How do the results match previous 1D models?

6.1 MECHANISMS

Dilatancy provides temporary stability, if due to a specific trigger the slope of submerged soil is steeper than internal friction. If the drop in pore pressure does not suffice, soil loses its stability and large volumes moves downstream in seconds. More densely packed soil induces larger drops in pore pressure and thereby slowly loses grains which fall downwards and (may) entrain water, during acceleration. This current can be quite strong and enhances the entrainment of particles at the bottom (erosion). This erosion is hindered by the same mechanism as the retrogressive breach, when the flow velocity is high. When slope angle decreases, sediment settles and eventually the flow loses all its particles. Due to hindered settling this can be far downstream and thereby the final slope angle can be gentle, which is shown during experimental studies. The initial breach height is thought to be limited, because the weight of the soil increases by breach height and therefore may lose its stability at an earlier moment. Therefore it is suggested that constant breaching is replaced by alternation of sliding and breaching, as described by (You et al., 2014). Larger volumes of soil suddenly lose their stability and result in higher velocities, thickness and density.

6.2 EQUATIONS

The expressions used in BreachFlow to model breach flows comprise three flow parameters (thickness, velocity and density), initial breach height and pre-specified soil properties. The continuity of sediment/water mixture and the continuity of solely sediment, and the momentum equation along slopes form the framework of the model. In HMBreach the continuity of sediment and water are derived separately and the concentration instead of the density is taken as a variable. BreachFlow is non-stationary, in contrast to HMBreach, since the objective was to compute the retrogression length.

The pressure term of the momentum equation depends only on the change in thickness of the current. However, if the pressure gradient is integrated over the depth by using a linear distribution (hydrostatic pressure assumption) the change in pressure due to the change in bed level is also included in the equation (1D depth averaged model).

6.3 NUMERICAL IMPLEMENTATION

A first order upwind scheme was developed for modelling. The model is however restricted because of the absence of any dissipative term. Transition between super- and subcritical flows provide too many fluctuations between two grid cells. This instability hinders continuation of the flow along slopes and makes it impossible to see under what angle the sediment finally settles. However, the entire erosion part is modelled and provides accurate results of a certain breach. Therefore the super-critical onset of the flow is modelled in detail and provides information of the retrogressive impact of the breach.

6.4 VALIDATION

In order to provide an accurate validation, BreachFlow has to be further improved. Critical is the transition between super- and subcritical flows. Up to now, the location of sedimentation can be observed but lacks the development of the settlement of grains. Therefore the slope angle cannot be calculated.

At the beginning of the breach flow, the changing breach height provides a first indication about the development in time. When larger amounts of sand fall down and entrains more water and sediment downstream, it amplifies the flow. However, the location where turbidity current loses it strength because of decreasing slopes is also important. Sediment carried far away from the breach decreases the final slope and has a negative impact on the retrogressive length.

The calculations in BreachFlow are based on a vertical transition between the breach face and the slope downstream. This provides a difference of the initial values because in this case the actual slope is 1:3. A closer look at this transition is required to be able to see how initial sand transport varies between different breach slopes. In BreachFlow the transitional parameters of Eke et al., 2011 are used, but results from simulations of fixed parameters show that the model is sensitive to other ratios of thickness, velocity and density.

Despite of the shortcomings of BreachFlow, it is a promising first step in order to predict retrogressive length of a breach flow. Instead of using the transport of sand, which is used in Retrobreach, this parameter is replaced by three flow variables. With respect to calculations, the numerical model has the advantage that all parameters can be changed rather easy, including the profile, which favours the usability.

6.5 RECOMMENDATIONS

6.5.1 NUMERICAL SCHEME

The first gain can be achieved by implementing a higher order scheme in order to handle shocks and discontinuities around hydraulic jumps (Li et al. 2013). An appropriate scheme might be the one of MacCormack (MacCormack, 1969), which is a second-order explicit scheme in time and space (appendix B). The MacCormack scheme is a so-called two-step ‘predictor-corrector’ scheme. The predictor step is first order accurate in space, which is unstable for positive propagation of internal waves. The corrector step is first order backwards in space and unstable for negative celerity. Overall, in combination both steps are second order accurate in space, and should yield stable results.

A second option is the use of an implicit scheme. Implicit methods require iteration to converge to stable solutions, which negatively affects computational efficiency. In addition, the use of a shock-capturing technique is also required to conserve mass and momentum at locations of shocks (appendix C). The complex expressions requires more effort in modelling, it however improves the model extensively and is therefore recommended besides the second order explicit scheme as first recommendation.

6.5.2 MODELLING PARAMETERS

In all simulations the expression for high erosion rates or fine sand with relatively low permeability is used, which is known as hindered erosion. Although, when the flow velocity has decreased extensively away from the breach, the classical formulation (Mastbergen & Van Den Berg, 2003) might be more accurate instead of the hindered erosion due to dilatancy effects (equation 2.2.2). Second, the wall velocity is considered to be constant throughout the entire breaching process. In-situ differences in soil (density, grain size and permeability) provide fluctuation of this wall velocity, and may even induce alternation between breaching and sliding. This is also important when further research is done to provide more information about the distribution of the sediment at the incoming boundary. Further, it is recommended to implement different soil layers, when it provides more accurate information regarding the effect of the wall velocity. It also will be possible to implement very large wall velocities, simulating liquefaction of loose layers. Third, the model uses the $D_{50}[mm]$ and thereby is restricted in modelling the effects of various grain size distributions. The role of fines is thought to be important for the turbidity current in maintaining its property. (Salaheldin, Imran, Chaudhry & Reed (2000). Therefore any modelling tends to underestimate the impact of currents, when using a constant $D_{50}[mm]$.

6.5.3 3D EFFECTS

When the 1D result provides accurate results and the model is able cope with large fluctuations in profile and hydraulic jumps the next step is to transform the model into 2D. In Mastbergen (2009) there is already an extension of the HMBreach model including the width. In addition, there are already other 2D models for modelling turbidity currents (Georgoulas, Angelidis, Panagiotidis & Kotsovinos, 2010; Kostic &Parker, 2006; Groenenberg, 2007), but none of them is coupled to retrogressive breach failure.

BIBLIOGRAPHY

Akiyama, J., & Fukushima, Y. (1985). SAFHL, Univ. of Minnesota, Ex.

Been, K., & Jefferies, M. G. (1985). A state parameter for sands. *Geotechnique*, *35*(2), 99-112.

Been, K., Jefferies, M. G., & Hachey, J. (1991). The critical state of sands. *Geotechnique*, *41*(3), 365-381.

Beinssen, K., Neil, D.T. and Mastbergen, D.R. (2014), Field Observations of Retrogressive Breach Failures at Two Tidal Inlets in Queensland, Australia, Australian Geomechanics. 49, 3, 55-63

Beinssen, K., & Neil, D. T. (2015, July). Retrogressive Breach Failure Events at Amity Point, Australia and their Interaction with Built Defences. In *The Twenty-fifth International Offshore and Polar Engineering Conference*. International Society of Offshore and Polar Engineers.

Bisschop, F., Visser, P., van Rhee, C., & Verhagen, H. J. (2011). Erosion due to high flow velocities: a description of relevant processes. *Coastal Engineering Proceedings*, *1*(32), sediment-24.

Bolton, M. D. (1986). The strength and dilatancy of sands. *Geotechnique*, *36*(1), 65-78.

Boussinesq, J. (1877). *Essai sur la théorie des eaux courantes* (Vol. 2). Imprimerie nationale.

Bradford, S. F. (1996). *Numerical modeling of turbidity current hydrodynamics and sedimentation*. University of Michigan.

Breusers, H. N. C. (1974). Suction of sand. *Bulletin of the International Association of Engineering Geology-Bulletin de l'Association Internationale de Géologie de l'Ingénieur*, *10*(1), 65-66.

Brownlie, W. R. (1981). *Compilation of alluvial channel data: laboratory and field* (p. 37). California Institute of Technology, WM Keck Laboratory of Hydraulics and Water Resources.

Cartigny, M. J., Postma, G., van den Berg, J. H., & Mastbergen, D. R. (2011). A comparative study of sediment waves and cyclic steps based on geometries, internal structures and numerical modeling. *Marine Geology*, *280*(1), 40-56.

Cesare, G. D., Schleiss, A., & Hermann, F. (2001). Impact of turbidity currents on reservoir sedimentation. *Journal of Hydraulic Engineering*, *127*(1), 6-16.

Choi, S. U., & Garcia, M. H. (1995). Modeling of one-dimensional turbidity currents with a dissipative-Galerkin finite element method. *Journal of Hydraulic Research*, *33*(5), 623-648.

CUR Aanbeveling 113, Oeverveiligheid bij zandwinputten, CUR, Gouda (2008)

Coleman, J. M. (1969). Brahmaputra River: channel processes and sedimentation. *Sedimentary Geology*, *3*(2), 129-239.

De Groot, M. B., (2008). Zettingsvloeiing bij ontgrondingskuil Oosterscheldekering, Deltares, versie september, 2008

De Groot, M. B., (2014). HMBreach/Retrobreach modellering inscharing. Deltares, memo 1207813-009-GEO-0006, versie december 2014.

De Koning, J. (1970). Neue Erkenntnisse beim Gewinnen und Transport von Sand im Spülproject Venserpolder. *VDI TagungBauen Im Ausland*, 1-9.

Di Cristo, C., Iervolino, M., & Vacca, A. (2006). Linear stability analysis of a 1-D model with dynamical description of bed-load transport. *Journal of Hydraulic Research*, *44*(4), 480-487.

Eke, E., Viparelli, E., & Parker, G. (2011). Field-scale numerical modeling of breaching as a mechanism for generating continuous turbidity currents. *Geosphere*, *7*(5), 1063-1076.

Garcia, M., & Parker, G. (1991). Entrainment of bed sediment into suspension.*Journal of Hydraulic Engineering*, *117*(4), 414-435.

Georgoulas, A. N., Angelidis, P. B., Panagiotidis, T. G., & Kotsovinos, N. E. (2010). 3D numerical modelling of turbidity currents. *Environmental fluid mechanics*, *10*(6), 603-635.

Groenenberg, R. M. (2007). *Process-based modelling of turbidity-current hydrodynamics and sedimentation*. TU Delft, Delft University of Technology.

Kamphuis, J. W., Davies, M. H., Nairn, R. B., & Sayao, O. J. (1986). Calculation of littoral sand transport rate. *Coastal engineering*, *10*(1), 1-21.

Kostic, S., & Parker, G. (2003). Progradational sand-mud deltas in lakes and reservoirs. Part 1. Theory and numerical modeling. *Journal of Hydraulic Research*, *41*(2), 127-140.

Kostic, S., & Parker, G. (2006). The response of turbidity currents to a canyon–fan transition: internal hydraulic jumps and depositional signatures. *Journal of Hydraulic Research*, *44*(5), 631-653.

Lambe, T. W., & Whitman, R. V. (1969). Soil Mechanics, 553 pp.

Lesser, G. R., Roelvink, J. A., Van Kester, J. A. T. M., & Stelling, G. S. (2004). Development and validation of a three-dimensional morphological model. *Coastal engineering*, *51*(8), 883-915.

Li, W., Vriend, H. J., Wang, Z., & Maren, D. S. (2013). Morphological modeling using a fully coupled, total variation diminishing upwind-biased centered scheme. *Water Resources Research*, *49*(6), 3547-3565.

Mastbergen, D. R., & Van Den Berg, J. H. (2003). Breaching in fine sands and the generation of sustained turbidity currents in submarine canyons. *Sedimentology*, *50*(4), 625-637.

Mastbergen, D. R. (2009). Oeverstabiliteit bij verdieping waterbodems: Rekenmodel HMBreach, Delft Cluster, DC 04 43 11

Mastbergen, D.R., Van den Ham, G., Cartigny, M., Koelewijn, A., de Kleine, M., Clare, M., Vellinga, A. (2015). Multiple flow slide experiment in the Westerschelde Estuary, the Netherlands. *Submarine Mass Movements and Their Consequences, 7th Int. Symp.,* Wellington: Springer

Meijer, K. L., & van Os, A. G. (1976). Pore pressures near moving underwater slope. *Journal of the Geotechnical Engineering Division*, *102*(4), 361-372.

Parker, G., Fukushima, Y., & Pantin, H. M. (1986). Self-accelerating turbidity currents. *Journal of Fluid Mechanics*, *171*, 145-181.

Pratson, L. F., Ryan, W. B., Mountain, G. S., & Twichell, D. C. (1994). Submarine canyon initiation by downslope-eroding sediment flows: evidence in late Cenozoic strata on the New Jersey continental slope. *Geological Society of America Bulletin*, *106*(3), 395-412.

Perng, A. T. H., & Capart, H. (2008). Underwater sand bed erosion and internal jump formation by travelling plane jets. *Journal of Fluid Mechanics*, *595*, 1-43.

Reynolds, O. (1885). Lvii. on the dilatancy of media composed of rigid particles in contact. with experimental illustrations. *The London, Edinburgh, and Dublin Philosophical Magazine and Journal of Science*, *20*(127), 469-481.

Richardson, J. F., & Zaki, W. N. (1954). The sedimentation of a suspension of uniform spheres under conditions of viscous flow. *Chemical Engineering Science*, *3*(2), 65-73.

Rowe, P. N. (1987). A convenient empirical equation for estimation of the Richardson-Zaki exponent. *Chemical Engineering Science*, *42*(11), 2795-2796.

Salaheldin, T. M., Imran, J., Chaudhry, M. H., & Reed, C. (2000). Role of fine-grained sediment in turbidity current flow dynamics and resulting deposits. *Marine Geology*, *171*(1), 21-38.

Sawyer, D. E., Flemings, P. B., Dugan, B., & Germaine, J. T. (2009). Retrogressive failures recorded in mass transport deposits in the Ursa Basin, Northern Gulf of Mexico. *Journal of Geophysical Research: Solid Earth (1978–2012)*, *114*(B10).

Simon, A., & Rinaldi, M. (2000). Channel instability in the loess area of the Midwestern United States.

Sokolnikoff, I. S., & Redheffer, R. M. (1966). Mathematics of physics and modern engineering. *New York: HcGraw-Hill*.

Spiegel, E. A., & Veronis, G. (1960). On the Boussinesq approximation for a compressible fluid. *The Astrophysical Journal*, *131*, 442.

Tabak, F. (2011) Analysis of Breach Flow Slides with HMBreach, Deltares, Delft

Terzaghi, K. (1925). Principles of soil mechanics, IV Settlement and consolidation of clay. *Engineering News-Record*, *95*(3), 874-878.

Terzaghi, K. (1957). Varieties of submarine slope failures: Proc. 8th Texas Conf. *Soil Mechanics and Foundation Eng., Sept*, 14-15.

Van den Ham, G.A., Mastbergen, D. R., Koelewijn, A.R., Ter Brake, C.K.E., Zomer, W.S., (2015) Eindrapport validatie-experiment zettingsvloeiing, Amersfoort, STOWA/ Flood Control IJkdijk.

Van Den Berg, J. H., Van Gelder, A., & Mastbergen, D. R. (2002). The importance of breaching as a mechanism of subaqueous slope failure in fine sand. *Sedimentology*, *49*(1), 81-95.

Van Kesteren, W. G. M., Steeghs, H. J. M. G., & Mastbergen, D. R. (1992). Pore water behaviour in dredging processes. In *Proceedings XIII World Dredging Conference* (pp. 598-615). Universal Publishing Corporation.

Van Rhee, C., & Talmon, A. M. (2000). Entrainment of sediment (or reduction of sedimentation) at high concentration. In *Proc., 10th Int. Symp. on Transport and Sedimentation of Solid Particles*. Wroclaw, Poland: Agricultural Univ. of Wroclaw.

Van Rhee, C., & Bezuijen, A. (1998). The breaching of sand investigated in large-scale model tests. *Coastal Engineering Proceedings*, *1*(26).

Van Rhee, C. (2010). Sediment entrainment at high flow velocity. *Journal of Hydraulic Engineering*, *136*(9), 572-582.

Van Rijn, L. C. (1984). Sediment transport, part I: bed load transport. *Journal of hydraulic engineering*, *110*(10), 1431-1456.

Van Rijn, L. C., & Kroon, A. (1992). Sediment transport by currents and waves. *Coastal Engineering Proceedings*, *1*(23).

Wilderom, N. H. (1979). Resultaten van het vooroeveronderzoek langs de Zeeuwse stromen. *Rijkswaterstaat, Nota*, *75*.

Winterwerp, J. C., de Groot, M. B., Mastbergen, D. R., & Verwoert, H. (1990). Hyperconcentrated Sand-Water Mixture Flows Over a Flat Bed. *Journal of Hydraulic Engineering*.

Winterwerp, J. C., Bakker, W. T., Mastbergen, D. R., & van Rossum, H. (1992). Hyperconcentrated sand-water mixture flows over erodible bed. *Journal of Hydraulic Engineering*, *118*(11), 1508-1525.

You, Y., Flemings, P., & Mohrig, D. (2012). Dynamics of dilative slope failure. *Geology*, *40*(7), 663-666.

You, Y., Flemings, P., & Mohrig, D. (2014). Mechanics of dual-mode dilative failure in subaqueous sediment deposits. *Earth and Planetary Science Letters*, *397*, 10-18.

APPENDIX A: RESULTS SLOPES

In this Appendix additional results are shown with the model BreachFlow by varying the breach height and the slope angle. The results are discussed in chapter 4.4.2

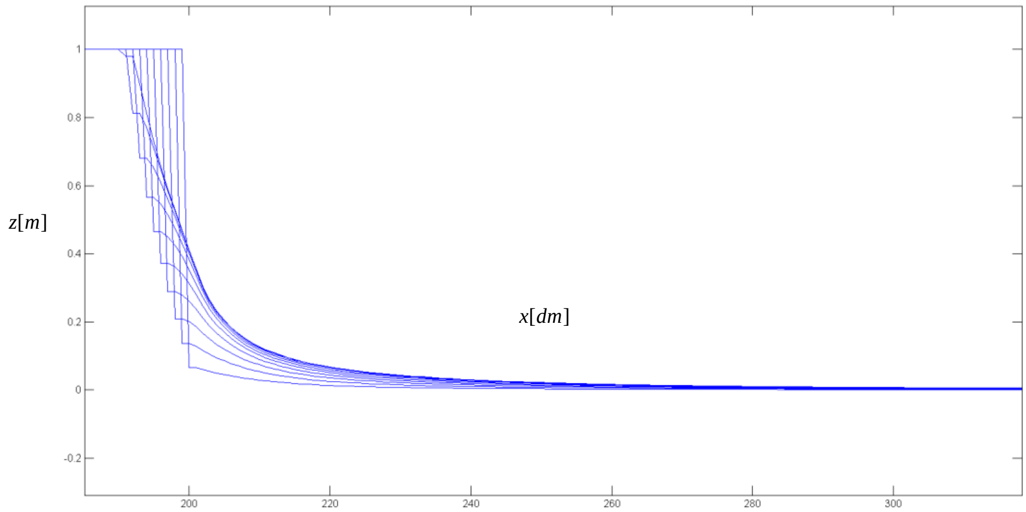

Figure A.1: breach height 1m, beta 0°

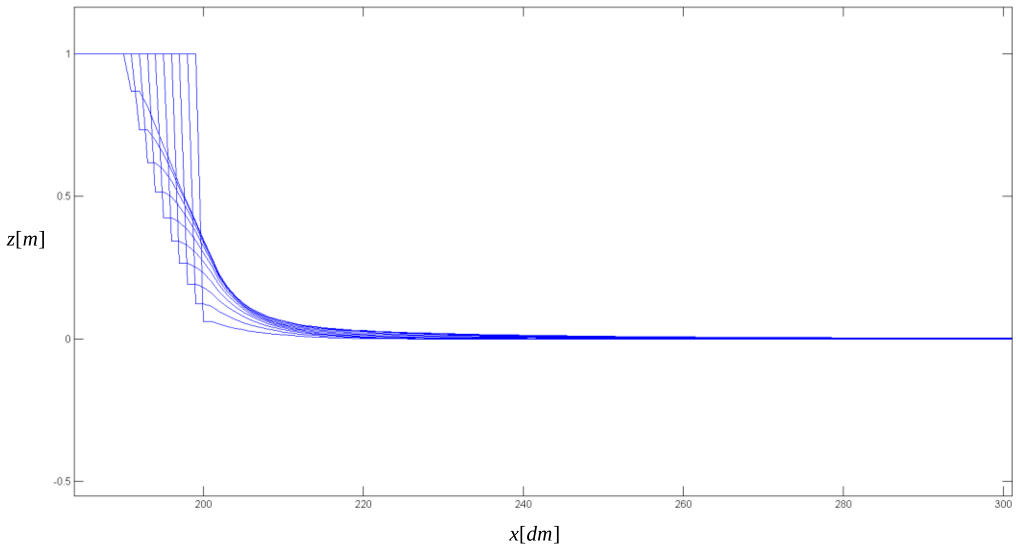

Figure A.2.1: breach height 1m, beta 18°

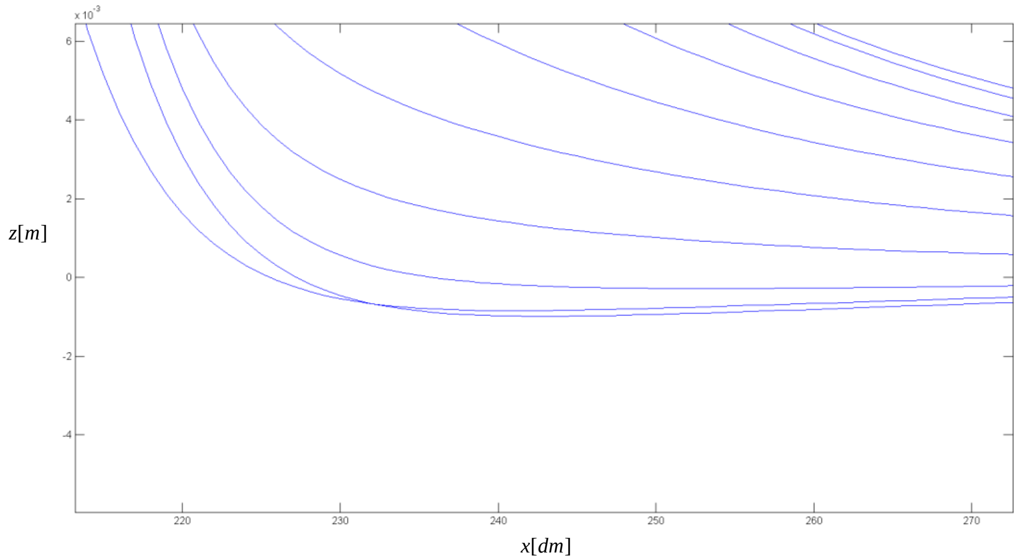

Figure A.2.2: detail breach height 1m, beta 18°

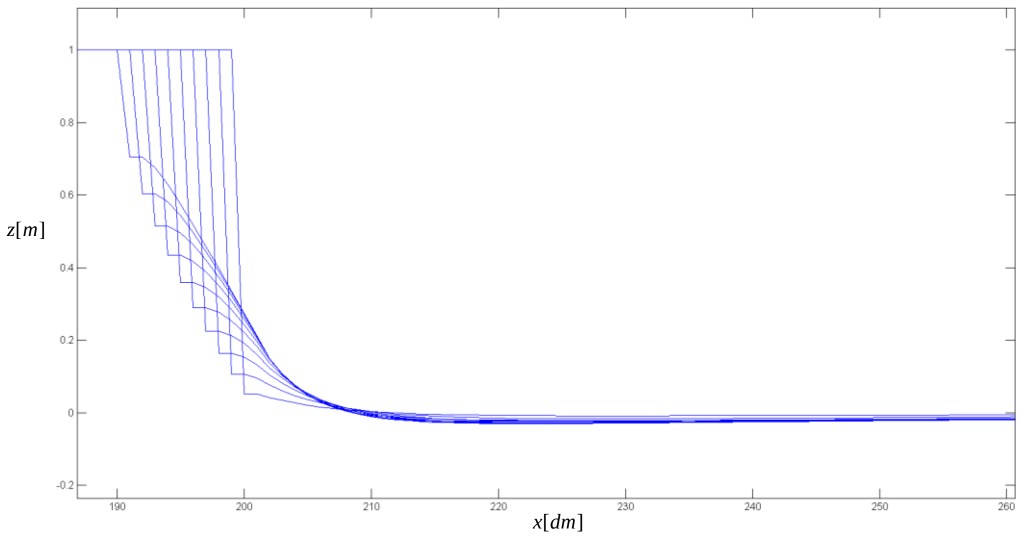

Figure A.3: breach height 1m, beta 30°

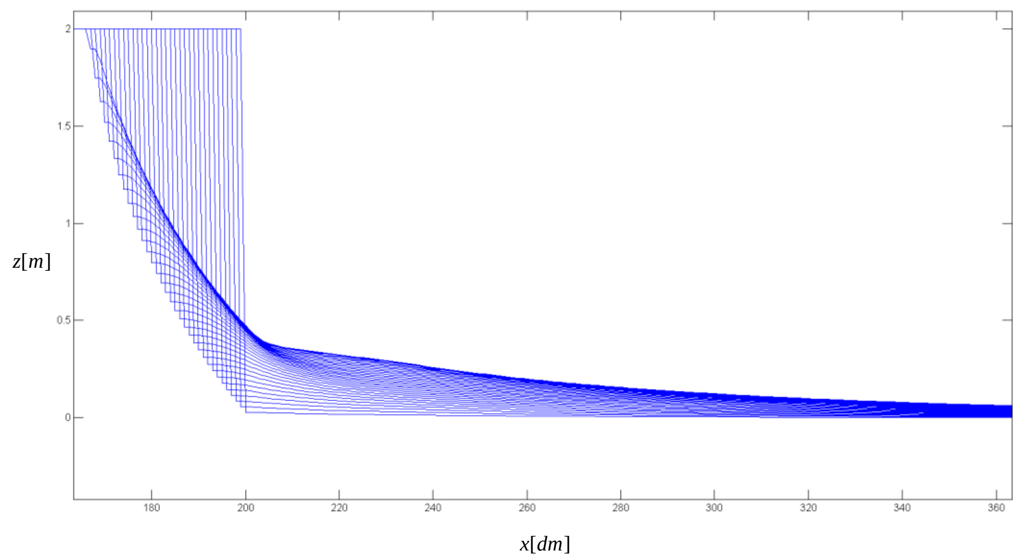

Figure A.4: breach height 2m, beta 0°

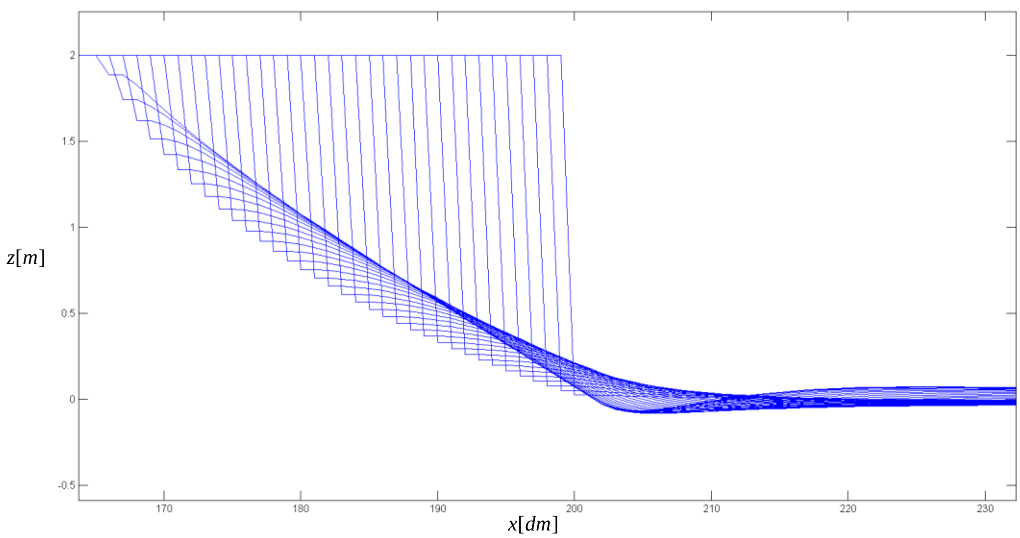

Figure A.5.1: breach height 2m, beta 10°

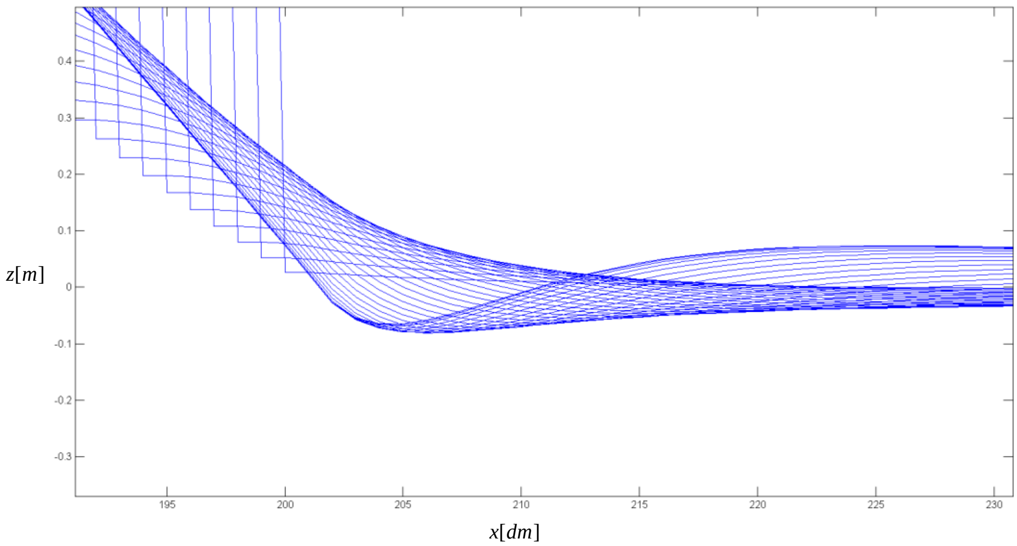

Figure A.5.2: detail breach height 2m, beta 10°

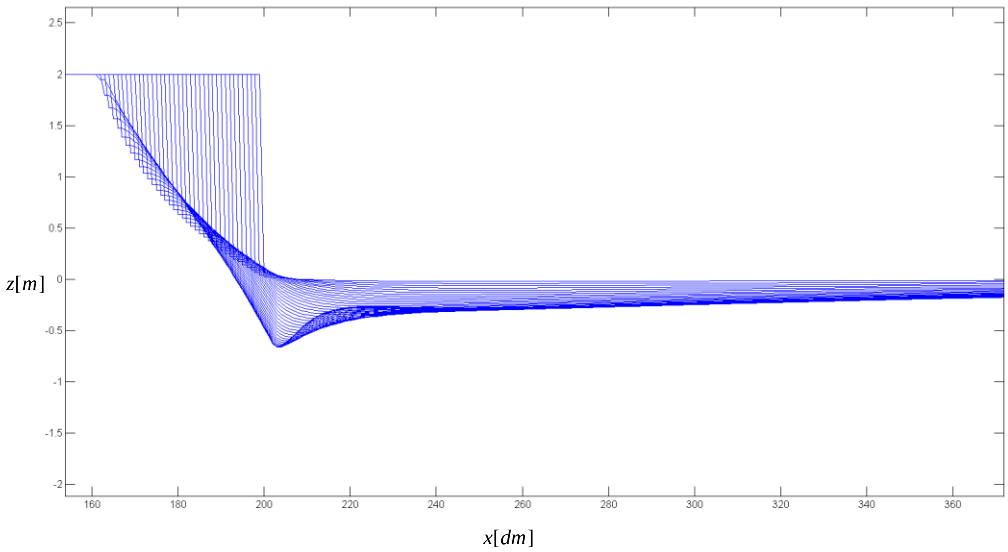

Figure A.6: breach height 2m, beta 20°

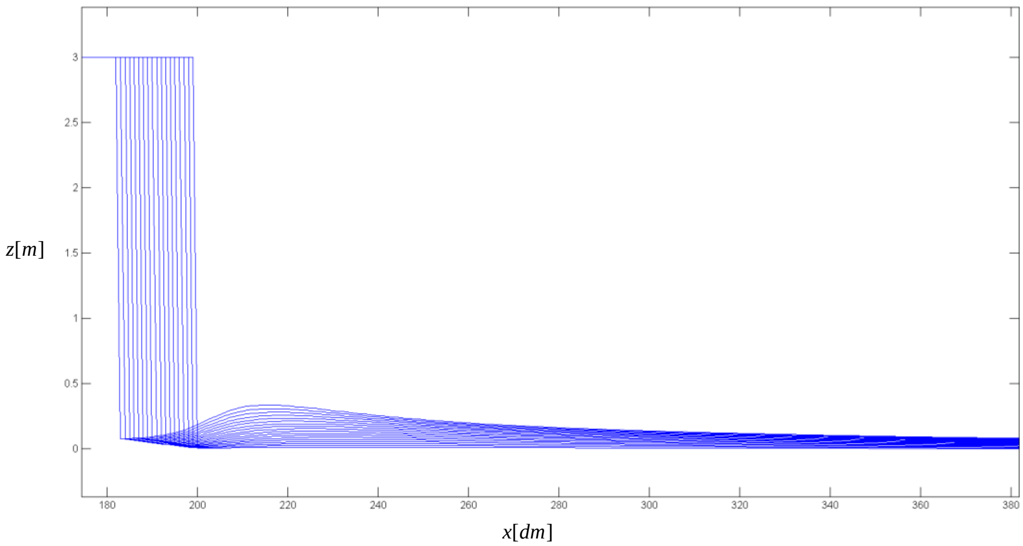

Figure A.7: breach height 3m, beta 0°

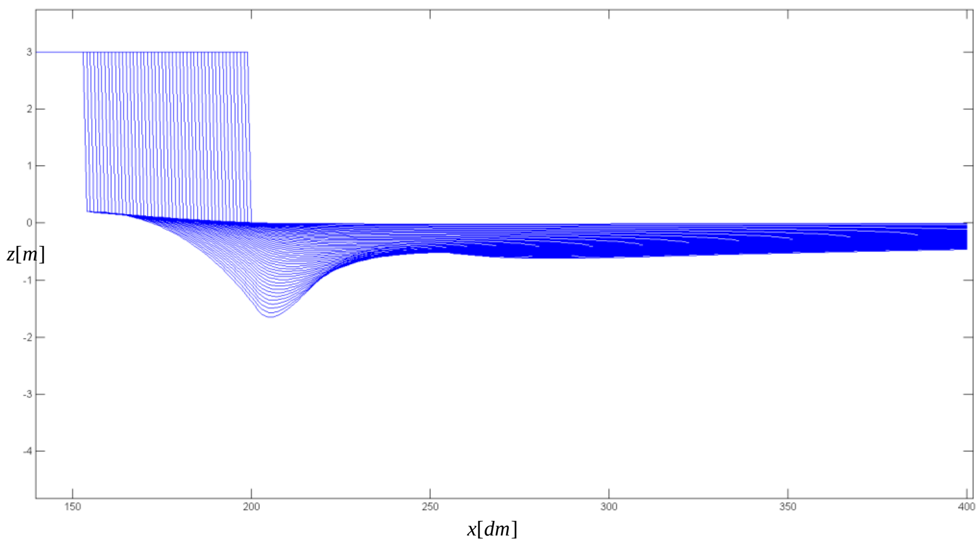

Figure A.8: breach height 3m, beta 10°

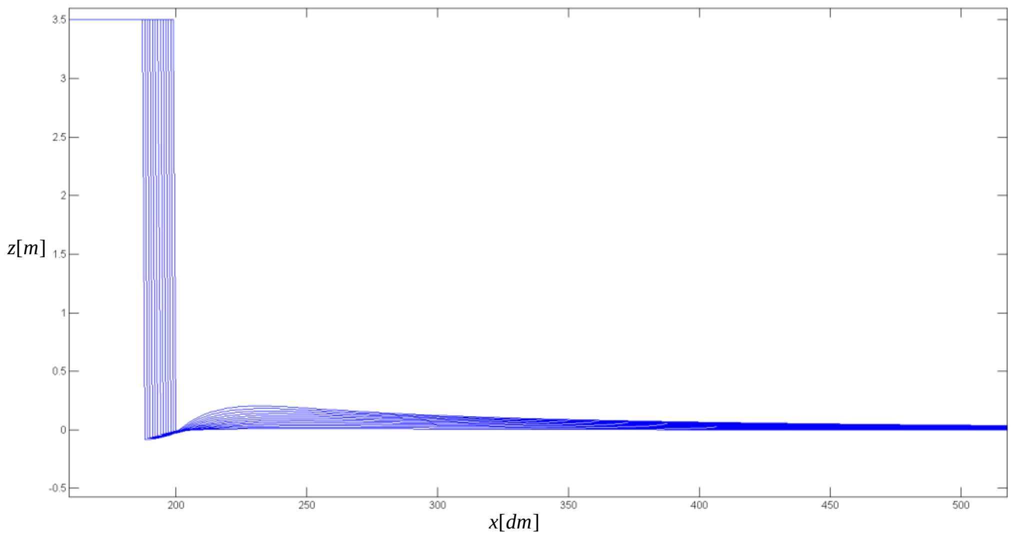

Figure A.9: breach height 3.5m, beta 0°

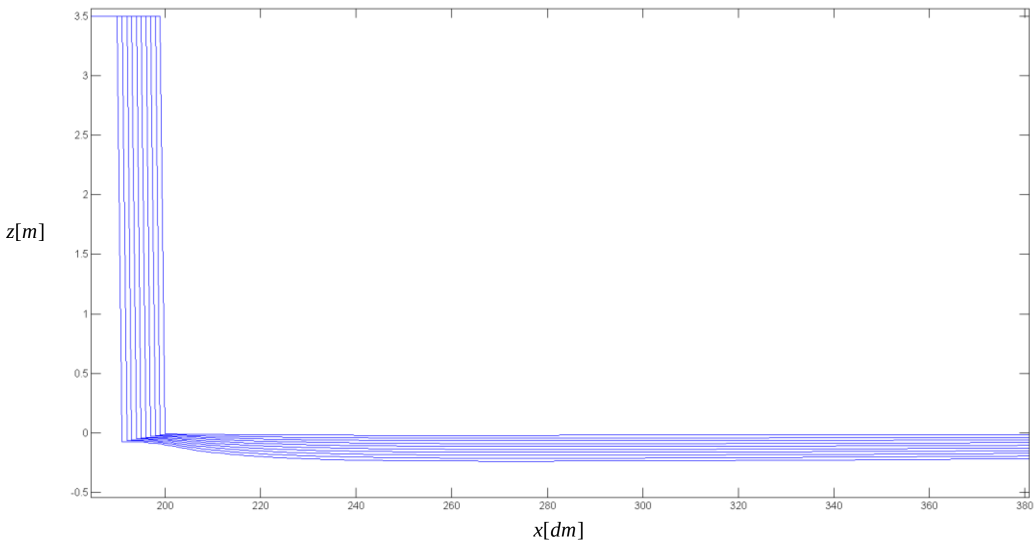

Figure A.10: breach height 3.5m, beta 10°

APPENDIX B: MACCORMACK SCHEME

The MacCormack scheme for continuity of sediment and water, continuity of water and the momentum equation resp. is shown by the quasi-linear systems:

$$M^{P,n+1} = M^n - \frac{\Delta t}{\Delta x}(M_{i+1}^n u_{i+1}^n - M_i^n u_i^n) + \Delta t q_i^n \;\; ; \;\; M^{C,n+1} = M^n - \frac{\Delta t}{\Delta x}(M_{i+1}^{P,n} u_{i+1}^{P,n} - M_i^{P,n} u_i^{P,n}) + \Delta t q_i^{P,n} \quad \text{(B.1)}$$

$$d^{P,n+1} = d^n - \frac{\Delta t}{\Delta x}(d_{i+1}^n u_{i+1}^n - d_i^n u_i^n) + \Delta t q_i^n \;\; ; \;\; d^{C,n+1} = d^n - \frac{\Delta t}{\Delta x}(d_{i+1}^{P,n} u_{i+1}^{P,n} - d_i^{P,n} u_i^{P,n}) + \Delta t q_i^{P,n} \quad \text{(B.2)}$$

$$F^{P,n+1} = F^n - \frac{\Delta t}{\Delta x}(F_{i+1}^n u_{i+1}^n - F_i^n u_i^n) + \Delta t q_i^n \;\; ; \;\; F^{C,n+1} = F^n - \frac{\Delta t}{\Delta x}(F_{i+1}^{P,n} u_{i+1}^{P,n} - F_i^{P,n} u_i^{P,n}) + \Delta t q_i^{P,n} \quad \text{(B.3)}$$

In which, superscripts P and C are the Predictor and Corrector steps, which are the intermediate solutions and q_i^n are the source terms. Combination of both steps for all three equations yield the stable solution (only momentum equations is shown):

$$F^{n+1} = \frac{1}{2}(F^{P,n+1} + F^{C,n+1}) \quad \text{(B.4)}$$

However, this scheme generates over and undershoots when slopes exceeds the difference in mean values of the fluxes at cell interfaces (i+1/2) and (i-1/2). Because the values at these points are first order approximated, the scheme requires additional information so the fluxes are within bounds. The additional information is applied by the use of TVD (Total Variation Diminishing) schemes, by which variables are discretized at cell interfaces instead of cell centres.

$$F_i^{n+1} = F^n - \frac{\Delta t}{\Delta x}(F_{i+1/2}^n u_{i+1/2}^n - F_{i-1/2}^n u_{i-1/2}^n) + \Delta t q_i^n \quad \text{(B.5)}$$

In which the flux interfaces (i+1/2) and (i-1/2) can be expressed as:

$$F_{i+1/2}^n = \frac{1}{2}(F_{i+1}^n + F_i^n) - \frac{1}{2}\frac{\Delta t}{\Delta x} A_{i+1/2}^n (F_{i+1}^n - F_i^n) \quad \text{(B.6)}$$

$$u_{i+1/2}^n = \frac{1}{2}(u_{i+1}^n + u_i^n) - \frac{1}{2}\frac{\Delta t}{\Delta x} A_{i+1/2}^n (u_{i+1}^n - u_i^n) \quad \text{(B.7)}$$

APPENDIX C: PARAMETERS IMPLICIT SCHEME

The expressions can also be solved implicitly, with the use of an iterative step. In this appendix the entire discretisation is shown and used as input for modelling. First, the three expressions from previous calculations and assumptions are shown. The sediment (C.1), water (C.2), mixture (C.3), and momentum equation (C.4) are derived from the 1D continuity and 1D momentum balance equations.

$$\frac{\partial cd}{\partial t}+\frac{\partial ucd}{\partial x}=(1-n_0)v_e\Big|_{z1} \tag{C.1}$$

$$\frac{\partial(1-c)d}{\partial t}+\frac{\partial(1-c)ud}{\partial x}=w_e\Big|_{z2}+n_0v_e\Big|_{z1} \tag{C.2}$$

$$\frac{\partial d}{\partial t}+\frac{\partial ud}{\partial x}=w_e\Big|_{z2}+v_e\Big|_{z1} \tag{C.3}$$

$$\frac{\partial(1+\Delta c)ud}{\partial t}+\frac{\partial(1+\Delta c)u^2d}{\partial x}+\Delta cg\cos\beta d\frac{\partial(d+z_1)}{\partial x}-\Delta c\,\mathrm{g}\sin\beta d+\frac{f_0+f_1}{8}(1+\Delta c)u_s^2+\frac{1}{2}g\cos\beta d^2\Delta\frac{\partial c}{\partial x}=0 \tag{C.4}$$

The expressions can be simplified by combining the variables $\rho_m ud=F$, as well as $\rho_m d$ which is expressed in terms of M . It simplifies equation (C.2), (C.3) and (C.4) by:

$$\frac{\partial M}{\partial t}-\rho_w\frac{\partial d}{\partial t}+\frac{\partial F}{\partial x}-\rho_w\frac{\partial ud}{\partial x}=(\rho_{m,z1}-\rho_w)v_e\Big|_{z1} \tag{C.5}$$

$$\frac{\partial d}{\partial t}+\frac{\partial ud}{\partial x}=w_e\Big|_{z2}+v_e\Big|_{z1} \tag{C.6}$$

$$\frac{\partial F}{\partial t}+\frac{\partial Fu}{\partial x}+(\rho_m-\rho_w)g\cos\beta d\frac{\partial d}{\partial x}-(\rho_m-\rho_w)\mathrm{g}\sin\beta d+\frac{f_0+f_1}{8}\rho_m u_s^2+\frac{1}{2}g\cos\beta d^2\frac{\partial}{\partial x}\rho_m=0 \tag{C.7}$$

If (C.6) is substituted into (C.5), it yields:

$$\frac{\partial M}{\partial t}+\frac{\partial F}{\partial x}=\rho_{m,z1}v_e\Big|_{z1}+\rho_w w_e\Big|_{z2} \tag{C.8}$$